Lithium-Ion Energy Storage Systems in Smart Grid Applications: Modeling and Analysis

BY

FRANCESCO REBAUDI
M.S., Politecnico di Torino, Turin, Italy, 2018
B.S., Universita' di Genova, Genoa, Italy, 2016

THESIS

Submitted as partial fulfillment of the requirements
for the degree of Master of Science in Mechanical Engineering
in the Graduate College of the
University of Illinois at Chicago, 2019

Chicago, Illinois

Defense Committee:

Suresh Aggarwal, Chair and Advisor
Reza Shahbazian Yassar
Massimo Santarelli, Politecnico di Torino

ACKNOWLEDGMENTS

I would like to express special appreciation to Professor Suresh Aggarwal, Professor Andrea Casalegno and Professor Massimo Santarelli who offered me the possibility of working on this interesting subject. They gave me precious and valuable suggestions which helped me to complete this research thesis. Furthermore, I desire to thank Arpit Maheshwari for his necessary knowledge concerning the cell model and the energy storage systems. Finally, I express my gratitude to my family and friends that have supported me during the studies.

FR

TABLE OF CONTENTS

TABLE OF CONTENTS (continued)

CHAPTER **PAGE**

TABLE OF CONTENTS (continued)

CHAPTER **PAGE**

LIST OF TABLES

LIST OF FIGURES

LIST OF FIGURES (continued)

FIGURE **PAGE**

LIST OF FIGURES (continued)

FIGURE **PAGE**

LIST OF FIGURES (continued)

FIGURE **PAGE**

LIST OF ABBREVIATIONS

AC	Alternating Current
AF	Aging Factor
BESS	Battery Energy Storage System
BNI	Beam Normal Irradiation
BSDG	Black Start Diesel Generators
BTM	Behind The Meter
CAES	Compressed Air Energy Storage
CCGT	Combined Cycle Gas Turbine
CAMS	Copernicus Atmosphere Monitoring Service (CAMS)
CEDA	Centre for Environmental Data Analysis
DC	Direct Current
DHI	Direct Horizontal Irradiation
DOD	Depth Of Discharge
DSO	Distribution System Operator
EA	Energy Arbitrage
EFC	Equivalent Full Cycle
EOL	End Of Life

LIST OF ABBREVIATIONS (continued)

ESS	Energy Storage
FFR	Firm Frequency Response
HT	Heat Transfer
HTC	Heat Transfer Coefficient
HV	High Voltage
ISO	Independent System Operator
IG	Island Grid
Li-Ion	Lithium-Ion
LIB	Lithium-Ion Batteries
LV	Low Voltage
MV	Medium Voltage
NMC	Lithium Nickel Manganese Cobalt Oxide
OCV	Open Circuit Voltage
RES	Renewable Energy Sources
RES-BESS	Renewable Energy Sources - Battery Energy Storage System
PS	Peak Shaving
PV	PhotoVoltaic
R&D	Research and Design

LIST OF ABBREVIATIONS (continued)

SEI	Solid Electrolyte Interface
SOC	State Of Charge
TSO	Transmission System Operator
UIC	University of Illinois at Chicago
UPS	Uninterruptible Power Supply

LIST OF ABBREVIATIONS (continued)

Symbol	Meaning	Unit
A	Area	m^2
AF	Aging Factor	€
A_b	cell bottom surface	m^2
A_l	cell lateral surface	m^2
A_t	cell top surface	m^2
BNI	beam normal irradiation	kW/m^2
C	cell capacity	Ah
C_N	cell nominal capacity	Ah
C_1	high frequency capacitance RC model	Farads
C_2	low frequency capacitance RC model	Farads
C_p	specific heat capacity	J/Kg/K
d_k	aging damage contribution	1
D	diffusion coefficient	1
D	total cumulative aging damage	1
DOD	depth of discharge	1
DHI	direct horizontal irradiation	kW/m^2
E	electrochemical potential	V
E_0	standard potential	V
E^0_{anode}	anode standard potential	V
$E^0_{cathode}$	cathode standard potential	V
F	Faraday's constant	96485 C/mol
h_b	cell bottom heat transfer coefficient	$W/K/m^2$
h_{le}	cell lateral external heat transfer coefficient	$W/K/m^2$
h_{li}	cell lateral internal heat transfer coefficient	$W/K/m^2$
h_t	cell top heat transfer coefficient	$W/K/m^2$
HT	cell heat transfer	W
I	current	A
I_C	current rate	1/h (C)
I_{C_1}	high frequency capacitor current	A
I_{C_2}	low frequency capacitor current	A
k_{AF}	aging factor coefficient	1
k_{alt}	altitude factor	1
k_{AF}	aging factor coefficient	1
m	chemical activity	1
M	cell mass	Kg

LIST OF ABBREVIATIONS (continued)

Symbol	Meaning	Unit
n	number of electron per reaction	1
N_{panels}	number of solar panels	m^2
$N_{turbines}$	number of wind turbines	1
Pess	battery power (discharging positive, charging negative)	kW
Pr	electricity prices	€/kWh
p_1	calendar aging capacity fade coefficient	1
p_2	calendar aging capacity fade coefficient	1
P_{solar}	solar electrical power output	kW
P_{wind}	wind electrical power output	kW
Q	charge throughput	Ah or EFC
R	universal gas constant	8.31446 $J/mol/K$
R	resistance	ohm
R_i	cell internal resistance	ohm
R_0	series resistance RC model	ohm
R_1	high frequency resistance RC model	ohm
R_2	low frequency resistance RC model	ohm
s	stoichiometric concentration	1
SOC	state of charge	1
t	time	days
T	temperature	K
T_c	cell temperature	K
V_{R_0}	series resistance voltage drop	V
V_{C_1}	high frequency capacitor voltage drop	V
V_{C_2}	low frequency capacitor voltage drop	V
V_{OC}	open circuit voltage	V
V_{OC}	open circuit voltage	V
v_{wind}	wind speed	m/s
α	cycle capacity fade coefficient	Ah/EFC
$\beta_0^{SOC_i}$	cycle aging coefficient of R_0 at SOC_i	ohm/EFC
$\beta_1^{SOC_i}$	cycle aging coefficient of R_1 at SOC_i	ohm/EFC
$\beta_2^{SOC_i}$	cycle aging coefficient of R_2 at SOC_i	ohm/EFC
ΔC_{cal}	calendar capacity fade	Ah
ΔG^0	Gibbs free energy	Joule
η_{solar}	PV conversion efficiency	1
η_{dhi}	diffuse horizontal irradiation collection efficiency	1
ρ	resistivity	A/V/m
τ	time	h

SUMMARY

Nowadays, modern smart grids require the implementation of Energy Storage Systems (ESS) in order to optimize the production, consumption and distribution of electrical energy. In particular, ESS add a degree of freedom to the system which allows to cover the mismatch between production and demand while providing other grid support services. Lithium Ion Batteries have proven to be mature to serve in several applications involving different stakeholders. In fact, their characteristics in terms of aging, specific power and response times are superior to other energy storage technologies.

The aim of the thesis is to develop and study a model which simulates a Lithium-Ion based storage system operating in some selected applications. The model is built in the MATLAB and Simulink environment, and it considers several aspects: electrical connections, thermal behavior, aging prediction, controlling and economic performance. Overall, the comprehensive model is developed thanks to large amounts of experimental data which make it accurate and flexible. Great relevance is given to the aging model which is designed starting from experimental results and fatigue algorithms: both calendar and cycle aging are considered.

Three relevant energy storage system applications are selected and studied: RES-BESS, energy arbitrage and island grid. In all cases a simulation of one year is performed employing the developed model after an accurate design procedure. The operating conditions of the storage system are checked and analyzed throughout the simulation. Aging is the main index to be evaluated to asses the sustainability of the application. Finally, depending on the specific

application, revenue sources are identified and calculated. With current prices of Lithium Ion batteries, all applications resulted to be hardly economically sustainable. However, considering the decreasing trend of prices, these applications may be very interesting in the medium and long term (about a decade) confirming the relevance of the research.

CHAPTER 1

INTRODUCTION

A traditional electrical grid, as shown in Figure 1, features always a one-way energy flux. This system design is suitable when energy is supplied constantly by conventional plants which exploit fossil fuels such as coal, gas and uranium. In fact, the electrical production of these kind of plants can be totally forecast and planned (exception for nuclear plants whose production can be only partially adjusted). Until 2000, the penetration of non-hydro Renewable Energy Sources (RES) was not relevant (below 2%) and energy was almost fully supplied by conventional plants [1]. Furthermore, there was not great interest in investing in modern and efficient electrical grids. Under these circumstances, basically, the main objective was planning the production and transporting electricity to the end user in a one-way flux as shown in Figure 1 [2].

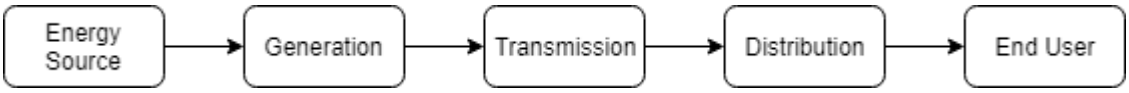

Figure 1: Traditional electrical grid

Nowadays, higher sustainability standards require upgraded and flexible electrical grids. Moreover, the employment of RES is the right path in order to guarantee a sustainable electricity

supply. Thanks to relevant R&D investment, RES are becoming cheap and competitive with conventional energy sources. The main renewable sources, exploited as distrubeted generators, are Wind Turbines and PhotoVoltaics (PV). These technologies are well developed and they can be integrated in existing grids easily. However, their energy output is often intermittent and cannot be planned [3]. Furthermore, energy demand variations add an additional stochastic variable. For this reason, balancing supply and demand is becoming increasingly challenging in terms of power, energy and frequency. Figure 2 shows how PV and Wind turbines had a penetration around 15% in the United Kingdom in 2016 (3% and 12% respectively) and they are expected to double within 2022 [4]. A RES penetration about 20% throughout a year implies that sometimes the power generated by RES exceeds 50%. This high and increasing RES production is one of the main reasons of Energy Storage System (ESS) employment but, as it will be explained, it is not the only one. In fact, modern electrical grids in order to be flexible, reliable and efficient need the possibility of storing energy.

Smart grids can fully take advantage of the increasing penetration of RES as they can face the related issues. A smart grid is an electrical grid which is purposely designed to effectively manage energy fluxes in presence of both centralized plants and distributed generators allowing multi-stakeholder interactions [5]. To achieve this task a smart grid relies on advanced sensors, controllers and energy storage systems. ESS are key factors in a smart grid providing an additional and necessary degree of freedom. Smart grids exploit ESS in synergy with distributed generators in order to achieve different tasks.

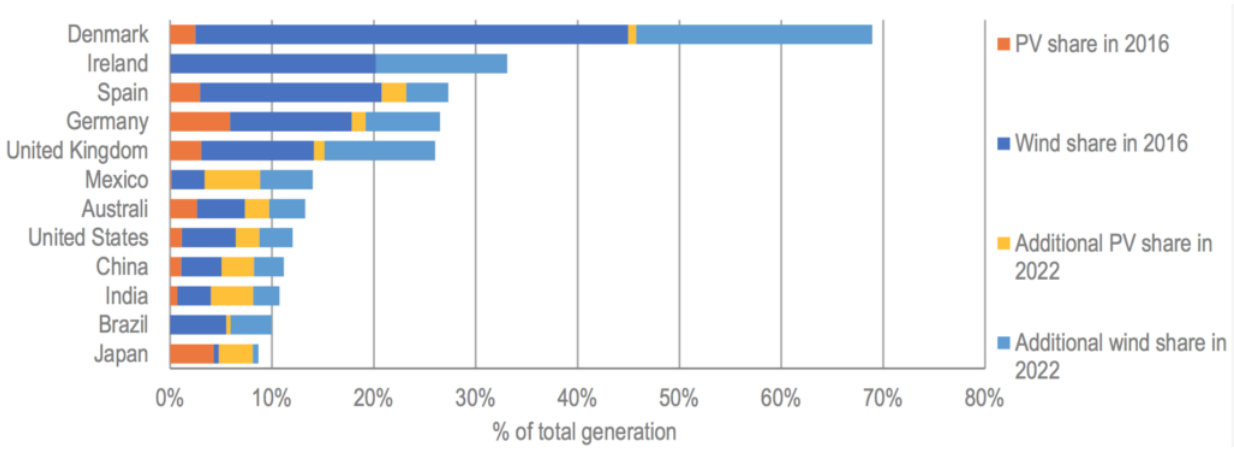

Figure 2: Wind and PV penetration in 2016 and 2022, Based on IEA data ©OECD/IEA, Reprinted with permission,Licence: www.iea.org/t&c

As shown in Figure 3, the energy storage system can be integrated at different levels of the grid. It can be connected, according to the application, to High Voltage (HV) transmission lines, to Medium Voltage (MV) primary distribution networks, to Low Voltage (LV) secondary distribution networks or directly to end users (behind the meter). The implementation of ESS guarantees an additional dimension allowing energy fluxes to be bidirectional. In general ESS can provide several services in different applications which will be discussed in the following chapter.

The focus of the thesis is reserved to Battery Energy Storage System (BESS) based on the lithium ion technology. A model is built on MATLAB and Simulink to simulate the behavior of a Lithium Ion Battery (LIB) ESS. Compared to other models built within literature this model include an advanced subroutine which predicts and assess aging effects making the simulation

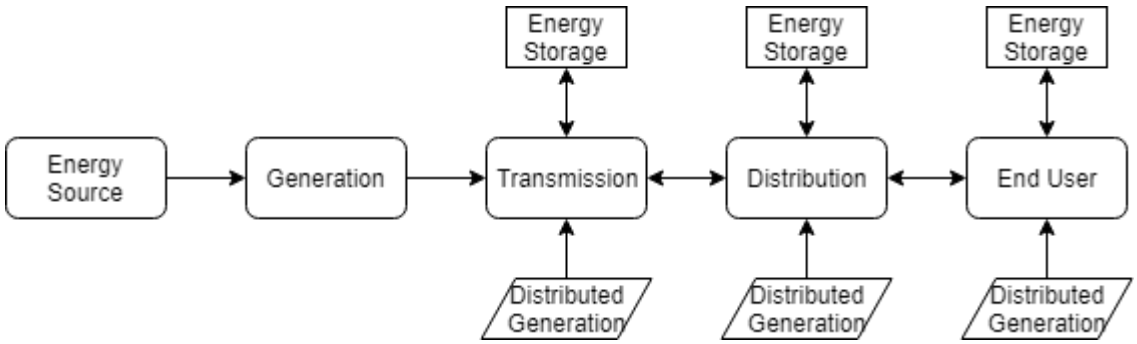

Figure 3: Power grid with storage and distributed generation

more accurate and the analysis more reliable. Next, the developed model is employed to perform a simulation lasting one year for some selected application.

The aim of the thesis consists in describing the procedure to build the BESS model and analyzing its results for some specific applications. In this way the feasibility and the opportunities of these applications are evaluated and discussed. A great relevance is given to the aging aspects of the battery which is the main index to evaluate the sustainability of the specific application.

The structure of the thesis is described in the following.

Chapter 2 describes all main applications involving battery energy storage systems. Applications are clustered and discussed considering different aspects: stakeholders, connection level, revenue sources, battery requirements etc.

Chapter 3 gives a brief overview on the ESS technologies. Next, the principles of operation and the components of lithium ion batteries are described. Moreover, the theoretical founda-

tions regarding LIB aging are discussed. Finally, some definitions about the batteries quantities employed in the model are described.

Chapter 4 describes the battery energy storage system model in all its aspects.

In Chapter 5 the model discussed in chapter 4 is employed to simulate the energy storage system in three different applications: RES-BESS, Island Grid and Energy Arbitrage. In all cases, the BESS is designed after an advanced design procedure which is presented as well as the system layout and topology. Next, the operating condition of the battery throughout the simulation are analyzed and discussed. Moreover, the economic performance as well as the aging results are evaluated.

CHAPTER 2

ENERGY STORAGE SYSTEMS: APPLICATIONS IN MODERN POWER GRIDS

This Chapter gives an overview on the applications regarding Energy Storage Systems (ESS) integrated in electrical grids. In particular, applications involving Lithium-Ion Batteries (LIB) are considered but some other technologies may be suitable as well. Applications are clustered and discussed considering different aspects: stakeholders, connection level, revenue sources and battery requirements.

LIB ESS can achieve several tasks which can be classified in different clusters. Each application involve different stakeholders and different designs of the energy storage system. In the following subsections applications are grouped according to the families listed below:

- Energy Services: the ESS achieve tasks related to the supply of electrical energy. Power is exchanged over long time intervals. Normally high capacity batteries are employed.
- Power Services: the ESS achieve tasks related to the supply of electrical power. Large amounts of power are exchanged over short time intervals. Normally high rated power batteries are employed.
- Ancillary Services and Grid Support: the ESS serve various tasks. ESS technical parameters depend on the specific application.
- Combined Applications: The ESS operates offering multiple services.

2.1 Energy Services

Energy services include all tasks having the exchange of electrical energy as main target. Contrary to power services, energy services exchange electricity over longer time intervals (usually longer than 15 minutes). Batteries operating in this field should have high capacities and long expected lives. In fact, they usually undergo several cycles at high Depth Of Discharge (DOD). Lithium ion batteries feature high energy density and longer cycle life compered to other electrochemical devices [6]. As it will be explained in this subsection, energy services can involve different stakeholders at different levels of the grid. Table I gives an overview on applications regarding energy services.

TABLE I: ESS ENERGY SERVICES APPLICATIONS

Task Family	**Application**	**Connecection Level**	**Revenue Source**	**Stakeholder**
Energy Services	Energy Arbitrage	Transmission Distribution	Energy Markets	Enterprise
	PV-BESS	End User	Energy Bill Savings Demand Charge Savings	Private Industry
	Load Leveling	Distribution	Energy Markets Grid investment Savings	Electric Utility DSO
	RES-BESS	Transmission Distribution	Energy Markets Grid Investments Savings	Enterprise Electric Utility
	Island Grid (IG)	Distribution	Grid Investments Savings Regulating Services	Electric Utility

2.1.1 Energy Arbitrage

Energy Arbitrage consists in taking advantage of the energy price volatility. Price volatility is mainly caused by variations in demand and supply. A high RES penetration, as explained in the previous section, increase supply uncertainty and, consequently, energy price volatility. This volataility cannot be exploited by conventional pumped hydro storage systems because of the fast fluctations. Usually BESS operating in energy arbitrage place buy and sell orders in the day ahead (and intraday) electricity market. This decision making procedure is based on forecasting and optimization algorithms which control the BESS (they will be discussed in the chapter about the model). The main target of the optimizer is to maximize profits considering, if possible, cell aging as well. Figure 4 shows energy price variations on a random day (01/12/2016) in the day ahead market in UK [7]. As it can be seen, the minimum price on that day was 0.0251 €/kWh whereas the maximum, almost four times higher, was 0.0930 €/kWh. Figure 5 illustrates prices distribution on hourly basis in UK in 2016 [7]. A high ESS penetration, which is not the case at present, would damp the volatility of the energy prices improving the performance of the grid but decreasing the profitability of ESS operating in this manner. For this reason ESS can be considered price taker or price maker according to their total influence on the market. Energy arbitrage applications usually involve enterprises or heavy industries with sufficient funds and know-how to operate in the energy market. Considering the volumes of the energy exchanged, connection to the grid is usually at the upper distribution or transmission level. Since LIB ESS have high energy densities, fast response time and good cycle life, they are considered suitable to provide energy arbitrage services. LIB prices are still too

high but they are decreasing constantly. Recent studies stated that energy arbitrage systems could be economically sustainable soon [8].

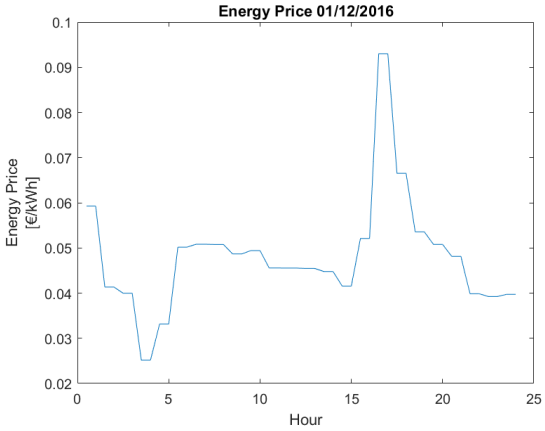

Figure 4: Energy prices in UK on 01/12/2016

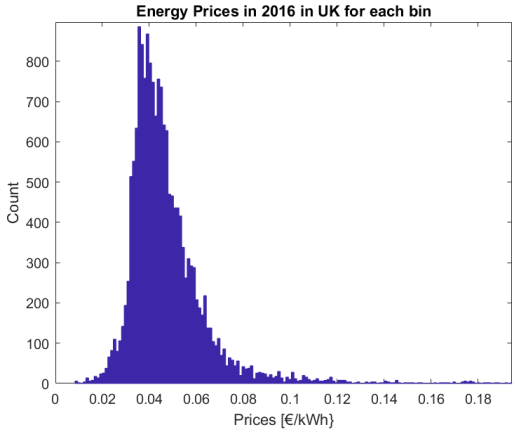

Figure 5: Energy prices in UK in 2016 per bin

2.1.2 PV-BESS

PV-BESS consists in storing the energy produced by Photo-Voltaic (PV) devices to maximize self consumption and, consequently, bill savings. This application usually regards end users such as residential customers or small industries. The whole system including the battery and the generator (PV) operates behind the meter [9]. Depending on the type of utility contract, PV-BESS allow savings both in terms of energy consumption and in terms of peak demand charges. Usually, peak demand charge savings are reserved to entities having business utility contracts. Anyway, an advanced PV-BESS can be controlled so that it takes into ac-

count energy price variations during the day (according to the market or to the utility contract) maximizing savings even further.

2.1.3 Load Leveling

Load Leveling implies damping the load profile of residential districts and small industries over a long time period (usually a day). During period of light loading (usually at night) energy is stored whereas, in case of high loading, energy is provided to the electrical grid. Unlike energy arbitrage whose target is to maximize revenue by trading energy, the objective of load leveling is minimizing load demand variations. By doing so, the distribution grid is relieved allowing savings in generation and grid support devices [10]. Finally, considering that usually energy prices are lower when demand is low and vice versa, load leveling should guarantee a revenue from the energy markets. Figure 6 shows the typical load profiles of 10000 households in the East Midlands for a day on January and June. As it can be seen, those load profiles would benefit from a LIB ESS operating in load leveling. The national grid in UK pays large users which can increase their demand during period of high RES output and low national demand through the demand turn up market. Participants should be able to demand at least 1 MW for an average delivery time of about 4 hours. Providers are paid based on the availability interval offered (availability fee) and on the energy absorbed (utilization fee). In 2016 the average utilization price of the demand turn up was 61 [£/MWh] [11].

2.1.4 RES-BESS

RES-BESS is a system which includes renewable energy sources and ESS. Contrary to PV-BESS applications, RES-BESS do not involve end users but rather enterprises operating in the

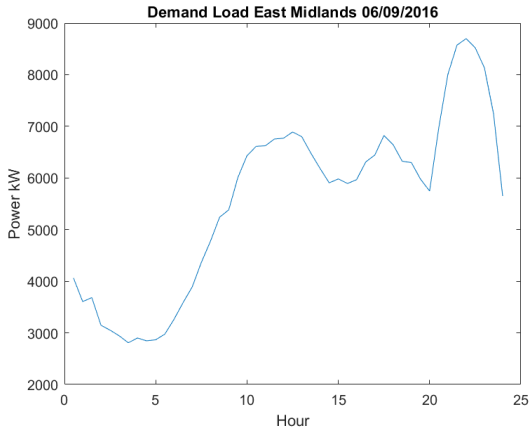

Figure 6: Load profile East Midlands, UK 06/09/2016

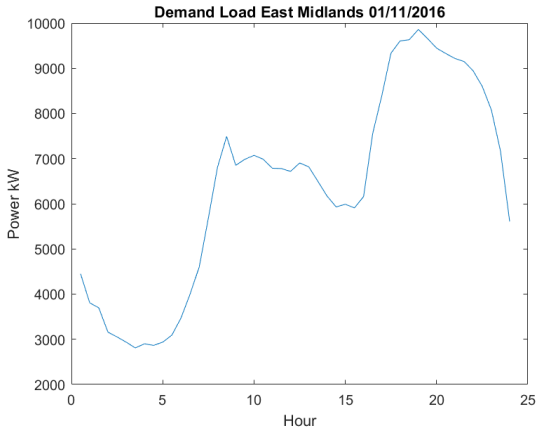

Figure 7: Load profile East Midlands, UK 01/11/2016

energy market. RES usually consist of wind and solar farms with high power outputs (usually higher than 1 MW). Considering the high amount of energy exchanged, the whole system is connected to the transmission lines or to the upper distribution network. The main reason for implementing energy storage systems in this kind of application is controlling the sale of energy: the intermittent and stochastic energy produced by the RES can be stored and sold when prices are higher maximizing profits. LIB systems operating in this kind of field have very high rated power and capacity. Moreover, controlling the BESS properly should allow RES feeders to avoid receiving sanctions from the Independent System Operator (ISO) and it could improve the quality of the energy/power sold. Precisely, sanctions can be inflected to enterprises selling unplanned energy volumes. Finally, an energy storage system integrated with RES can also

avoid excessive ramping rates during the supply of energy which are sanctioned by the ISO. A detailed description about the control of the ramping rate is given in paragraph 2.2.2.

2.1.5 Island Grid

An island grid is a portion of the distribution network which is made fully or partially independent from the external transmission lines. In an island grid the electrical production is provided by distributed generators (mainly RES such as PV and wind turbines) whereas the load is represented by houses or small factories. Energy storage systems are employed in an island grid in order to cover the mismatch between production and consumption with a relieving effect for the external grid. In this way, the energy exchanges between the island grid and the external grid are minimized making the system more efficient and sustainable. Moreover, an island grid implies lower transmission line investments and savings in balancing services. In fact, an ESS integrated in an island grid, besides covering the mismatch between production and demand, provides voltage support, frequency regulation and operating reserve. Overall, an energy storage system operating in this manner fulfills several tasks, and thus, the island grid can be considered as a combination of different application. As a case study, the Minami-Soma Substation exploits a LIB ESS with a rated power of 40 MW connected to the distribution grid. It controls the balance between renewable energy supply and demand, which depends on weather, by storing exceeding renewable electricity and supplying a distribution grid located in Minami-Soma [12].

2.2 Power Services

Power services include all tasks having the exchange of electrical power as main target. Contrary to energy services, power services exchange electricity over shorter time intervals (usually shorter than 15 minutes). LIB are suitable for this kind of duty considering the higher power density compered to other electrochemical devices (redox,lead-acid etc.). Moreover, the response time of LIB ESS is shorter compered to other mechanical storage systems (hydro-pumped, Compressed air etc.) allowing fast interventions on a millisecond timescale [13]. An overview on power services is given in Table II.

TABLE II: BESS POWER SERVICES

Task Family	**Application**	**Connecection Level**	**Revenue Source**	**Stakeholder**
Power Services	Peak Shaving	End User	Demand Charge Savings	Industry
	Ramping	Distribution Transmission	DSO/ISO regulations	RES Feeders
	Operating Reserve	Generation Transmission	Operating Reserve Markets	Plants Enterprise
	Frequency Control	Transmission Distribution	Frequency Regulation Markets	Plants Enterprise

2.2.1 Peak Shaving

Peak Shaving (PS) has the purpose of reducing peak demand [14]. It usually interests companies with business utility contracts which have peak demand fees. The demand charge is

directly proportional to the highest power demand in the billing period. Sometimes it can be even higher than the electrical energy usage charge. For this reason, implementing a PS BESS could be very attractive for industrial customers with highly variable loads. Peak Shaving may also interests distribution system operators to gain a relieving effect on the distribution grids (in this case the application is similar to Load Leveling 2.1.3).

2.2.2 Ramping Control or Capacity Farming

Ramping control (or Capacity Farming) consists in controlling the output of energy sources subjected to fluctuations [15]. The ramping rate [Watt/s] is the first time derivative of energy output. High ramping rates could cause voltage and power swings in the electrical grid. Therefore, to comply with system operator regulations, high ramping rates should be avoided. RES feeders, which are strongly subjected to weather-dependent output, could benefit from the employment of ramping control energy storage systems. In this manner they could maintain the power generation at the committed level. Ramping control is accomplished over small time intervals in the region of few minutes. LIB ESS are suitable for this task because of low-self discharge, fast response and high power density. RES-BESS, discussed in 2.1.4, operate similarly but over longer time intervals and with different targets.

2.2.3 Operating Reserve

To control the mismatch bewtween production and consumption, to keep frequency stable and to guarantee a reliable service an operating reserve of 15-20 % of the total generation should be kept ready to intervene. Capable of making intervention on a millisecond timescale, LIB BESS can be effective operating reserves [16]. The BESS operating in this field are maintained at

a high state of charge ready to respond to generation interruptions while conventional additional generators are activated. Using BESS in operating reserve could help conventional generators to operate at the optimum power output. Moreover, they can eliminate the need of having generators running idle. The national grid in UK requires two kind of operating reserve services: the Fast Reserve and the Short Term Operating Reserve.

The Fast Reserve involves generators or ESS which can be ready to supply or absorb minimum 50 MW for 15 minutes within 2 minutes. On average, providers are called for 5 minutes 10 times a day [17]. The revenue sources, which are listed below, consist in an availability fee, a nomination fee and an utilization fee [17].

- Availability [£/h]: Payment for the hours a provider has offered to make the service available. On average 260 £/h.
- Nomination/positional fee [£/h] (optional): Payment for being called upon to provide the service. On average 120 £/h.
- Utilization fee [£/MWh] : Payment based upon the amount of energy delivered in a certain intervention. On average 100 £/MWh.

The Short Term Operating Reserve interests providers connected to the transmission or distribution lines which can supply at least 3 MW for a minimum of 2 hours within 240 minutes (even if 20 minutes are preferable). Typically the service is requested in the morning and evening windows when the eletrical energy demand has its daily peaks. The revenue sources consist in an availability fee (on average 4.25 £/hour/MW in 2016) and and an utilization fee (on average

150 £/MWh in 2016) [18]. Providers cannot offer other services during the tendered availability windows.

2.2.4 Frequency Control

The main objective of frequency regulators is to keep the electrical grid frequency at 50 Hz in Europe or 60 Hz in the U.S.A. Frequency regulation is one of the most attractive application regarding BESS. Frequency deviations are mainly caused by mismatches in demand and supply. A high RES penetration decreases the employment of large conventional generators which are obliged to offer frequency regulation. Therefore, new frequency regulators should be integrated to compensate the growth of RES. Considering the high power and the fast response, LIB ESS have demonstrated to be suitable to operate in the frequency regulation market. Frequency control applications can be classified according to the duration of the average intervention [19]:

- Primary Frequency Regulation: Response provided within 10 seconds and sustained for further 20 seconds.
- Secondary Frequency Regulation: Response provided within 30 seconds and sustained for further 30 minutes.
- High Frequency response: Response provided within 10 seconds and sustained indefinitely.

Frequency regulation is accomplished feeding high amount of power in the transmission line. The primary frequency regulation is the most attractive for LIB ESS because lower amount of energy are exchanged. BESS operating in this kind of market are usually kept at a medium state of charge to be ready to absorb or release high amount of power. The transmission system

operator (TSO) , which is responsible for keeping the frequency stable, remunerates enterprises offering frequency regulation [20]. In UK, the national grid accepts providers that can be ready to dispatch at least 1 MW 24/7. There is a tender process by which providers are selected. Enterprises can offer only one or a combination of response times (resumed in the previous list). There are three revenue sources for enterprises joining this market [19]:

- Availability [£/hour]: Payment for the hours a provider has tendered to make the service available.
- Window initiation fee [£/window]: Payment for each frequency response window instructed in the tendered frames.
- Nomination fee [£/hour]: Payment for being called upon to provide the service.
- Response energy fee [£/MWh] : Payment based upon the amount of energy delivered in a certain intervention.

Offering primary frequency regulation can be highly remunerative. Recent studies assessed that returns per year range between 15000 £/MW and 20000 £/MW [21].

2.3 Ancillary and Grid Support Services

This subsection summarizes all BESS applications having auxiliary and grid support purposes. These tasks usually involve system operators. Frequency control and operating reserve can be considered ancillary services as well but they have been classified power services due to the recurring high power exchanges. Modern grid support devices, such as BESS, allow savings

in terms of grid maintenance and in grid reinforcement investments. Table III gives an overview on ancillary and grid support applications regarding LIB BESS.

TABLE III: BESS ANCILLARY AND GRID SUPPORT SERVICES

Task Family	**Application**	**Connection Level**	**Revenue Source**	**Stakeholder**
Ancillary and Grid Support Services	Black-Start	Transmission Generation	TSO contract BSDG savings	Enterprise Plants
	UPS	End User	Reliability Savings	Critical Users
	Voltage Support	Distribution	Grid Investment Savings	DSO

2.3.1 Black Start

Black start is the ability of restoring the generators of a plant without relying on the external transmission grid. In fact, after a serious failure in the eletrical grid, there might not be available power to restart the main generators and the entire system may collapse. For this reason, plants usually have small auxiliary diesel generators called Black Start Diesel Generators (BSDG) providing the black start service. However, keeping this high capacity in standby is uneconomical. Hydro pumped energy storage systems are often used in black start processes but distances between the coupled generators should be limited to avoid excessive impedance. In 2017, an electric utility in Southern California has successfully implemented a LIB energy storage system providing the black start service. It successfully restored a 44 MW Combined Cycle Gas Turbine (CCGT) from an idle state [22]. Considering the fast response time, the

high power output and the low self-discharge, LIB ESS have proven to be very effective in this application[23]. This kind of service is remunerated by the transmission system operator [24]. In UK, the national grid pays providers for the availability [£/settlement period] to offer black start services. Moreover, it pays for each black start test [£/MW]. Among others requirements, providers should be ready to supply instantaneously at least 35 MW with limited frequency variations. LIB ESS can be very precise at controlling output frequency compared to mechanical generators [22].

2.3.2 Uninterruptible Power Supply

Some kind of end users (such as hospitals, computer servers etc.) requires a high power supply reliability: they cannot withstand a black out [25]. Uninterruptible Power Supply (UPS) systems provide electrical energy in case of supply interruptions. LIB UPS have proven to be mature considering the low self-discharge and the limited calendar aging. The benefit of implementing a BESS UPS consists in an enhanced reliability. Finally, possible savings are made if alternative solutions are more expensive.

2.3.3 Voltage Support

Distribution system operators, among several other tasks, have to keep the voltage stable in the distribution grid. The voltage fluctuations mainly depend on variations of RES output and on changes of demand because of the impedance of the transmission cables [26]. ESS can stabilize the voltage on distribution grids through active and reactive power supply. Voltage support devices need to be fast and powerful but only little energy is required. For this reason LIB ESS are suitable for this duty. Considering that a market in this field does not exist, this

application involves distribution operators. The revenue stream is represented by saving in alternative voltage support solutions.

2.4 Combined Applications

BESS can operate providing multiple services simultaneously. At present many multi-purpose BESS are being evaluated. Often, single applications do not guarantee enough returns to cover the investment and the operational costs [27]. Instead, providing an additional service, usually overcomes the increased degradation costs. However, it can be really challenging to design a BESS for multiple applications which have specific requirements (cell performance, BESS size, grid connections etc.). Moreover, each task require a definite control method: for example, BESS operating in frequency control should be kept at medium SOC whereas in Black-Start they need to be always almost fully charged. Nevertheless, with accurate design procedures and flexible controlling, multi-purpose BESS can be very interesting.

An innovative multi-use BESS application consists in creating an island-grid which have already been discussed in paragraph 2.1.5. In this scenario, the battery energy storage system fulfills all tasks regarding the energy distribution in that island-grid: voltage stabilization, frequency control, load leveling and operating reserve. Furthermore, in the presence of RES integrated in the same island-grid, the energy exchanged with the external transmission grid can be minimized. The advantages in terms of revenue, savings and sustainability can be very attractive [28]. Finally, combining Electrical Vehicle (EV) batteries with smart grids (containing BESS as well) can be very interesting [29].

CHAPTER 3

ENERGY STORAGE SYSTEM TECHNOLOGIES: LITHIUM ION BATTERIES

Considering that storing energy can interest several applications, researchers have been developing various technologies. Obviously each application, as discussed in the previous chapter, has specific needs requiring a suitable energy storage system. To give an overview, the main energy storage system technologies employed as of today are listed below [30] [31] [32].

- Pumped hydro systems: This technology consists in exploiting gravity to store and supply energy. In particular, water is elevated in reservoirs with pumps in order to store energy. When energy is needed the water is released and its mechanical energy is converted in electrical energy by turbines. This technology can manage great amounts of energy in a simple way, and thus, it is the most popular energy storage system. However, the response times can be very long compared to other technologies making pumped hydro systems inappropriate for some specific applications.
- Compressed Air Energy Storage (CAES): This technology aims at storing energy by exploiting air. In particular, air is compressed with a compressor and stored in a pressurized underground cavern. When electricity is demanded, this air is heated and expanded in turbines producing mechanical energy which is converted in mechanical energy by alter-

nators. The total efficiency of this technology is about 45 %. However, it can be increased to about 70 % through the utilization of the heat produced during the compression stage.

- Flywheels: With this technology exceeding electrical energy accelerates a spinning mass whose mechanical energy is exploited when energy is demanded. The response times are very low enabling the system to operate in frequency regulation.
- Thermal systems: Thermals systems aim at converting exceeding energy in thermal energy which can be stored in thermal energy storages. When needed, this energy can be utilized to supply thermal energy to either end users or plants.
- Superconducting Magnetic Energy Storage: With this technology the electrical energy is converted and stored in magnetic fields.
- Super-capacitors: This technologies consists in storing exceeding electrical energy in electrostatic fields. These systems have very high power densities, low response times and long lifetimes. However, they lack in energy density which is about 5 Wh/Kg. The implementation of super-capacitor is very interesting: they can be implemented alongside other ESS technologies to manage the fast fluctuations in energy demand or supply.
- Electrochemical batteries: Electrical energy is converted and stored in chemical energy. These technologies include solid state batteries and flow batteries. These systems have good specific energy and specific power as well as excellent response times (in the region of tenths of seconds). However, batteries have a limited lifespan which can make their integration expensive.

Considering that the target of the thesis is to evaluate the implementation of a lithium ion battery as an energy storage system the attention is focused on this technology.

3.1 Lithium Ion Batteries

Figure 8 illustrates the number of existing and operating Lithium Ion Battery (LIB) ESS worldwide [33]. Overall, larger Battery Energy Storage System (BESS) ranging between 5 MW and 100 MW are connected directly to high voltage transmission lines or to primary distribution networks. Medium size BESS are linked to lower distribution levels and they have usually a rated power between 100 kW and 5 MW. Finally, BESS can be connected also behind the meter in houses or industries and they have a rated power usually around 10 kW for houses and much higher for industries.

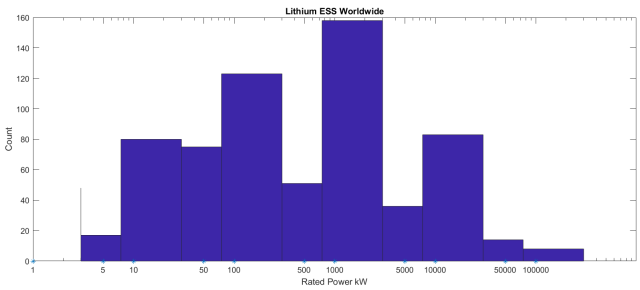

Figure 8: Lithium ESS worldwide per rated power

Lithium Ion batteries are an interesting trade-off between flywheels and pumped hydro systems which are the most spread solutions. In fact, pumped hydro systems can supply or demand

huge amounts of energy taking long response times though. On the other hand, flywheels or supercapacitors have short response times and excellent power densities but they cannot store great amounts of energy. Lithium Ion batteries can store moderate amounts of energy with good response times and interesting power densities. Compared to other electrochemical batteries, lithium ion batteries show a great performance in terms of power/energy density and cycle life as shown in the Ragone diagram [34].

3.1.1 Structure and Components

Lithium Ion cells can have different shapes: cylindrical, pouch and prismatic. Cylindrical cells are cheaper because they can be manufactured with fully automated processes. The downside of these cells is the packing density which is not really relevant for ESS. For these reasons, cylindrical cells are the most popular in ESS applications [35]. The main components of a LIB are the negative electrode, the positive electrode and the electrolyte.

The negative electrode, is oxidized during discharge releasing electrons to the external circuit. This component should have a low electrochemical potential as well as a good energy density. The state of the art material for the negative electrode is the graphite which allows lithium ions to intercalate into it [34]. This material is less effective in terms of specific charge density compared to metallic lithium materials. However, graphite is chosen for safety and for practical reasons. Moreover, graphite is a good conductor enabling the movement of the electrons to the current collector. During charging, the volume of the graphite can increase by 10 % which is determinant for cycle life as it will be explained in the following section.

The positive electrode , during discharge gets reduced meaning that it accepts electrons from the external circuit. Contrary to the negative electrode, there are many materials which can be employed to build the positive electrode. Three families of materials are usually used: Layered Metal Oxides, Spinels and Phosphates [36] [34]. Spinels have high electrochemical standard potentials (around 4.1 V with graphite) but they lack in stability leading to a fast aging. Phosphates have a discreet stability but they have lower standard potentials (around 3.4 V with graphite). Layered Metal oxides are the most popular materials used as positive electrodes because they have a good cycle stability as well as a high standard potential. Lithium ions can intercalate between the layers of metal oxide forming alloys. Although many types of metal layered oxide are in the market, the lithium-Nickel-Manganese-Cobalt-oxide (NMC) is one of the most popular. In fact, it represents an excellent trade-off between lifespan, cost, energy density and safety. Considering that the BESS model developed within the scope of the thesis is based on a NMC:C cell, the attention is focused on these materials.

The electrolyte has to be conductive for ions but insulating for electrons. For LIB the elctrolyte is usually composed of lithium salts such as lithium hexafluorophosphate ($LiPF_6$), lithium tetrafluoroborate ($LiPF_4$) and lithium perchlorate ($LiClO_4$) dissolved in an organic solvent like propylene carbonate (PC), ethylene carbonate (EC), diethyl carbonate (DEC) and dimethyl carbonate (DMC) [34]. Some other additives may be added to allow the formation of the SEI.

In addition to the electrodes and to the electrolyte, the cell is composed of other materials which do not take part in the chemical reactions such as the separator and the the current

collectors. The separator avoid the electron transfer between the electrodes which would result in a short circuit inside the cell.

3.1.2 Principles of Operation

All reaction in the cell are driven by a change of the Gibbs free energy ΔG^0 as show in Equation 3.1: n is the number of electrons involved in the reaction, F is the Faraday's constant and V_{OC} is the open circuit voltage. The Gibbs free energy tends to decrease to reach an equilibrium position during discharge. Instead, during charging, the energy is supplied by the DC current increasing the Gibbs free energy.

$$\Delta G^0 = -n \cdot F \cdot V_{OC} \tag{3.1}$$

V_{OC} is the the voltage difference at the terminals when no current is flowing. It depends on the materials which compose the electrodes and it can be calculated exploiting the galvaninc series as a difference between the oxidation potential of the anode and the reduction potential of the cathode as illustrated in Equation 3.2.

$$V_{OC} = E^0_{cathode} - E^0_{anode} \tag{3.2}$$

During discharging, lithium ions migrate from the anode to the cathode moved by the electrochemical potential. In this transfer each ion leaves an electron which flows in the external circuit from the positive electrode to the negative electrode releasing energy. Therefore, the negative electrode acts as an anode getting oxidized whereas the positive electrode, the anode,

is reduced. The complete reaction during discharging is shown in Equation 3.3: M represents the metals which compose the cathode (such as cobalt, nickel and manganese).

$$LiC_6 + Li_{1-x}MO_2 \rightarrow C_6 + LiMO_2 \tag{3.3}$$

During charging the process is inverted and it is powered by the energy supplied by the external circuit. The electrons migrate from the positive to the negative electrode moved by the external voltage. Therefore, the positive electrode is oxidized acting as an anode: lithium ions move from the solid phase to the electrolyte releasing electrons. Vice versa, the negative electrode acts as a cathode and it gets reduced: lithium ions intercalate inside the graphite absorbing the electrons. The overall reaction is shown in Equation 3.4.

$$C_6 + LiMO_2 \rightarrow LiC_6 + Li_{1-x}MO_2 \tag{3.4}$$

3.1.3 Aging Mechanisms

Each kind of lithium ion battery suffers an aging process which slowly decreases its performances during operation (cycle aging) and idle times (calendar aging). The most relevant aging effects on LIB are impedance rise and capacity fade which are caused by various factors. In this section all major aging mechanisms are analyzed according to the cell component involved: the solid electrolyte interface, the anode and the cathode.

3.1.3.1 Solid Electrolyte Interface

The Solid Electrolyte Interface (SEI) is a relevant component in a LIB because it protects the electrolyte from the reduction at the anode. In fact, electrolyte components tend to decompose at the surface of the graphite electrode during charging. A correct design of the electrolyte composition can prevent this mechanism by the formation of a stable SEI at the first charging which acts as an electronic insulator. Therefore, being also highly conductive for Lithium Ions, the SEI is a necessary component for the Lithium-Ion cell. However, a real SEI does not fully insulate the negative electrode causing the SEI to growth gradually even after the first charging process. The initial thickness of the SEI is usually 0.2 μ [37].

The first factor producing the growth of the SEI is the impurity of the anode surface as well as of the SEI itself. In fact, these impurities can lead to areas with an higher electrical conductivity causing electron migration. Equation 3.5 analytically describes this phenomena: it has to be highlighted how higher SOC (namely higher OCV) are expected to accelerate the growth rate of the SEI [38].

$$l_{SEI} = \sqrt{l_{SEI,initial}^2 + \frac{2 \cdot K \cdot OCV}{\rho} \cdot t} \tag{3.5}$$

Where l_{SEI} is the SEI thickness, K is a correlation coefficient and ρ is the resistivity of the SEI.

SEI growth is also caused by electron diffusion which regards especially homogeneous systems. In this case the governing variables are illustrated in Equation 3.6 [38].

$$l_{SEI} = \sqrt{l_{SEI,initial}^2 + 2 \cdot K \cdot D \cdot c_0 \cdot t} \tag{3.6}$$

Where K is a correlation coefficient, F is the Faraday's constant, D is the diffusion coefficient and c_0 is the concentration of electrons in the solid electrolyte interface near the external border.

Finally, an other mechanisms which induce SEI growth is the fact that during cycling some parts of the SEI are rebuilt. In fact, graphite volume varies (by about 10-20 %) as lithium is intercalated causing damage to the SEI layers.

Overall, an increase of the SEI thickness leads to a decrease in the cell capacity because an amount of active lithium is consumed by SEI building. Moreover, considering that the SEI has a lower conductivity in comparison with the electrolyte, SEI growth implies an increase of the ohmic resistance of the cell.

3.1.3.2 Anode

During cycling the anode which is composed of graphite can undergo a mechanical degradation. In fact during operation, as said before, the graphite volume varies causing mechanical stresses. Morevoer, intercaleted lithium ions can form large conglomerates with solvent molecules leading to exfoliation of graphene. In general, mechanical degradation implies an increase in cell impedance. Furthermore, it leads to a capacity decrease because some part of the damaged anode material could become unable to store lithium [37].

An other aging mechanism affecting the anode is Lithium Plating. It refers to the precipitation of metallic lithium around the anode during charging. This phenomena is mainly caused by high current rates, which accumulate lithium on the anode surface, and by low temperatures, which affect the intercalation. Overall, Lithium plating increases cell impedance and decreases cell capacity as precipitated lithium hinders the intercalation process. In extreme cases, lithium plating can cause short circuit through the formation of long dendrites.

3.1.3.3 Cathode

In comparison with the Anode, the cathode does not undergoes relevant aging processes. Some minor factors (such as corrosion, surface film formation and mechanical stresses) are observed and they can imply a slight impedance rise [39].

3.1.4 Definitions

In this section some definitions regarding lithium ion batteries are given.

Capacity

The capacity of the cell (C) is measured in Ah. It represents the total charge which can be delivered during a full discharge (namely from the upper and lower cut-off voltages which are given by the manufacturer). The value of the capacity depends on the material of the electrodes and on their size. Moreover, the capacity is affected by the temperature and the discharge rate. In particular, higher discharge rates tend to decrease the capacity. For this reason the capacity has to be measured at specific operating conditions. To build the cell model, the capacity is measured with the procedure described in paragraph 4.1.1.1 while the nominal capacity is specified by the manufacturer.

State Of Charge

The State Of Charge (SOC) is the variable which measures the remaining charge of a cell. It can be expressed with a dimensionless number (between 0 and 1) or with a percentage. Equation 3.7 shows how the state of charge can be computed: obviuoulsy the starting SOC ($SOC(t_0)$) must be known. Usually cells are cycled between intermediate SOC (i.e. $0.15 < SOC < 0.9$) to avoid excessive degradation due to aging.

$$SOC(t) = SOC(t_0) - \frac{1}{C} \cdot \int_{t_0}^{t} I(\tau) d\tau \tag{3.7}$$

Charge Troughput and Equivalent Full Cycle (EFC)

The Charge Troughput refers to the total charge released and accepted by the cell during operation. As shown in Equation 3.8, the charge troughput depends on the current flowing in the cell. From a chemical point of view, this value is directly proportional to the transfer of the active material (lithium ions) during a specific timestep. The Charge Troughput can be expressed in Ah or in EFC. The Equivalent Full Cycle (EFC) is equal to twice the nominal capacity of the cell.

$$Q(t) = \int_{t_0}^{t} |I(\tau)| \, d\tau \tag{3.8}$$

Depth Of Discharge

The Depth Of Discharge (DOD) measures the amplitude of each cycle. Its computation is shown in Equation 3.9. As it will be explained, the DOD is a variable which strongly affects cell aging.

$$DOD = \int_{t_0}^{t} \frac{|I(\tau)|}{2C} \cdot d\tau \tag{3.9}$$

Current Rate

The current rate I_C is employed to asses the charging and discharging rates. It is computed with Equation 3.10 and expressed in C which has a the dimension of h^{-1}. Its value should not be confused with the current I which is expressed in Ampere. As an example, a current rate equal to 1 C would charge or discharge the cell in one hour. Excessive current rates should be avoided to reduce the cycle aging of the cell.

$$I_C = \frac{I}{C_N} \tag{3.10}$$

Damage

Damage is a variable introduced to predict the life expectancy of a cell during operation. It is described in 4.3.1.2 and 4.3.1.1.1.

CHAPTER 4

BESS: MODEL

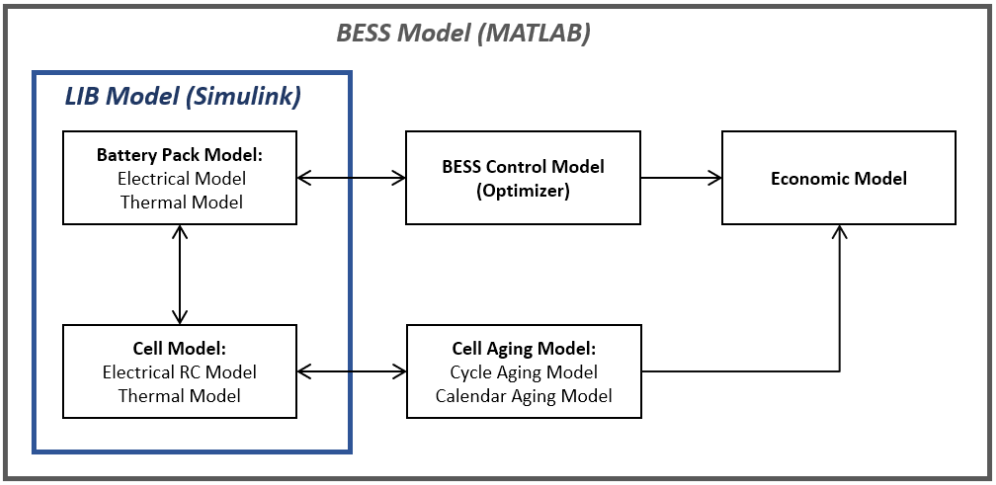

Figure 9: BESS model overview

In this chapter the Battery Energy Storage System (BESS) model is described. This model has been designed during this thesis research to simulate a lithium ion based ESS during operation and it can be employed in different applications. As shown in Figure 9, the *BESS model* is composed of different submodels which interact in the MATLAB environment. The *cell model* simulates the electrical and thermal behavior of single cells. Next, *the battery pack model* arranges different cells to form cell modules taking into account thermal and electrical

connections. The two aforementioned models are built on Simulink and they compose the *LIB model* (Lithium-Ion Battery) as shown in Figure 9. *The BESS control model* controls the LIB and it is based on an optimizer (on MATLAB) which operates according to the specific application. The control model is designed to perform a simulation of 1 year. Moreover, the aging effects are evaluated by the *cell aging model* (on MATLAB) which has a relevant impact in the simulation. Finally the *economic model* asses revenues and costs (mainly degradation costs) according to the application. The *BESS model* is designed to be flexible in order to simulate the battery energy storage system in different applications.

4.1 Cell Model

The cell of the battery can be modeled following various approaches available within literature. These models can be classified in three main families which feature different levels of complexity. The choice of approach depends on the research interest: from cell design to system simulation etc.

- Electrochemical Models: This kind of models are usually built to study the physics of the cell. Reactions, energy and momentum transports for each component are identified and modeled starting from fundamental physical concepts. Large sets of differential equations with an accurate spatial resolution are produced and they have to be solved. This approach is computationally demanding requiring numerous parameters but it gives precise and detailed results. Usually, electrochemical models are built in research and design to optimize the performance of the cell [40].

- Mathematical Models: Empirical equations, based on experimental results, are used to predict cell quantities (SOC, Capacity, efficiency etc.). For example, Peukert's law describes the capacity of rechargeable batteries at different discharge currents whereas Shepperd's equation predicts the cell voltage during quasi-stationary discharge. Few parameters are required and the computational effort is low. However, these models are abstract and they do not produce precise results [41].
- Electrical Models (Equivalent Circuit): Electrical models use a combination of lumped electrical components such as resistors, voltage sources and capacitors in order to predict the response of the battery. The parameters of these components are set starting from experimental results. Some correlations between the impedances and physio-chemical processes can be found. Moreover, a thermal model can be built in parallel in order to take into account temperature dependence and aging. The precision of the results of electrical models are a trade-off between Mathematical Models and Electrochemical Models: an accuracy around 1-5% is reached [42]. However, electrical models are not suitable for studying and improving the design of the cell.

Considering that the target of the thesis is to study a BESS implemented in a smart grid, the Electrical Model is the most appropriate approach because it is an effective trade-off between accuracy,computational effort and complexity. Moreover, starting from the electrical model it is possible to build a thermal model.

4.1.1 Cell Electrical Model: the RC circuit

The cells tested are commercial US18650V3 Lithium-Ion batteries produced by the Sony Energy Devices Corporation. They are standardized cylindrical NMC cells (18650) with a diameter of 18 mm and a height of 65 mm. The anode active material is graphite whereas the cathode one is Li(NiMnCo)O_2. It is a well performing high current cell, Table IV summarizes its technical specifications [43].

TABLE IV: TECHNICAL SPECIFICATIONS SONY US18650V3 AT 23 °C

Nominal Capacity	2.25 Ah (0.2 C discharge at nominal voltage)	Height	65 mm
Rated Capacity	2.15 Ah (0.2 C discharge)	Diameter	18 mm
Nominal Voltage	3.7 V	Weight	43.6 g
Cut-Off Voltage	2.5 V	Rated Energy	8.33 Wh
Upper Cut_Off Voltage	4.2 V	Specific Energy Density	191 Wh/kg

As explained in 4.1 an equivalent-circuit model is built in order to predict the behavior of this cell. A first order RC model requires few computational effort but it does not produce precise results. In particular, long time relaxation phenomena are not well predicted [44]. For this reason, a second order RC model, which is shown in Figure 10, is chosen. This model is composed by a voltage source V_{OC}, a series resisor R_0 and two RC branches. EIS Electrochemical Impedance Spectroscopy on NMC lithium cells confirms that this simplified model can be sufficiently reliable [45]. The resistances and the capacitances of this equivalent

circuit are discussed progressively and their estimation is explained in section 4.1.1.2. The capacity and the voltage source are discussed in 4.1.1.1.

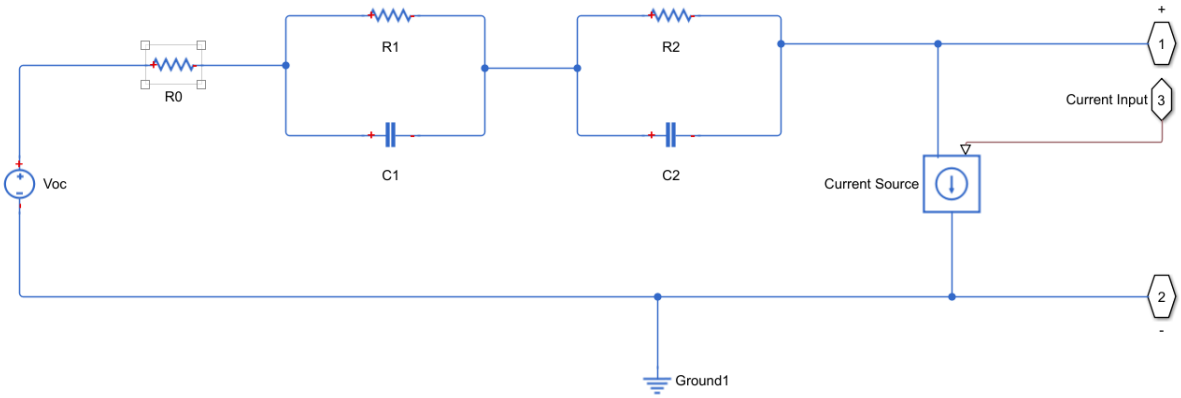

Figure 10: Second order equivalent RC model

The whole model is developed in Simulink thanks to the Simscape libraries. The model is designed so that each simple cell receives a current in input with a short time step (in the order of tenths of seconds) and returns some data as shown in Figure 11 (terminal voltage, terminal voltage, SOC, cell temperature, power dissipated for transport-diffusion phenomena and capacity). The input current depends on the control algorithm which is based on an optimizer. This section deals about the electrical model of the cell.

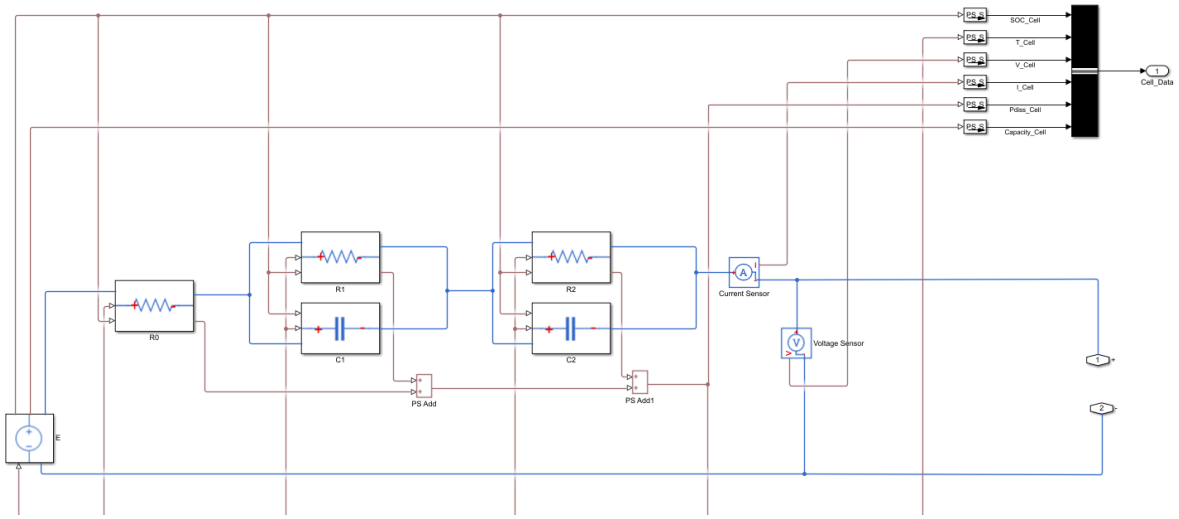

Figure 11: Cell electrical model

4.1.1.1 Source V_{OC}, SOC and Capacity C

The capacity of the cell is assessed thanks to a sequential discharging cycle at C=0.5 with 20 relaxation periods of 90 minutes. The discharge is performed until the lower Cut-Off voltage (see Table IV) is reached. The temperature of the cell is kept at 20 °C thanks to a climatic chamber. The procedure is repeated at 45 °C in order to have a correlation between capacity and temperature. Figure 12 and Figure 13 show how the relaxation periods are much longer than the discharging periods. In this way the cell can be considered at quasi-equilibrium conditions producing an accurate capacity estimation.

Finally, once reached the lower cut-off voltage, the total charge throughput is read and it represents the capacity. In particular, at T=20°C C=2.1599 Ah and at T=45 °C C=2.2342 Ah.

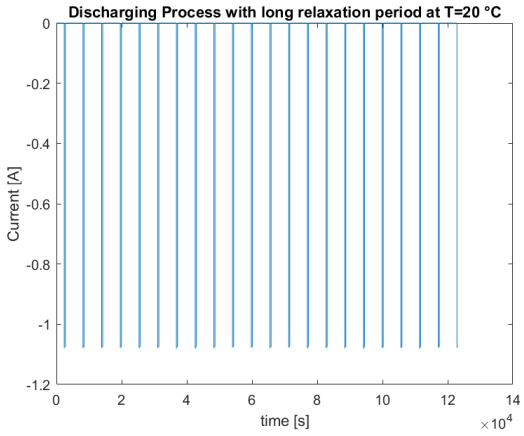

Figure 12: Discharging currents with long relaxation periods at T=20 °C

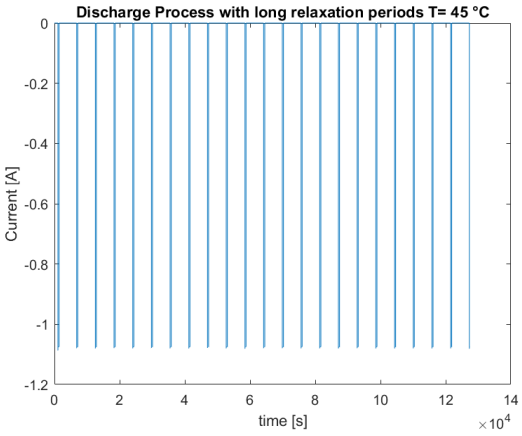

Figure 13: Discharging currents with long relaxation periods at T=45 °C

A linear interpolation is performed by the model in order to evaluate the capacities for other temperatures.

As far as the state of charge is concerned, this is calculated by the model at each time step k taking into account its starting value and the charge throughput as shown in Equation 4.1. As discussed previously, this capacity is temperature dependent.

$$SOC(k+1) = SOC(k) + \Delta t \cdot \frac{I(k)}{C(T)} \tag{4.1}$$

Obviously, the maximum value of the SOC is 1 meaning a fully charged cell whereas SOC=0 represents a fully discharged cell.

The voltage source of the RC equivalent circuit is represented by V_{OC} shown in Figure 10 which is the Open Circuit Voltage (OCV). Theoretically, if the cell stays at equilibrium condi-

tions, the electrochemical potential E of each electrode is determined by the Nernst equation (Equation 4.2) [46].

$$E = E^0 - \frac{RT}{nF} ln(\prod_{i}^{reactants} m_i^{s_i}) \tag{4.2}$$

Where E^0 is the standard potential, m_i is the activity of the specific reactant i with a stoichiometric concentration s_i. Overall, the standard potential of both electrodes depend on the concentrations of the reactants (SOC). However, phase transitions make the relationship between V_{OC} and SOC non linear and a deep knowledge on the reactants is required. For these reasons, deriving the V_{OC} curve with this kind of approach can be very difficult. Therefore, this curve is produced exploiting the experimental data obtained from the same cycles discussed previously and shown in Figure 12 and Figure 13. This kind of approach can be very accurate considering that long relaxation intervals allow the internal processes to decay sufficiently. Figure 14 and Figure 15 show the voltages measured continuously during these discharging cycles at different temperatures.

It can be seen how relaxation intervals let the OCV to recover. Therefore, the voltages (V_{OC}) are read after these long relaxation intervals (90 minutes) at different levels of the SOC. Approximately, 20 readings are made from SOC=1 and SOC=0. V_{OC} are derived at T=20 °C and at at T=45 °C. A linear interpolation is performed by the Matlab model between data points in order to obtain continuous functions in the SOC and temperature domains (Figure 16 and Figure 17). Table V resumes the results at specific SOC. An additional data point is

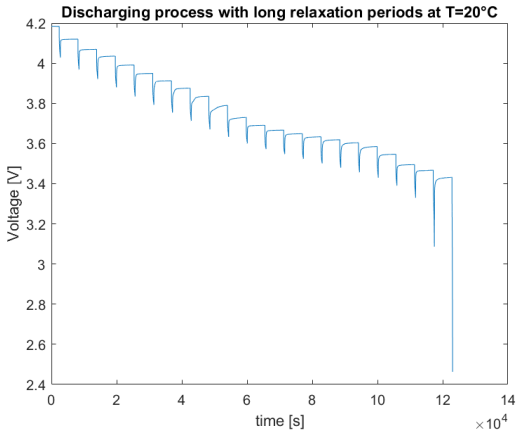

Figure 14: Discharging voltage curve with long relaxation periods at T=20 °C

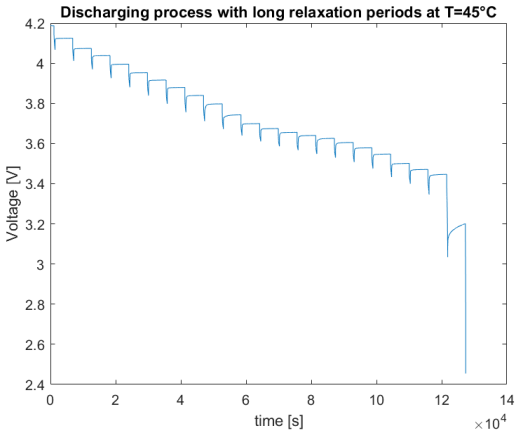

Figure 15: Discharging voltage curve with long relaxation periods at T=45 °C

inserted in the table at SOC=0.025 considering that in that region the OCV curve is very steep and the linear interpolation needs an extra data point to be accurate.

TABLE V: OPEN CIRCUIT VOLTAGE READINGS

SOC	0	0.025	0.1	0.2	0.3	0.4	0.5	0.6	0.7	0.8	0.9	1
OCV 20 °C	3.128	3.430	3.483	3.574	3.617	3.650	3.699	3.806	3.895	3.978	4.064	4.184
OCV 45 °C	2.799	3.254	3.468	3.552	3.613	3.649	3.695	3.800	3.890	3.975	4.065	4.187

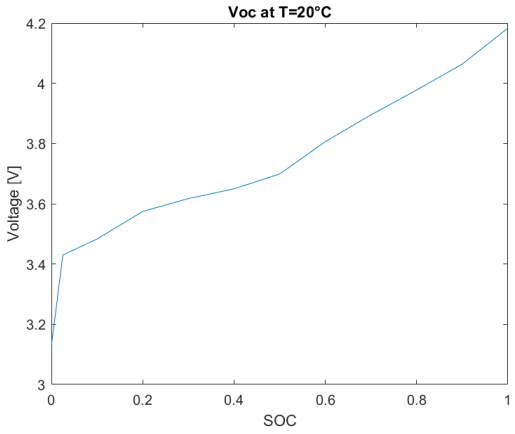

Figure 16: Open circuit voltage curve at T=20 °C

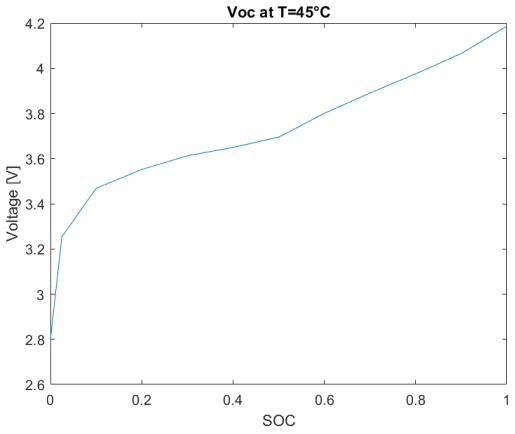

Figure 17: Open circuit voltage curve at T=45 °C

The pattern of the OCV curves (Figure 16 and Figure 17), which is rather steep and with slope changes approximately at SOC=0.55 and at SOC=0.18, is typical for a NMC lithium cell [47].

4.1.1.2 Parameter Estimation: Capacitances and Resistances

The electrical circuit of the RC model can be resolved using a system of equations with a time step index k. This procedure is necessary to compute the remaining parameters of this circuit: the Capacitances and the Resistances. The starting point is Equation 4.3 which is a voltage equilibrium: $V_{OC}(SOC, T)$ has been determined in paragraph 4.1.1.1, $V(k)$ is the terminal voltage which knwon and measured during the pulse cycles. $V_{R_0}(k)$, $V_{C_1}(k)$, $V_{C_2}(k)$ are the voltage drops due to the related capacitor or resistor. $I(k)$ is the circulating current which is known and imposed during pulse cycles as well as the temperature T. The SOC is

computed through Equation 4.1 and depend on the time integral of $I(k)$ and on the capacity of the cell already measured (4.1.1.1). Next, the Ohm's law determines Equation 4.4 and Kirchhoff's current law implies respectively Equation 4.5 and Equation 4.5. Finally, the charge law of the capacitor allows to obtain two differential equations which have been discretized in Equation 4.7 and Equation 4.7.

$$V(k) = V_{OC}(SOC, T) + V_{R_0}(k) + V_{C_1}(k) + V_{C_2}(k) \tag{4.3}$$

$$V_{R_0} = I(k) \cdot R_0(SOC, T) \tag{4.4}$$

$$I_{C_1}(k) = I(k) - \frac{V_{C_1}(k)}{R_1(SOC, T)} \tag{4.5}$$

$$V_{C_1}(k+1) = V_{C_1}(k) + \Delta t \cdot \frac{I_{C_1}(k)}{C_1(SOC, T)} \tag{4.6}$$

$$I_{C_2}(k) = I(k) - \frac{V_{C2}(k)}{R_2(SOC, T)} \tag{4.7}$$

$$V_{C_2}(k+1) = V_{C_2}(k) + \Delta t \cdot \frac{I_{C_2}(k)}{C_2(SOC, T)} \tag{4.8}$$

The whole system is resolved with the parameter estimator of Matlab. This tool iteratively guesses the unknown parameters $(R_0, R_1, R_2, C_1, C_2)$ trying to minimize the sum of squared differences between the measured terminal voltage and the simulated one. Since these parameters depend on the SOC, the estimation is performed using twenty pulse cycles (0.5 C) at different levels of the state of charge. Moreover, these parameters are also temperature dependent as well: therefore, the procedure is accomplished at T=20 °and T=45 °C. Figure 18 shows that the

difference between the simulated and the measured terminal voltage is minimal both for T=20 °C and T=45 °C: the estimation seems to be very reliable. Figure 19 and Figure 20 illustrate the cost functions: at T=45 °C the estimation is less accurate for low state of charges due to boundary effects.

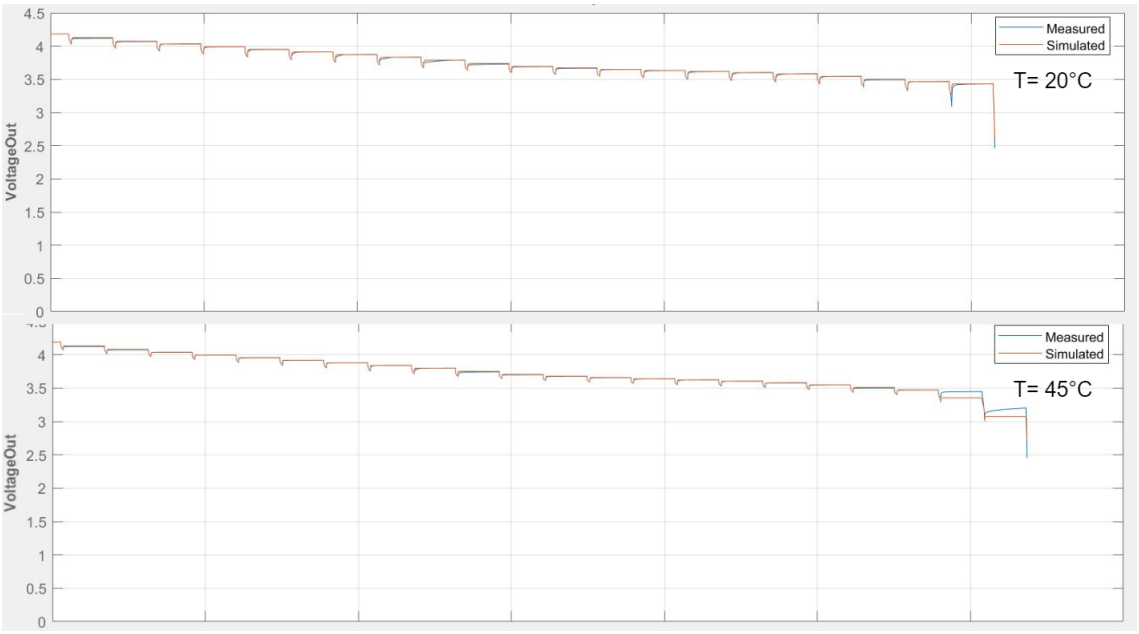

Figure 18: Measured and Simulated terminal voltage at T=20 °C and at T=45 °C

In the following paragraphs a brief analysis on the parameters extracted with this procedure is given. Table XI and Table XII, in the appendix, give all estimated RC parameters.

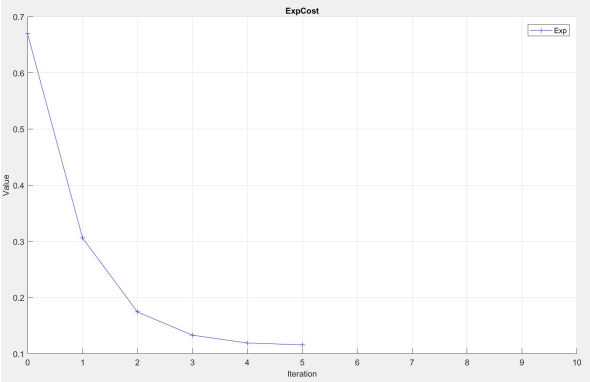

Figure 19: Estimation cost function at T=20°C

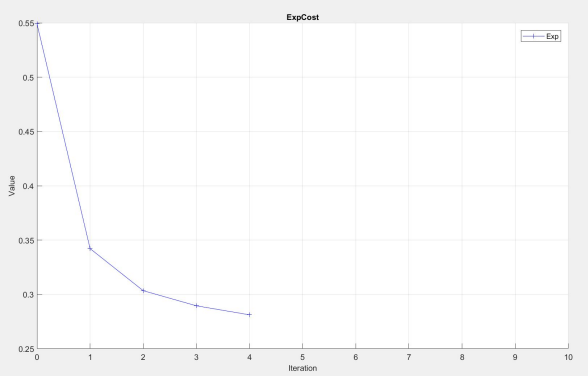

Figure 20: Estimation cost function at T=45°C

4.1.1.2.1 Resistance R_0

The values of the resistance R_0 are extracted thorough the procedure just explained in 4.1.1.2. This resistance represents all behaviors due to diffusion process having very low time constants (in the region between 0s and 1s). Physically, it depends on ionic resistances (electrolyte and separator) and electronic resistances (collectors and electrodes) [46]. Figure 21 shows how R_0 is approximately 0.045 ohm at T=20 °C. It slightly decreases (Figure 22) at higher temperatures T=45 °C.

4.1.1.2.2 High Frequency RC

The high frequency RC circuit represents all diffusion processes having a low time constant (on average of the order of seconds). The time constant of the high frequency RC circuit is calculated through Equation 4.9 and it measures the time the capacitor takes to charge at 63 % . The estimation procedure for R_1 and C_1 is described in section 4.1.1.2. As illustrated in Figure 23, R_1 on average is lower than R_0 and it lightly decreases as temperature increases.

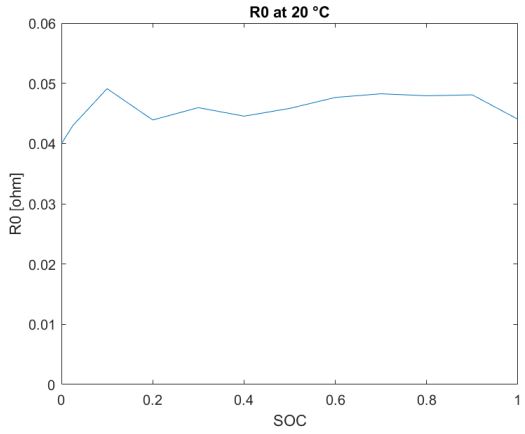

Figure 21: R_0 at different SOC, T=20 °C

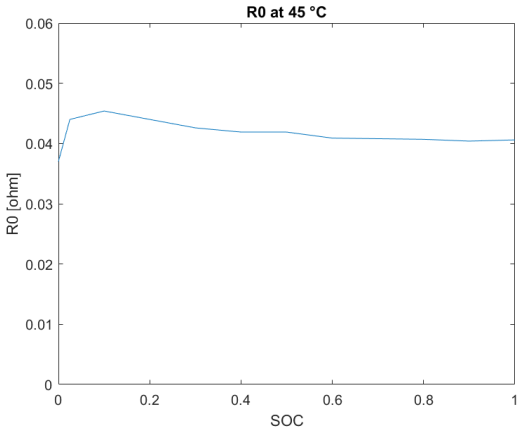

Figure 22: R_0 at different SOC, T=45 °C

Figure 24 shows the capacitances of the high frequency capacitor: higher capacitances are assessed for lower temperature. Regarding the time constants, it can be noticed from Figure 25 that the higher frequency RC circuit has on average τ_1=1 s at T=45 °C and τ_1=5 s at T=20 °C. This is due to the fact that diffusion processes are hindered by lower temperatures. At SOC=0 much higher R_1 and τ_1 are estimated due to boundary effects.

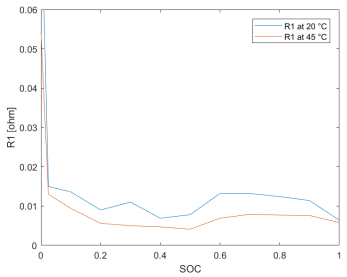

Figure 23: R_1 at different SOC

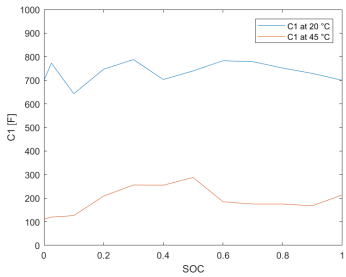

Figure 24: C_1 at different SOC

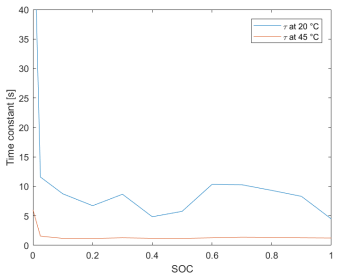

Figure 25: τ_1 at different SOC

$$\tau_1 = R_1 * C_1 \tag{4.9}$$

4.1.1.2.3 Low Frequency RC

The low frequency RC circuit represents all diffusion processes having an high time constant (in the order of tens of seconds). Analogous consideration can be made for the low frequency RC branch. In particular, the resistances and the capacitances are higher for lower temperatures resulting in a higher time constant. Once again, higher resistances, not shown in Figure 26, are assessed for a state of charge close to zero.

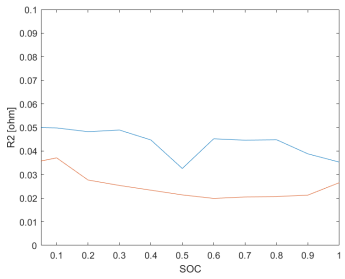

Figure 26: R_2 at different SOC

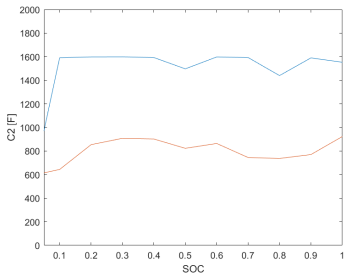

Figure 27: C_2 at different SOC

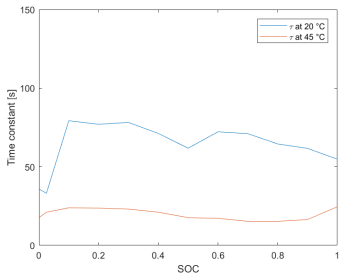

Figure 28: τ_2 at different SOC

4.1.2 Cell Thermal Model

Considering that many parameters of the RC model as well as aging depend on temperature a cell thermal model is built. Therefore, the main target of the thermal model is determining the temperatures of each cell continuously during the simulation.

First of all, the heat generation inside each cell (P_{gen} in Equation 4.10) is composed of two components.

$$P_{gen} = I^2 \cdot R_i(SOC, T) + I \cdot T \cdot \frac{\delta V_{OC}(SOC, T)}{\delta T} \tag{4.10}$$

The first term of Equation 4.10, known as polarization heat, is due to the Joule heating effect of the cell caused by ionic resistances (separator, electrolyte) and electronic resistances (electrodes, collectors). This phenomena is exothermic during both charging and discharging. The internal resistance R_i is the sum of all resistances of the RC circuit (R_0, R_1, R_2). Considering that the polarization heat is directly proportional to the square of the current, high current rates should be avoided to keep the temperature of the cell within suitable conditions.

The second term of Equation 4.10 is the entropic reversible heat and it is caused by the entropy change during the reactions. $\frac{\delta V_{OC}}{\delta T}$ is the entropic heat coefficient which can be calculated using the open circuit voltage curves determined in section 4.1.1.1 for T=20 °C and T=45 °C. In this way an entropic heat coefficient which depends on the SOC is obtained. In the case of the cell studied (Sony US18650V3) the entropic heat is always exothermic during discharging and endothermic during charing.

$$M \cdot C_p \cdot \frac{dT_{cell}}{dt} + HT = I^2 \cdot R_i(SOC, T) + I \cdot T \cdot \frac{\delta V_{OC}(SOC, T)}{\delta T} \tag{4.11}$$

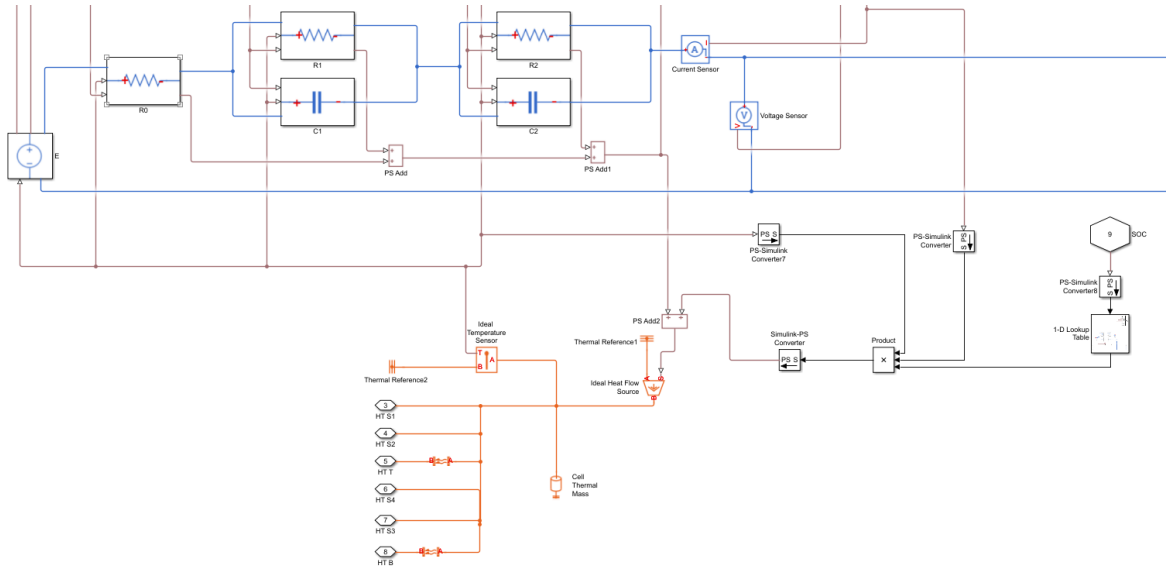

Figure 29: Cell thermal model simulink

Next, after having computed the heat generation of each cell, an heat balance is determined in Equation 4.11. The first left-hand side term is the change in internal energy where C_p is the specific heat capacity and M is the mass of the cell. The value of C_p for a Sony US18650V3 cell is $1.04kJ/Kg/K$ [48]. M is 44.6 g as shown in Table IV. The second left-hand side term is the Heat Transfer which is composed of various components: depending on the cell module layout, a single cell can exchange heat with other cells and/or with the external environment. A deeper

insight of this term is given in the section dealing with the battery module 4.2.1. Finally, the right hand-side of Equation 4.11 is the already discussed heat generation.

The entire thermal model of the cell is built using Simulink as showed in Figure 29. Ports 3,4,5,6,7,8 are the heat transfers which depend on the cell position in the battery module: it will be discussed later.

4.2 Battery Pack Model

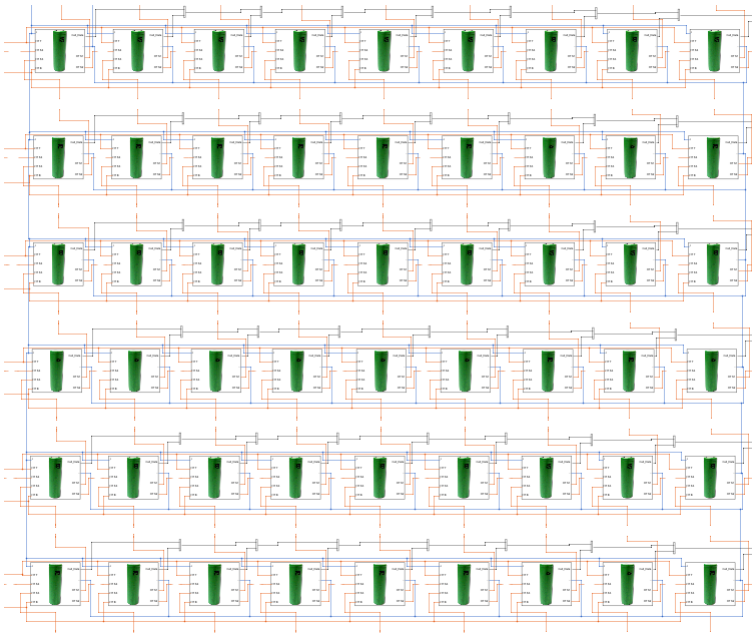

Figure 30: Cell module: thermal and electrical connections

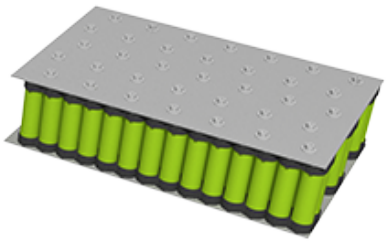

Figure 31: Cell module

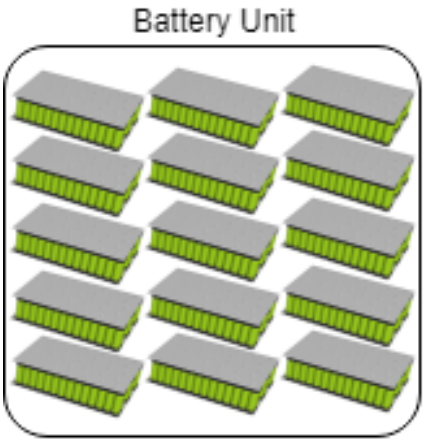

Figure 32: Battery unit

In this section it is described how cells, already modeled in Simulink in the previous sections, are connected in order to form an entire battery pack. The cells considered are Sony US18650V3 which have been already discussed in 4.1.1 and whose properties are summarized in Table IV.

First of all, 54 cells are placed side by side, as shown in Figure 31 in order to form a cell module. The resulting rectangle is formed by 6x9=54 cells. All cells in a module are connected in parallel so that the nominal capacity of a single module is around 116 Ah but the voltage remain the same as a single cell. Figure 30 shows the arrangement of cells in a module as well as the electrical and thermal connections which are modelled in Simulink. Next, 15 modules are connected in series to form a single battery unit having 55,6 V as nominal voltage and 116 Ah as nominal capacity. This battery unit has a nominal power around 6.5 kWh. These technical features are similar to state of the art battery units for ESS applications on the market [49]. Finally, several battery units are connected in order to form a battery pack. In particular,

ten units are arranged in series so that an output voltage close to 600 V is reached. This is a typical value for large scale ESS (in the region of MW): from 600 V the DC output is converted to AC and stepped up to the desired voltage which depends on the connection level [50]. In the common case of connection to the primary distribution network (Medium Voltage) the output AC voltage is 11 kV (UK). The number of battery packs arranged in parallel is a design variable which depends on the application. Battery packs are composed of several battery units to guarantee reliability. In fact, if a single battery pack contained directly all cell modules a single cell failure could imply failure of the whole pack. Instead, adopting the chosen arrangement, a failure of a unit in the battery pack can be detected easier enabling a fast solution [50].

This large number of cells and modules requires advanced electronic components which act as a Battery Management System (BMS). A BMS includes the Thermal Management System (TMS) and the Energy Management System (EMS) [51]. In general, these systems equalize the SOC and the temperatures of each single cell. In order to achieve this task passive or active balancing can be adopted. In passive balancing energy surpluses are dissipated with resistors, whereas in active balancing they are redistributed among cells. Obviously, the second approach is more efficient but passive balancing is simpler and cheaper. The description of these systems (BMS, TMS, EMS) is beyond the objective of the thesis.

4.2.1 Cell Module Thermal Model

The thermal model of single cells has already been discussed in subsection 4.1.2 where it is described how joule and reaction effects produce an internal heat generation. In this section

it is discussed how cells exchange heat with the external environment and with adjacent cells. The cell arrangement in a cell module, discussed in the previous section, has to be considered in order to take into account all heat exchanges. In fact, each cell, depending on its position in a module, exchange heat differently. The main assumption is that all cell modules in the battery units behave equally and exchange heat with the external environment through natural convection whose temperature is controlled. Cells are considered as cylinders whose dimension are listed in Table IV. All cells exchange heat through six surfaces: top, bottom and four equal lateral surfaces. A cell module, as described in the previous section, is composed of 54 cells arranged in parallel (side by side) to form a 9x6 rectangle. Corner cells are localized at the four corner of the battery module, border cells are on the perimeter of the battery module (excluding corner cells) and internal cells are placed in the internal area of the battery module. All cells exchange heat through the bottom and top surfaces with the external environment equally. Instead, lateral heat exchanges depend on the position of the specific cell. Internal cells exchange heat with the four adjacent cells through the four equivalent lateral surfaces as shown in Figure 33. Border cells exchange heat with the external environment through one lateral surface and with the three adjacent cells as illustrated in Figure 34. Corner cells exchange heat with the external environment through two lateral surfaces and with the two adjacent cells (Figure 35).

The values of the Heat Transfer Coefficients (HTC) are depicted in Table VI [52] [53]. The top heat transfer coefficient (h_t) mainly depend on the natural convection between the cell top surface (A_t) and the external environment. Similarly the bottom heat transfer coefficient (h_b)

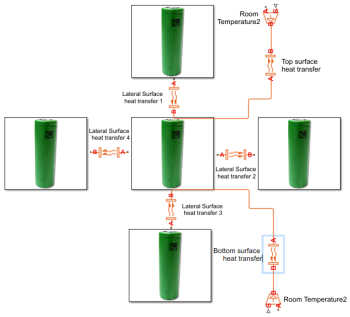

Figure 33: Heat transfer internal cell

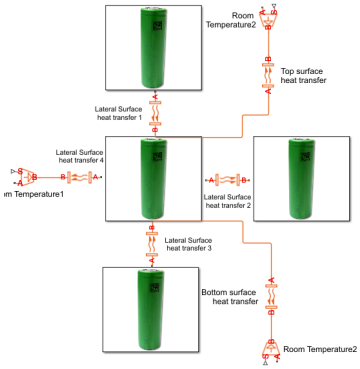

Figure 34: Heat transfer border cell

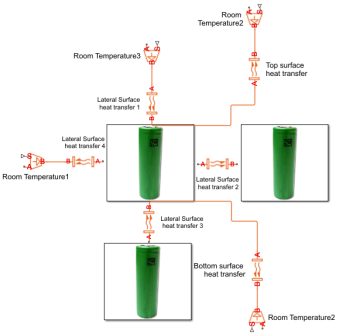

Figure 35: Heat transfer corner cell

regard the bottom surface (A_b): its value is slightly lower in comparison with the top HTC because the flux of heated air, which tend to rise, is hindered by the bottom surface of the cell module. The lateral-internal heat transfer coefficient (h_{li}) depends on the HT between lateral surfaces (A_l) of adjacent cells. Finally, the lateral-external HTC (h_{le}) represents the heat transfer between the cell lateral surfaces and the external environment and it regards only border or corner cells.

TABLE VI: HEAT TRANSFER COEFFICIENTS

	Top (cell-environment)	Bottom (cell-environment)	Lateral-Internal (cell-cell)	Lateral-External (cell-environment)
HTC $[W/K/m^2]$	9.9	8.8	6.0	11.6

Overall, Equation 4.11 describes the heat balance of each cell where HT is the total heat transfer which is determined thanks to Equation 4.12, Equation 4.13 and Equation 4.14 for internal, border and corner cell respectively.

$$HT = h_b \cdot A_b \cdot (T - T_{ext}) + h_t \cdot A_t \cdot (T - T_{ext}) + \sum_{c=1}^{4} h_{li} \cdot A_l \cdot (T - T_c) \tag{4.12}$$

$$HT = h_b \cdot A_b \cdot (T - T_{ext}) + h_t \cdot A_t \cdot (T - T_{ext}) + h_{le} \cdot A_l \cdot (T - T_{ext}) + \sum_{c=1}^{3} h_{li} \cdot A_l \cdot (T - T_c) \tag{4.13}$$

$$HT = h_b \cdot A_b \cdot (T - T_{ext}) + h_t \cdot A_t \cdot (T - T_{ext}) + h_{le} \cdot 2A_l \cdot (T - T_{ext}) + \sum_{c=1}^{2} h_{li} \cdot A_l \cdot (T - T_c) \tag{4.14}$$

Where T is the temperature of the cell taken into account and $T_{c=1,2,3,4}$ are the temperature of the adjacent cells.

The whole cell module is modeled in Simulink as shown in Figure 30 where both electrical and thermal connections are visible. This model receives in input a current controlled by the optimization algorithm which will be discussed later. The output is represented by the electrical response of the cell module where each cell behaves differently due to aging and thermal effects. Moreover, time series regarding several quantities (temperatures, SOC, voltages, RC parameters, powers dissipated etc) are recorded for each cell during the entire simulation. As far as temperatures are concerned an example result of the thermal model is visible in Figure 36 showing the cell temperatures evolution during a standard day of operation. Moreover, Figure 37 illustrates the temperature distribution in a cell module after discharging at 0.5 C.

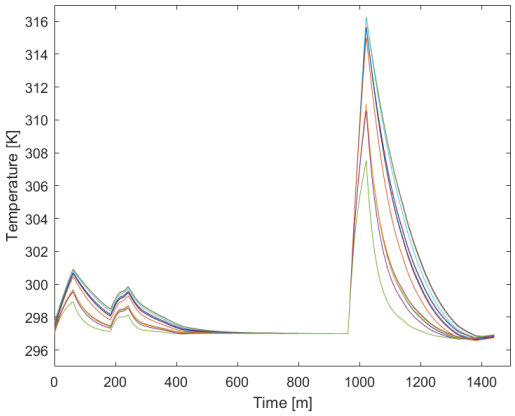

Figure 36: Cell temperatures during a standard day of operation

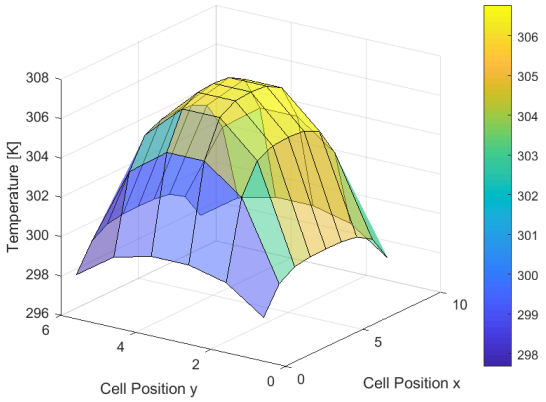

Figure 37: Cell temperatures distribution in a cell module

4.3 Cell Aging Model

Cell aging is an essential factor implemented in the model. In fact, employing a LIB ESS in a smart grid can be extremely expensive in terms of degradation costs. For this reason, in order to conduct a significant analysis cell aging is taken into account. Moreover, an effective optimizer, which control the BESS during operation, should take into account cell aging as well. The chemistry beyond cell aging mechanisms has already been discussed in section 3.1.3. Some mathematical models, which are directly derived from the physics of the phenomena, have been developed within literature. Although these models are very accurate, they require a challenging setting of numerous parameters and a high computational effort [54]. Therefore, a model based on experimental results, which is proposed by many authors, is built and implemented in the LIB model [55]. All aging tests were performed by other authors on Sony (US18650V3) cells

which have already been introduced in subsection 4.1.1. The raw data about the experimental results are provided by those authors and they are available within literature [55] [56] [57]. This data is exploited to build a cell aging model. The main variables affecting aging are the SOC, the temperature, the Depth Of Discharge (DOD) and the current rate. Unfortunately, the relationships between aging (in terms of capacity fade and impedance rise) and the aforementioned influencing variables are based mainly on experimental results and they are often nonlinear.

In the BESS model, starting from the time series data of some cell quantities (SOC, temperature, DOD, Current), aging is evaluated by the MATLAB code. More precisely, during the entire simulation, at the end of each day, capacity fade and impedance rise are determined for each cell differently. In fact, as explained is section 4.2, each cell in a cell module undergo different temperatures and currents according to its position in a cell module. Finally, the resistances and the capacities are updated daily for each cell.

Two kind of aging can be identified: cycle aging and calendar aging. Cycle aging affects cells during operation whereas calendar aging deteriorates all cells during operation as well as during idle times. Separating these causes of aging during the experiments is not trivial. In fact, cycle aged cells undergo calendar aging as well. Vice versa, calendar aged cells have to be electrically characterized during the tests regularly producing cycle aging. If the battery is utilized regularly, the influence of cycle aging can be an order of magnitude higher in comparison with calendar aging [55] [58].

4.3.1 Cycle Aging

Cycle aging as well as calendar aging causes capacity fade and impedance rise. The End Of Life (EOL) of the cell is always accompanied by a sharp capacity fade primarily. For this reason, capacity is the main variable needed to asses the remaining life of the cell. In general, cycle aging exhibits distinctive stages with specific capacity fade rates as shown in Figure 38. Initially, the capacity decays at a high rate but for a limited amount of time (first stage). This behavior is due to the initial formation of the SEI. Next, during the majority of the battery life, the capacity fades linearly at a limited rate (second stage). This decay is attributable to the SEI continuous repairs and to the degradation of the graphite condition. Finally, usually around 80 % of remaining capacity, the cell undergoes a sharp and nonlinear capacity fade (third stage). This is caused by the occurrence of lithium plating. When a cell enters this nonlinear stage it is no longer usable and it reaches the end of life. It is common to describe the capacity fade of the first two stages with a linear function. The following paragraphs describe how cycle aging effects (the end of life, the capacity fade and the impedance rise) are taken into account in the LIB model. The main variables influencing cycle aging are the DOD, the current rate I and the temperature T. Finally, in section 4.3.1.2 the procedure to evaluate cycle aging effects for cells cycled at variable operating condition is described.

4.3.1.1 Cycle Aging effects: End Of Life, Capacity Fade and Impedance rise

4.3.1.1.1 End Of Life (Damage)

Commonly, the End Of Life (EOL) is defined as the point where the capacity reaches 80 % of its initial value. However, an alternative and more accurate approach consists in assuming

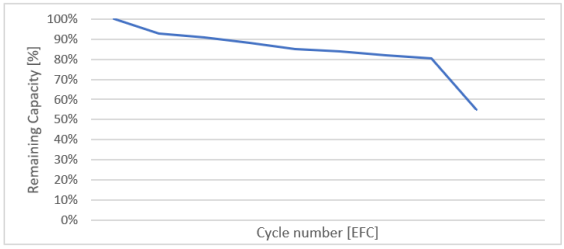

Figure 38: Stages during cycle aging

the point where the third stage begins as the end of life of the cell (see 4.3.1). More precisely, the beginning of the third stage is assumed as the point where the local slope of the capacity decrease becomes the double of the overall one (Equation 4.15). In fact, reached that point, the capacity will completely decay in few tens of EFC making the cell unusable. This approach is more accurate considering that the third stage may begin before or after 80 % of remaining capacity depending on the operating conditions. This phenomena is visible in Figure 41 and Figure 42. The results of the experiments are listed in Equation 4.15 where the cell lifetime is expressed in terms of Equivalent Full Cycles (which is directly related to the charge throughput Q)[55]. In these cases, the cells are cycled at fixed operating conditions (DOD, I, T) during the whole lifetime. Figure 39 shows how higher temperature tends to increase the lifespan of the cell. This is mainly due to the fact that lithium planting occurs earlier at lower temperature. However, keeping the cells at high temperatures strongly increases the calendar aging as it will be explained. Figure 40 illustrates how, generally, higher current rates reduce cell lifetime. As far as the DOD is concerned, lower lifespans are observed in cells cycled at intermediate DOD. In section 4.3.1.2 the procedure to evaluate cycle aging effects for cells cycled at variable

operating condition is described: the quantity named Damage will be introduced to evaluate the remaining life to the EOL. However, to be more conservative, both damage and capacity should be evaluated to asses the remaining life of the cell: these two approaches usually lead to similar results.

$$\left|\frac{C(k)-C(k-1)}{Q(k)-Q(k-1)}\right| \geq 2 \cdot \left|\frac{\Delta C_{tot}}{Q_{tot}}\right| \tag{4.15}$$

TABLE VII: EQUIVALENT FULL CYCLES TO THE END OF CELL LIFE

T [°C]	20	20	20	20	20	20	20	20	20	45	45	45	45
I [C]	1	1	1	1	1	2	2	2	2	1	1	2	2
DOD [%]	25	50	75	90	100	25	50	75	100	50	100	50	100
EOL [EFC]	1151	435	238	291	719	683	245	226	406	839	873	811	929

4.3.1.1.2 Capacity Fade

As shown in Figure 38, the capacity fade during the first and the second stage (that is the cell lifespan) can be predicted by a linear function. Once again, this function depends on the operating conditions (DOD, current rate I and temperature T). Taking into account the considerations made in the previous paragraph, the capacity fade is computed separately from the end of life. However, obviously there is a strict connection between end of life and capacity fade. For this reason, physics considerations have been made in the previous paragraph. Fig-

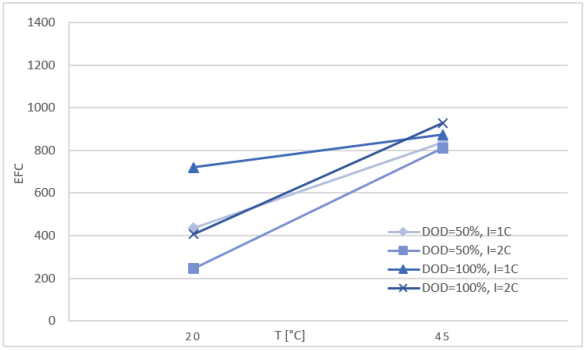

Figure 39: EOL temperature dependence

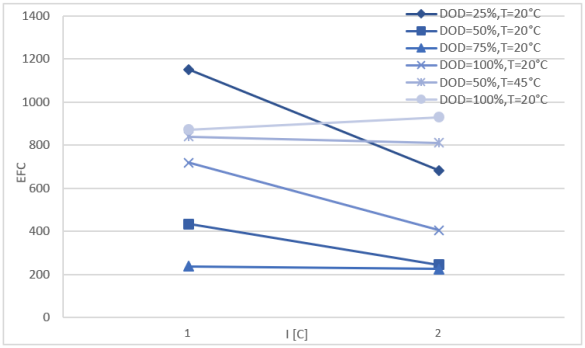

Figure 40: EOL current dependence

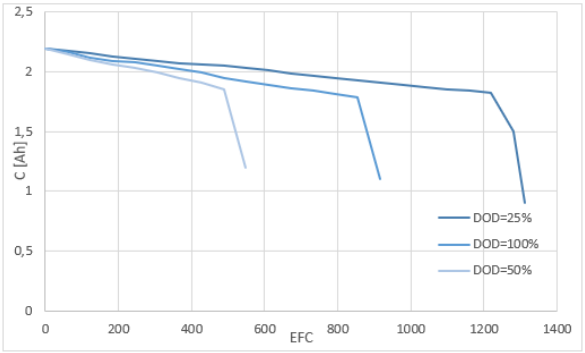

Figure 41: Capacity fade at T=20 °C, I=1C

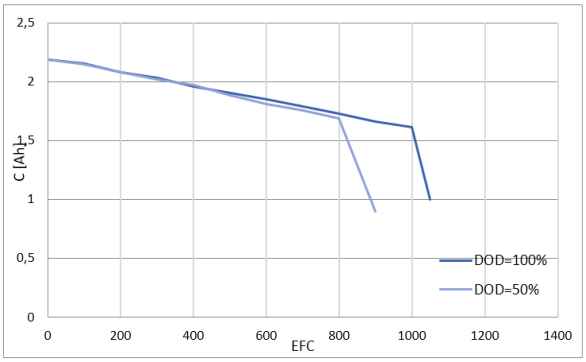

Figure 42: Capacity fade at T=45 °C, I=1C

ure 41 and Figure 42 show the capacity fade for some cycles. It can be noticed how the first two stages can be modeled by a linear function for each operating condition. Equation 4.16 is the linear equation which allow to predict the capacity fade according to certain input variables (DOD,T,I). The parameter α is set with a linear regression technique exploiting the experimental data. Table VIII illustrates the values of α for each operating condition [55]. During

the BESS simulation, as it will be explained later, the capacity of each cell is computed and updated daily.

$$C(t) = C_0 - \alpha(DOD, T, I) \cdot EFC(t) \tag{4.16}$$

TABLE VIII: CAPACITY FADE α COEFFICIENTS

T [°C]	20	20	20	20	20	20	20	20	20	45	45	45	45
I [C]	1	1	1	1	1	2	2	2	2	1	1	2	2
DOD [%]	25	50	75	90	100	25	50	75	100	50	100	50	100
Alfa E-04 [Ah/EFC]	2.61	5.58	6.36	7.54	4.57	3.49	8.47	13.4	6.71	5.98	5.75	6.09	6.41

4.3.1.1.3 Impedance Rise

In general, during cycle aging, the values of the resistances of the RC model tend to increase. From a theoretical point of view, the growth of the SEI and the deterioration of the electrodes (especially the anode) cause the resistances to increase: a deeper description of this phenomena is given in section 3.1.3. Once again, this behavior can be simulated with linear functions whose parameters β are fitted thanks to the experimental data. Considering that the RC model is composed of three resistors, three equation (Equation 4.17, Equation 4.18 and Equation 4.19 are built to predict the impedance rises of the RC model. Moreover, the resistances of each resistor strongly depend on the SOC. Therefore, each SOC_i requires a specific β. All these

parameters β are listed in the appendix in Figure 132, Figure 133 and Figure 134 [55]. During the BESS simulation, all resistances changes are computed and updated daily.

$$R_0^{SOC_i}(t) = R_0^{SOC_i}(t_0) - \beta_0^{SOC_i}(DOD, T, I) \cdot EFC(t) \tag{4.17}$$

$$R_1^{SOC_i}(t) = R_1^{SOC_i}(t_0) - \beta_1^{SOC_i}(DOD, T, I) \cdot EFC(t) \tag{4.18}$$

$$R_2^{SOC_i}(t) = R_2^{SOC_i}(t_0) - \beta_2^{SOC_i}(DOD, T, I) \cdot EFC(t) \tag{4.19}$$

4.3.1.2 Cycle Aging Model: rainflow counting algorithm and Miner rule

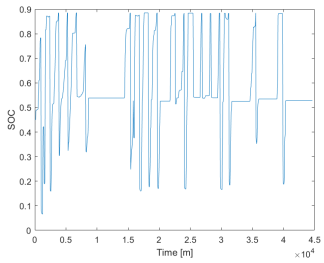

Figure 43: SOC variations in standard operating condition

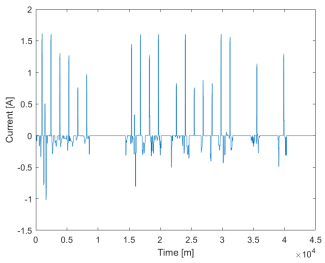

Figure 44: Current variations in standard operating condition

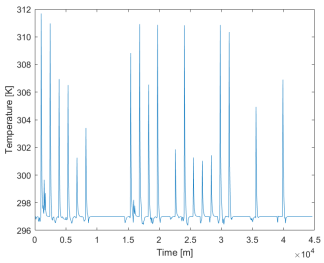

Figure 45: Temperature variations in standard operating condition

All linear models discussed in the previous paragraphs are based on the assumption that the cell is cycled at fixed DOD, Current I and temperature T. Unfortunately, during real operation each cell of the BESS undergoes variable cycles. Figure 43, Figure 44 and Figure 45 show how

the main variables influencing cycle aging vary during a month of standard operation. For this reason the rainflow counting algorithm (or bathtube method) is implemented in the aging model [59] [60]. This method allows to count cycles for each level of DOD. In this manner, after having associated temperatures T and current rates I, each cycle is related to determined operating condition (DOD, T, I). Next, the equations discussed in the previous paragraphs are employed in order to determine aging effects for each single operating cycle.

In particular, as far as capacity fade is concerned, Equation 4.20 allows to compute the capacity fade caused by each cycle k. Subsequently, these contributions are summed with Equation 4.21 to compute the total capacity fade. EFC_k is a measure of the charge throughput for each cycle k. Figure 48 and Figure 49 show capacity fade contributions and cumulative capacity fade in a month of standard operating condition. Although they undergo different temperatures, there are not great differences between internal and external cells in the module. This is due to the fact that there is a compensation effect: cells will higher remaining capacity suffer more charge throughput during cycling and thus they will age more rapidly. This is an advantageous consequence of having connected the cells in parallel.

The same procedure is adopted to assess the impedance rises of the resistors. Equation 4.22 is employed to asses partial impedance rises for each cycle k at each SOC i. Next, all these rises are summed in Equation 4.23. This procedure is repeated for the three resistor of the RC circuit because they have different β values as explained in the previous paragraph. Figure 50, Figure 51 and Figure 52 show the resistance cumulative increase in a month of standard operating condition: all values are referred to SOC=50 %.

$$\Delta C_k = \alpha_k(DOD_k, T_k, I_k) \cdot EFC_k \tag{4.20}$$

$$C(t) = C_0 - \sum_{k=1}^{k_t} \Delta C_k \tag{4.21}$$

$$\Delta R_k^{SOC_i} = \beta_k^{SOC_i}(DOD_k, T_k, I_k) \cdot EFC_k \tag{4.22}$$

$$R(t)^{SOC_i} = R_0^{SOC_i} + \sum_{k=1}^{k(t)} \Delta R_k^{SOC_i} \tag{4.23}$$

$$d_k = \frac{EFC_k}{EOL_k(DOD_k, I_k, T_k)} \tag{4.24}$$

$$D = \sum_{k=1}^{k(t)} d_k \tag{4.25}$$

The end of life is computed exploiting the Palmgren-Miner rule. This method allows to asses damage caused by a cyclic variant loading. With Equation 4.24 partial damages due to each cycle k, distinguished by known operating condition, are calculated. EOL_k is a measure of the charge throughput to the end of life for the specific cycle k. Next, all contributions are summed with Equation 4.25 to obtain the total cumulative damage D. The condition of end of life is reached when D equals 1. Usually, as expected, at the end of life the capacity is about 80% of the initial value. Despite being generally employed in materials science for the

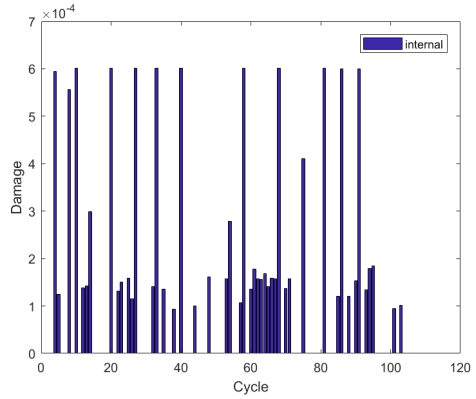

Figure 46: Damage contributions in a month of standard operating conditions

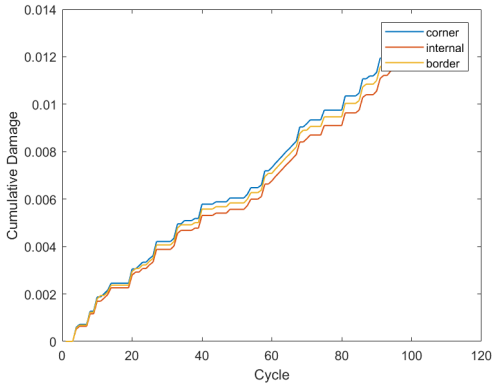

Figure 47: Cumulative damage in a month of standard operating conditions

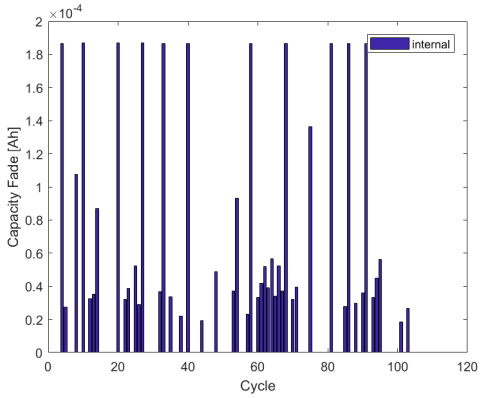

Figure 48: Capacity fade contributions in a month of standard operating conditions

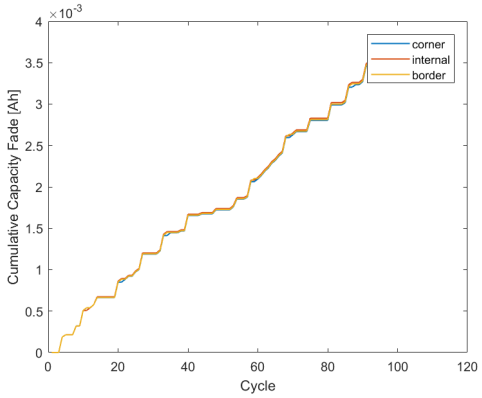

Figure 49: Cumulative capacity fade in a month of standard operating conditions

fatigue prediction, the Palmgren-Miner method is adopted in damage estimation for lithium ion batteries as well [61] [62] [63]. Figure 46 and Figure 47 show damage contributions and cumulative damage in a month of standard operating condition. As expected internal cells suffer less damage considering that lithium plating occurs at lower temperatures. However, as far as calendar aging is concerned, high temperatures strongly increase aging.

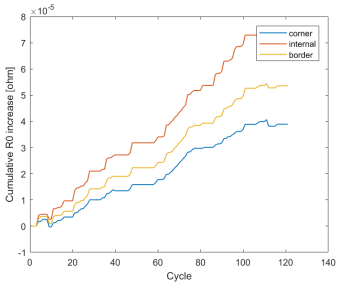

Figure 50: Cumulative resistance R0 increase in a month of standard operating conditions

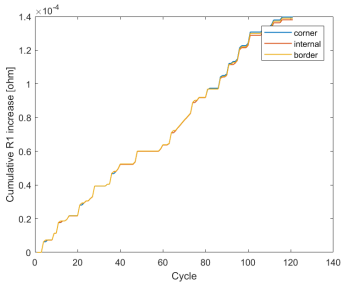

Figure 51: Cumulative resistance R1 increase in a month of standard operating conditions

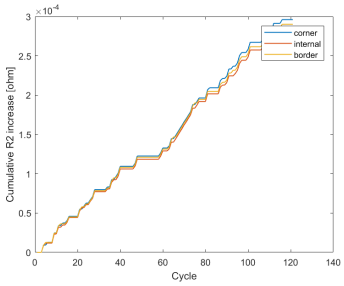

Figure 52: Cumulative resistance R2 increase in a month of standard operating conditions

In the BESS model the computation of all these quantities is performed daily for each cell separately. Moreover, the cell parameters affected by aging (capacity fade, impedance rise) are updated continuously in order to take into account the decay of the cell performance during the simulation. Finally, cumulative damageg are analyzed to asses the sustainability of the BESS in each specific application.

4.3.2 Calendar Aging

Similarly to cycle aging, calendar aging causes capacity fade and impedance rise. From a chemical point of view, SEI growth implies the reduction of active lithium, and thus, capacity fade. Equation 3.5 and Equation 3.6 describe the SEI growth. As it can be noticed from the equations and from Figure 53, higher SOC and higher temperatures increase the growth of the solid electrolyte interface enhancing calendar aging effects. For this reason, during operations, excessive temperatures should be avoided. As a secondary effect, the SEI growth

causes an increase of the cell impedance. However, this contribution is negligible compared to the impedance rise due to cycle aging. For this reason the BESS model does not include the computation of the impedance rise caused by calendar aging.

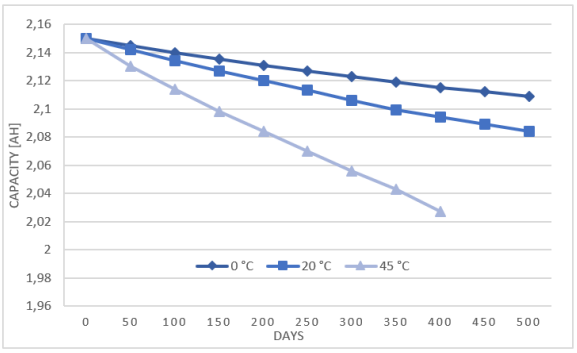

Figure 53: Calendar aging capacity fade: experimental results

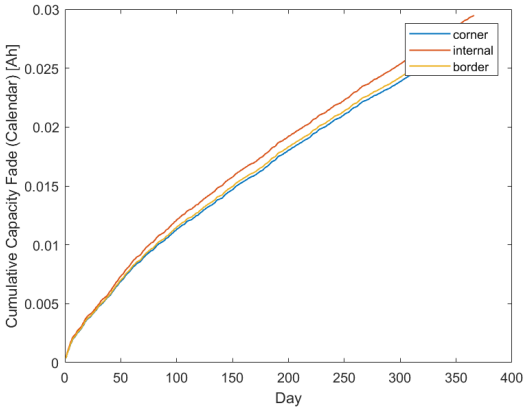

Figure 54: Calendar aging capacity fade: model results

Many equations can predict the capacity fade caused by calendar aging. From the fitting of experimental tests Equation 4.26 resulted to be the most accurate with a mean fit accuracy of 1.34. The two coefficients p_1 and p_2 depends on the state of charge and on the temperature according to Table IX. Considering that, during operation, the cell is cycled, the values of the SOC and of the temperatures are averaged. Figure 53 shows the capacity fade due to

calendar aging simulated by the BESS model. As expected, internal cells subjected to higher temperatures, undergo a higher calendar capacity fade.

$$\Delta C_{cal} = C_0 \cdot (1 - p_1(SOC, T) \cdot t^{p_2(SOC,T)}) \tag{4.26}$$

TABLE IX: CALENDAR AGING: CAPACITY FADE COEFFICIENTS

T °C	20	20	20	20	20	20	45	45
SOC [%]	10	25	50	75	80	100	50	100
p1	3.53e-06	6.28e-05	1.71e-04	5.01e-04	7.3e-04	2.18e-04	6.8e-04	2.05e-04
p2	1.62	1.02	0.854	0.656	0.683	0.862	0.782	1.05

4.4 Control Algorithm: the Optimizer

The lithium battery model, which is built mainly on Simulink, is controlled by an optimization algorithm written on Matlab. The optimizer is based on a nonlinear solver (fmincon) which tries to minimize a cost function. In parallel, the LIB model continuously receives in input the current which is the decision variable determined by the optimizer. More precisely, the variable determined by the optimizer is the battery power which is then converted in current thanks to the known terminal voltage (Table V). The setting of the optimizer depends on the BESS specific application. As a matter of example it is described how the optimizer operates in case

of a BESS acting in energy arbitrage (see paragraph 2.1). The control algorithms of the other applications differ only in the cost function.

In case of Energy Arbitrage (EA) the optimizer tries to minimize the cost function showed in Equation 4.27. $Pess_i$ is the decision variable and it is the output power at each time step i. $Pess_i$ is assumed positive during charging and negative during discharging. Pr_i is the energy price in the day ahead auction market on an hourly base. The time step adopted Δt is half an hour and the optimization is run daily at midnight. A shorter time step would be useless considering that energy price varies hourly and it would considerably increase the computational effort. With this cost function f_{EA} it is clear that the optimizer tries to maximize profit exploiting price volatility. Therefore, the battery is discharged when energy prices are higher and charged when prices are lower as shown in Figure 55 and Figure 56. However, the battery controlled in this way would take advantage of every price variation, even the smaller ones causing an excessive and useless aging. For this reason, depending on the application, a further factor AF (Equation 4.28) is implemented in the cost function to take into account aging during the decision making process. The Aging Factor (AF) is equal to the total power throughput multiplied by an aging factor coefficient which is the degradation cost per power throughput [€/kWh]. Obviously this is a very rough estimate; real aging is computed after the optimization process during the simulation. Moreover, the value of the aging factor coefficient is chosen very low to avoid battery underuse.

During the optimization some constraints have to be satisfied and they are considered by the optimizer. Firstly, the SOC has be contained between 0 and 1 even if a range between

0.2 and 0.9 is optimal to avoid excessive aging. An additional constraint is needed so that the battery starts the day always at the final SOC of the previous day. This constraint also takes into account the SOC deficit produced by the power dissipated. Moreover, $Pess_i$ has to be limited to avoid excessive discharge and charge current rates (usually 1.5 C for discharging and 1 C for charging). Finally, additional constraints are added depending on the application.

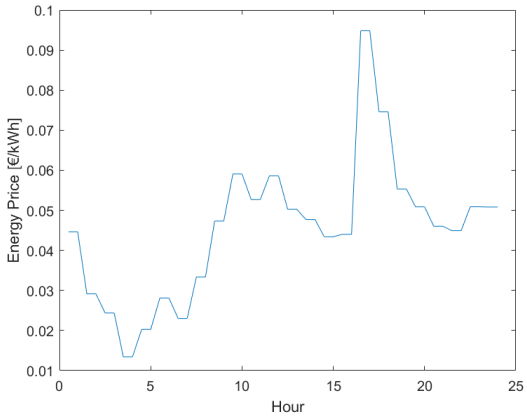

Figure 55: Energy prices on a standard day 01/01/2016

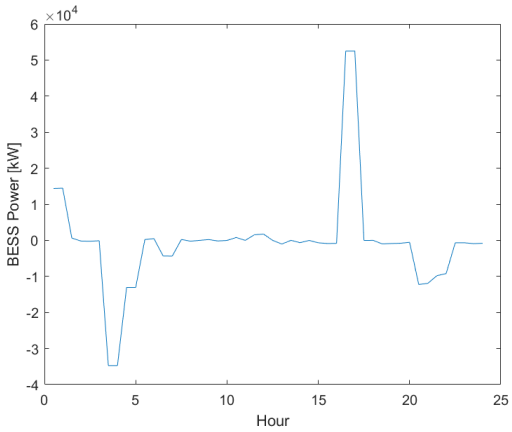

Figure 56: BESS power on a standard day of energy arbitrage

$$f_{EA} = -\sum_{i=1}^{48} \Delta t \cdot Pess_i \cdot Pr_i + AF_i \tag{4.27}$$

$$AF_i = \sum_{i=1}^{48} \Delta t \cdot (k_{AF} \cdot Pess_i) \tag{4.28}$$

The decision making process is performed by the optimizer daily. The results are given in input at the LIB simulink model which simulate the battery real behavior.

4.5 Economic Model

Different applications can have specific revenue sources. For this reason, the economic model will be discussed separately for each application. In general, it is difficult to evaluate accurately the value proposition for energy storage systems. In fact, in some cases benefits can be qualitative or spread among different stakeholders.

As far as degradation (aging) costs are concerned, these are computed multiplying the cumulated damage of the energy storage system by its price.

CHAPTER 5

BESS: APPLICATIONS

In this chapter the battery energy storage system is studied in various applications. A detailed description of the BESS model is given in chapter 4 whereas chapter 2 resumes common ESS applications. In particular three applications, listed in Table X, are analyzed. In all cases a simulation of one year (2016) is performed running the developed BESS model. The operating conditions of the ESS are checked and discussed throughout the simulation. Although a great amount of data is produced, the attention is mainly focused on battery aging and on the economic performance of the energy storage system during the whole year.

TABLE X: ANALYZED LIB ESS APPLICATIONS

Application	**RES-BESS**	**Island Grid**	**Energy Arbitrage**
Target (Cost Function)	Maximize Earnings	Minimize Energy Bought	Maximize Earnings
System Composition	BESS+RES	BESS+RES+LOAD	BESS
Connection Level	Transmission Upper Distribution	Distribution	Transmission Upper Distribution
Stakeholder	RES Feeders	Electric Utility	Enterprise
Revenue Source	Energy Market DSO/ISO regulations	Energy Market Grid Investments Savings Regulating Services	Energy Market
Secondary Revenue Source	STOR market (Operating Reserve)		FFR market (Frequency Regulation)

As illustrated in Table X, in some cases, the BESS is implemented in a system composed of RES and residential loads as well. For this reason, before going into any detail regarding the single applications, the RES and load models are discussed.

5.1 RES and Electrical Load: Models

Considering that the attention of the entire research is focused on the battery energy storage system, the RES and the electrical Load models are only superficially discussed. All data regarding RES output and power demand is referred to the East Midlands (UK) in 2016.

5.1.1 RES

As shown in Table X, the renewable energy sources are included in the system in two cases. The RES considered are Wind and PhotoVoltaic (PV) which are the most suitable to be implemented in a smart grid. In fact, the intermittent and unpredictable behavior of these sources makes the battery energy storage system very useful. Moreover, these distributed generators are advanced and their prices are competitive and steadily decreasing.

5.1.1.1 Wind Power Output

The wind power eletrical output is computed starting from real data. The Centre for Environmental Data Analysis (CEDA) provides historical wind measurements for different locations [64]. Considering that the load profiles are referred to the East Midlands (UK), the chosen measurement station is located in Coningsby. This anemometer gauges wind speed, wind direction and wind gusts on an hourly basis. Next, a wind turbine is selected in order to convert the wind data in electrical power output employing the wind power curves. To choose a proper wind turbine an analysis on the average wind speed in the east midlands is performed. Figure 57

shows the wind speed distribution during the whole year whose average was 5.6 m/s. The wind turbine DW54 of class IIIA, which is suitable for lower wind (on average 7.5 m/s), is selected. The DW54 produced by EWT is a modern IIIA wind turbine designed for the distributed energy generation [65]. It has a nominal power of 500kW and an operating wind range between 3 m/s and 25 m/s. Figure 58 shows the power curve of this wind turbine which is used to convert the historical wind speed in power output. The power output distribution per single DW54 turbine in 2016 is showed in Figure 59. It has to be highlighted that, being the rotor at 50 meters high from the ground, an altitude correction factor (k_{alt}) is integrated in the conversion as shown in Equation 5.1.

$$P_{wind_i} = k_{alt} \cdot N_{turbines} \cdot f(v_{wind_i}) \tag{5.1}$$

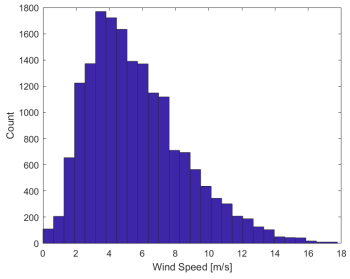

Figure 57: Wind speed distribution in 2016

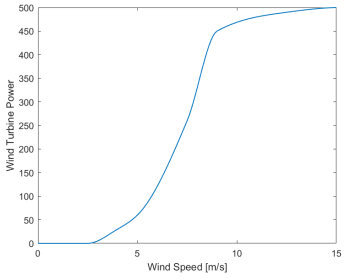

Figure 58: Power curve of the wind turbine DW54

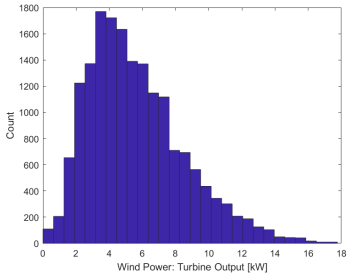

Figure 59: Turbine power output distribution in 2016

At this point, the power output on an hourly basis per wind turbine in 2016 is known. The number of turbines remains a design variable and it will be discussed case by case according to the BESS application.

5.1.1.2 Solar Power Output

Similarly to wind power, the solar power output in 2016 is computed starting from real data. In this case the Copernicus Atmosphere Monitoring Service (CAMS) provides timeseries of various irradiations on an hourly basis [66]. The physical quantities needed to obtain an electrical power output per square meter are the Beam Normal Irradiation (BNI) and the Diffuse Horizontal Irradiation (DHI). In fact, these radiations can be converted in electrical power by photovoltaic solar panels. The power output P_{solar} at each time step i is computed with Equation 5.2. The DHI, contrary to the BNI, is not totally gathered by the solar panel which is oriented towards the sun. Therefore, η_{dhi} represents the amount of diffuse radiation which is collected by the tilted solar panels and it is assumed about 0.75 [67]. Next, η_{solar} is the conversion efficiency of the solar panel: it measures the amount of collected radiation which is converted in electrical power. The result of Equation 5.2 is a timeseries of solar power electrical output per square meter on an hourly basis in 2016. Also in this case, the PV surface (N_{panels}) remains a design variable and it will be discussed in the single BESS applications case by case. Figure 60 and Figure 61 illustrate the DHI and the BNI distributions measured in the East Midlands (UK) in 2016 (null radiations are filtered). Figure 62 shows the solar power output distribution per square meter.

$$P_{solar_i} = N_{panels} \cdot \eta_{solar} \cdot (BNI_i + \eta_{dhi} DHI_i) \tag{5.2}$$

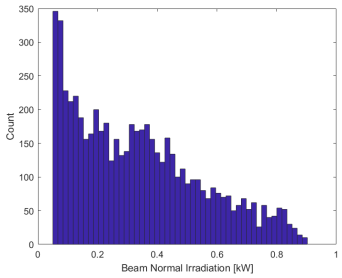

Figure 60: BNI distribution in 2016

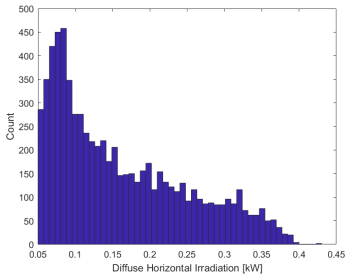

Figure 61: DHI distribution in 2016

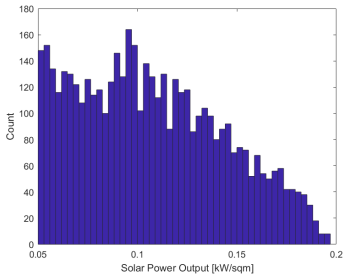

Figure 62: Solar power output distribution in 2016

5.1.2 Electrical Load Model

The electrical power demand is computed with a stochastic algorithm. The model is based on the computation of the single appliances employed within the domestic environment [68]. Next, the single domestic units are summed with a montecarlo algorithm to produce the electrical demand profiles of 10.000 houses with a peak of 10 MW for each day [69] . All data produced in this way is referred to the district of Rushey Mead and Belgrave in Leicester (UK) in 2016. In particular, the electrical demand profiles are known with a time step of 1 minute. The electrical load model was not developed within this thesis research: a detailed description can be found in

literature [69] [68]. Figure 63 and Figure 64 show typical electrical demand profiles in different seasons.

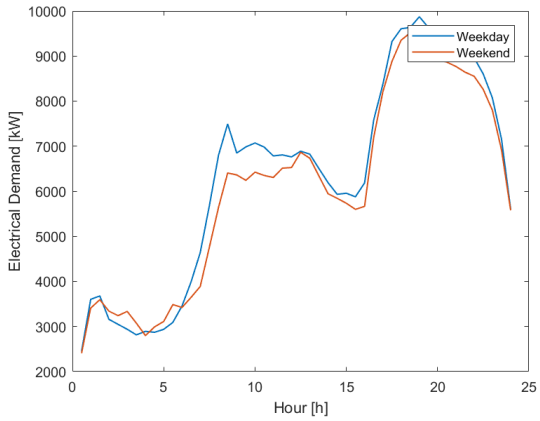

Figure 63: Electrical load standard profiles in January

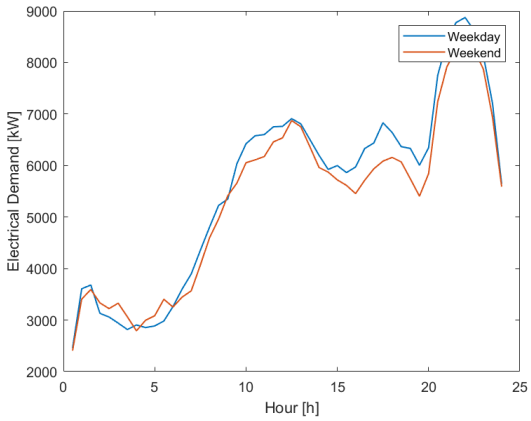

Figure 64: Electrical load standard profiles in July

5.2 RES-BESS

In this application the BESS is integrated in a system which includes renewable energy sources. Implementing an ESS guarantees an additional degree of freedom to the system which allows to control the sale of the electrical energy produced by wind turbines and photovoltaic panels. Therefore, energy can be sold when prices are higher maximizing profits which is the primary revenue source of an ESS operating in this application.

Moreover, an additional revenue source which can be considered in the RES-BESS application is operating in the reserve market as a Short Term Operating Reserve (STOR) provider.

Finally, considering that RES output is weather-dependent, the storage system can help the provider to supply the committed generation level with an acceptable ramping rate. In this way, RES feeders can comply with the regulations of the system operator avoiding possible sanctions.

Figure 65 shows how the BESS is integrated in the system. The energy produced by the RES can be supplied directly to the external grid or stocked in the storage system. In this specific application the energy flux is mono-directional meaning that energy can only be supplied to the external grid: the energy storage is charged with RES output. The electrical energy is sold through the day ahead energy market and the STOR market.

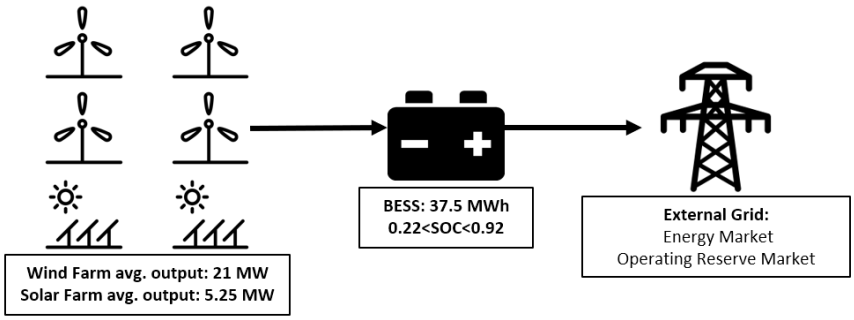

Figure 65: RES-BESS overview

5.2.1 Design and Sizing Procedure

In this application , the main target of the BESS consists in maximizing profits by controlling the sale of energy through the energy market. Sizing the BESS as well as the RES is crucial to achieve this task properly. The main design variable to be set is the proportion between RES average output and BESS nominal capacity. The nominal capacity of the battery is decided according to the regulations of the national grid in UK. In fact, there are not strict regulations regarding the energy market (sale of energy: first target) but a provider willing to enter the short term operating reserve market must supply 3 MW for a minimum of 2 hours (as discussed in paragraph 2.2.3). To comply with this regulation, the minimum remaining energy during operation has to be always higher than 6 MWh. Thus, the BESS nominal capacity is fixed at 37.5 MWh so that it can always provide that amount of energy considering that, during standard operation in the energy market, the SOC is always kept above 0.22. At this point, knowing the BESS capacity, the RES are sized in terms of number of wind turbines and surface of PV in order to maximize the ESS performance. To achieve that, some simulations lasting one year (2016) are performed changing the RES penetration while the BESS nominal capacity is fixed at 37.5 MWh. During these simulations the wind power output is kept 4 times higher than the solar one. The RES penetration is expressed as the ratio between RES average power output and BESS nominal capacity. Figure 66 shows that a RES penetration about 70 % (26.25 MW) seems to be optimal to maximize the BESS yearly revenue which is computed with the procedure described in paragraph 5.2.2.3. On the one hand, higher RES penetrations would not be fully exploited by the BESS which has a fixed capacity. On the other hand, lower

RES penetrations would not employ the operating capacity of the storage system. Figure 67 demonstrates the same idea with the average power (both discharging and charging) of the ESS which is an index of its utilization.

At this point solar and wind power penetrations are studied separately in order to asses which RES maximize the BESS performance the most. The overall RES average output has already been fixed at 26.25 MW. Figure 68 shows the yearly revenue for different solar penetrations (the remaining penetration is represented Wind). To make an example a penetration of 40 % of solar would imply 60 % of wind. The result of this analysis is that a solar/wind ratio of 1/4 seems to be optimal. As expected, the energy storage system is more effective with wind power production. In fact, solar power is always produced during daytime when energy prices are generally higher. On the contrary, wind turbines produce also at night when prices are very low: ESS can store that energy. Moreover, considering that the whole analysis is referred to the East Midlands in UK, it would be unrealistic to design a system with a high solar output.

It has to be mentioned that all these preliminary design simulations are performed employing only the optimizer. Running real simulations (with the simulink LIB model) during this design phase would have been excessively computationally demanding. The complete model, whose results are described in the following paragraphs, is run with the design parameters just determined.

Figure 70 gives an overview on the topology of the system [70] [71]. All electrical power coming from the RES is converted in controlled voltage DC in order to control all power fluxes. Sold energy, after being converted in alternate current, is stepped up with a transformer to

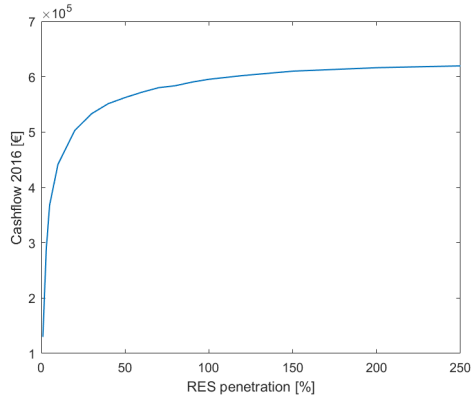

Figure 66: ESS yearly revenue for different RES penetrations (RES-BESS)

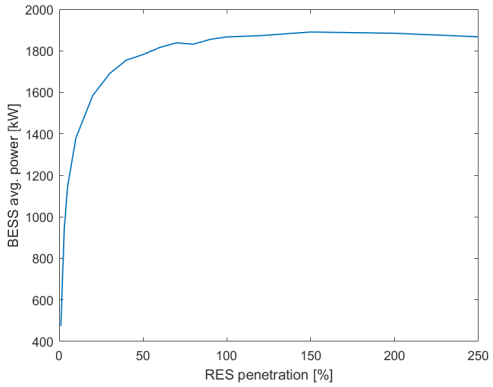

Figure 67: ESS average power for different RES penetrations (RES-BESS)

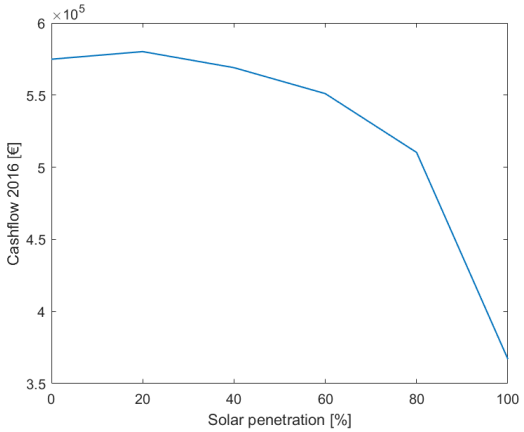

Figure 68: ESS yearly revenue for different solar penetrations (RES-BESS)

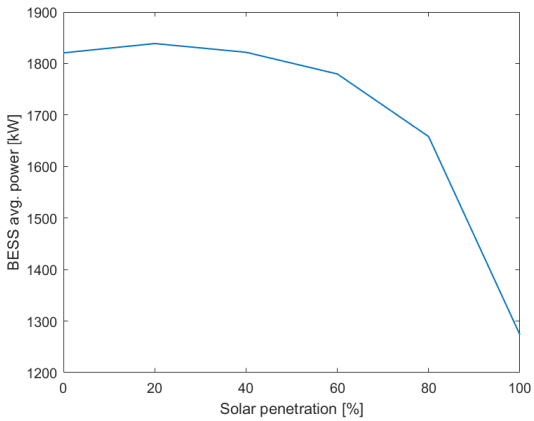

Figure 69: ESS average power for different solar penetrations (RES-BESS)

the desired voltage. A similar topology, which can be adopted in this application, is composed by a common AC bus instead of the DC one [72]. Topologies are not analyzed in detail but the efficiencies of the different converters are taken into account by the BESS model during the simulation. Considering the great amount of exchanged electrical power, the BESS is connected

to the high voltage transmission lines (400 kV or 275 kV in UK) or to the upper distribution line (132 kV in UK). In UK these power lines are directly owned by the national grid making possible to operate in the operating reserve market as well.

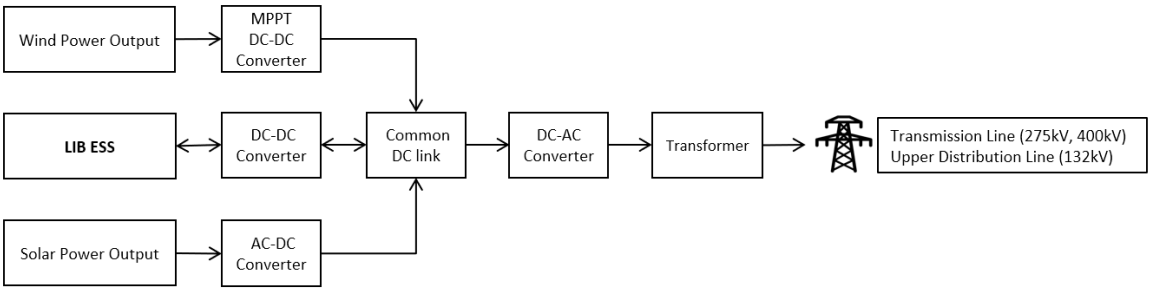

Figure 70: RES-BESS topology

5.2.2 Simulation Results

After the design procedure, a simulation lasting one year (2016) is performed employing the BESS model (with the LIB model as well) initialized with the input defined in the design process.

5.2.2.1 System analysis

The cost function of the optimizer in the RES-BESS application is the same employed in energy arbitrage (Equation 4.27). However, in this case, the BESS can be charged only with the energy produced by the RES: no energy demand is envisaged. Figure 71 illustrates the number of hours for each state of the battery throughout the whole year. As expected,

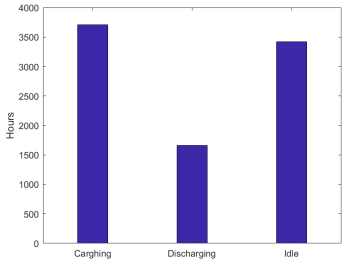

Figure 71: Charging, Discharging and Idle (RES-BESS)

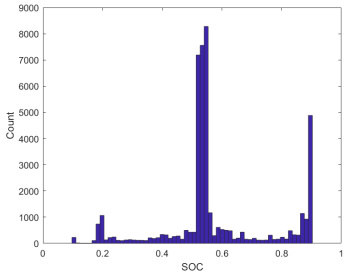

Figure 72: SOC distribution (RES-BESS)

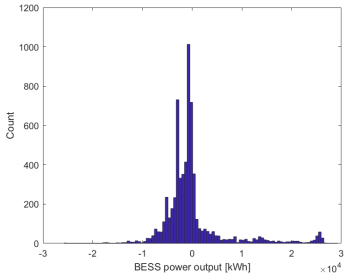

Figure 73: BESS power distribution (RES-BESS)

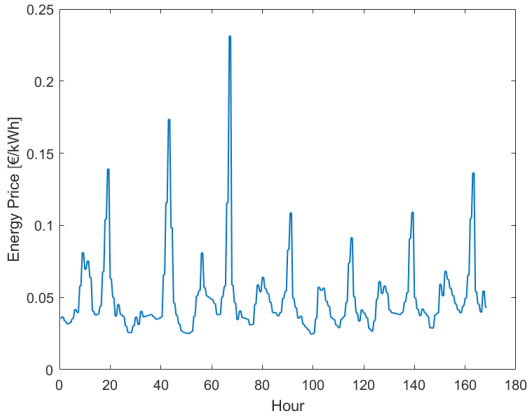

Figure 74: SOC profile during the first week of October 2016 (RES-BESS)

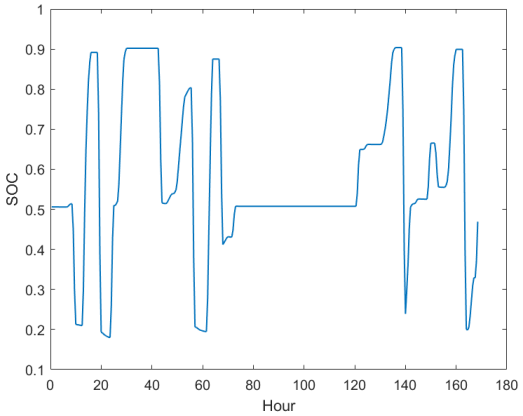

Figure 75: Energy prices during the first week of October 2016 (RES-BESS)

charging take longer than discharging because it depends on the RES output which can be very limited sometimes. Moreover, the charging rate is limited to avoid excessive aging. The battery stays idle when the volatility of energy prices is limited or the RES output is low. Overall, the BESS results to have an utilization factor about 60 %. Figure 72 shows the SOC distribution throughout the year. Intermediate state of charges are very recurrent considering that the starting SOC for each day is set at 50 % in order to maximize the flexibility of the system.

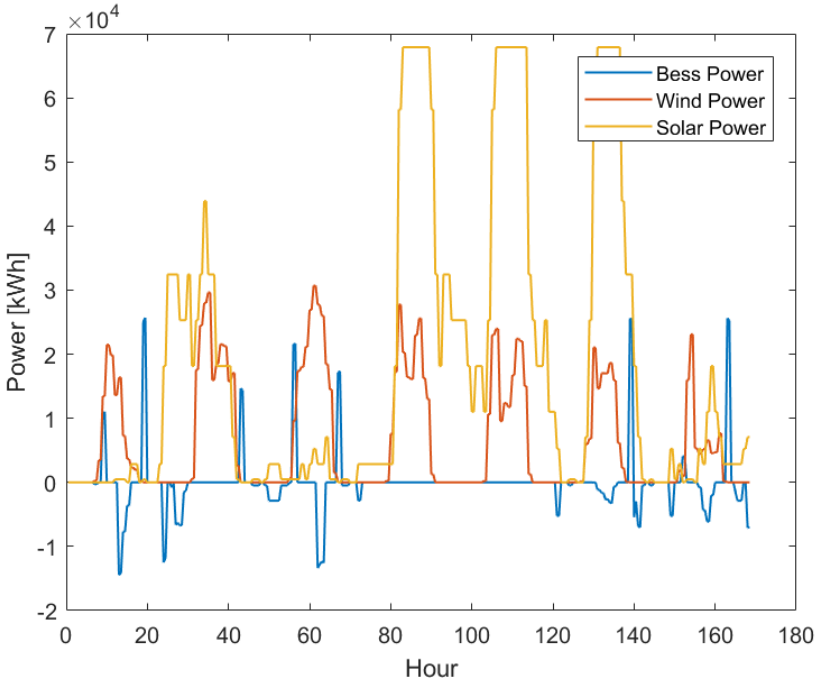

Figure 76: System power outputs during the first week of October 2016 (RES-BESS)

Edge SOC are also considerably recurrent because they are constraints. In fact, the battery SOC is kept between 0.92 and 0.22 to avoid excessive DOD and to be ready to dispatch in the short term operating reserve which is the secondary revenue source of the system. Figure 73 shows the distribution of the BESS power during 2016. The skewness of this curve is due to the fact that the system tends to sell energy very rapidly to exploit the peaks of the energy price. Figure 74, Figure 76 and Figure 75 illustrates how the system operate in a standard week (the first week of October 2016). As it can be noticed a BESS operating in this way is exploiting price volatility but it does not fully control the RES output.

5.2.2.2 Aging analysis

As described in the chapter dealing with the model, aging is evaluated daily during the simulation. It has to be reminded that the optimizer is set to avoid excessive aging through Equation 4.27. In particular, low differences in energy prices are not exploited by the system. Otherwise the BESS would be always in operation undergoing an excessive aging. As a first step the maximum temperatures reached by each cell in the cell module during the whole simulation are checked and showed in Figure 77. These values results to be within the operating range recommended by the manufacturer which is 60 °C [73]. Also the maximum current rates and SOC are checked: they stay within the set set. Figure 78 and Figure 80 show the damage for each cell during and after the simulation. As expected border and corner cells undergo a higher damage because they are cycled at lower temperatures accelerating lithium plating. On the other hand, as shown in Figure 79 the final capacity fade is more equally distributed between cells. This is due to the fact that, as visible in Figure 81, internal cells suffer a more severe calendar aging because of the higher temperatures. To predict the expected life of the battery both damage and capacity fade are checked. The total capacity fade at the end of the year is about 3 % of the initial nominal capacity. Therefore, theoretically, the BESS can be cycled at these conditions for about 6 years before reaching 20 % of capacity fade which is the maximum allowable. Similarly, at these operating conditions, the cell would reach a damage equal to one after about 7 years. As expected the results are very similar: taking the most pessimistic scenario (capacity fade) the life estimation is 6 years. Further details about the difference between capacity fade and damage are given in 4.3.

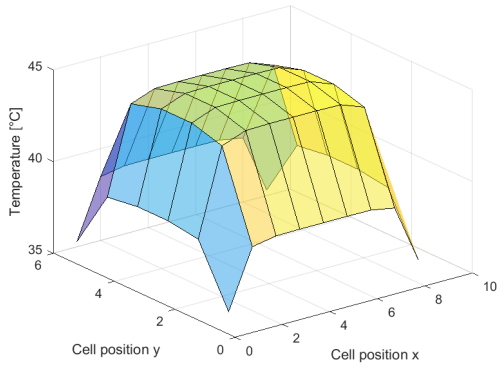

Figure 77: Max temperature reached by each cell during the simulation (RES-BESS)

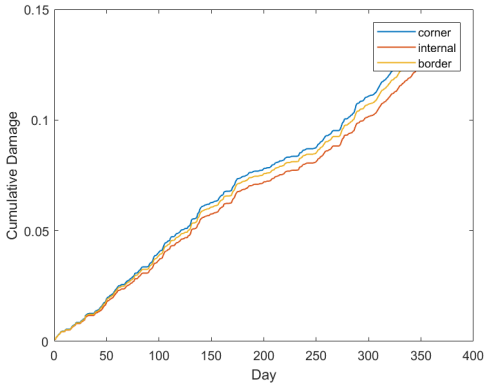

Figure 78: Cumulative damage (RES-BESS)

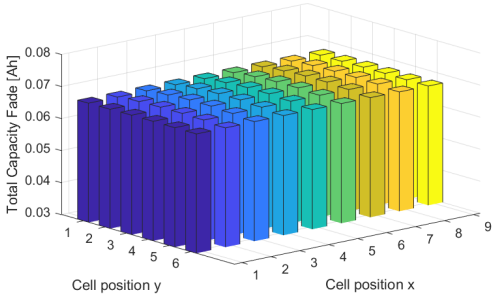

Figure 79: Final capacity fade reached by each cell (RES-BESS)

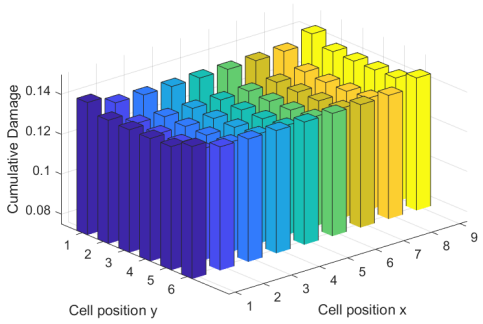

Figure 80: Final damage fade reached by each cell (RES-BESS)

As far as the resistances are concerned, Figure 83 and Figure 84 illustrate how R2 results to undergo a higher increase compared to R1 and R0. There are not great differences between different cells: internal cells suffer a slightly higher resistance increase for R0 but a minor one for R1 and R2. All cell resistances are updated daily throughout the whole simulation

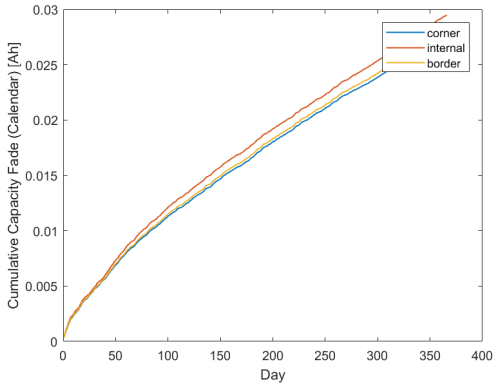

Figure 81: Cumulative capacity fade (calendar) (RES-BESS)

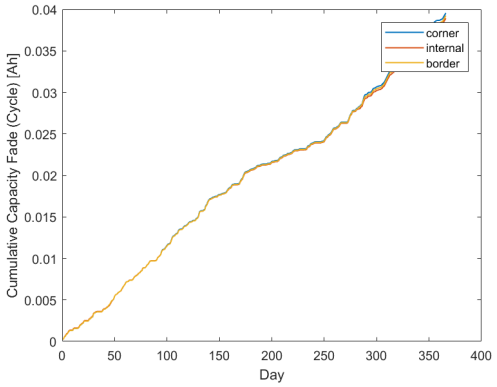

Figure 82: Cumulative capacity fade (cycle) (RES-BESS)

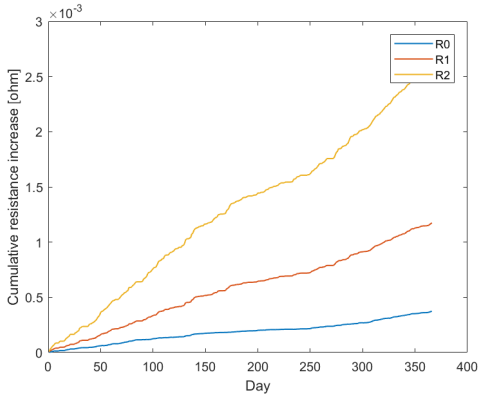

Figure 83: Resistances increase at SOC = 80 % for an internal cell (RES-BESS)

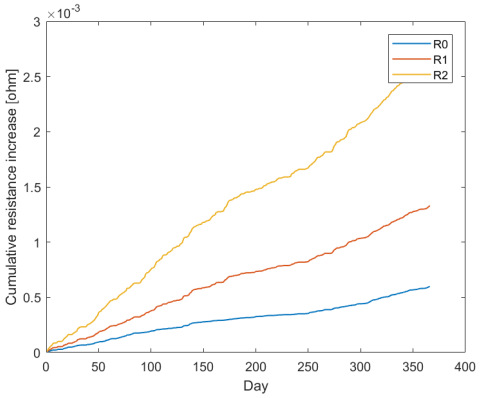

Figure 84: Resistances increase at SOC = 30 % for an internal cell (RES-BESS)

5.2.2.3 Economic results

Nowadays, NMC lithium ion battery prices hover between 170 and 320 €/kWh but they are expected to decrease [74] [75]. For example, according to Bloomberg they should be lower than 100 €/kWh by 2030 [76]. Nowadays, the cost of the whole battery energy storage system designed for this application should be around 6.500.000 €.

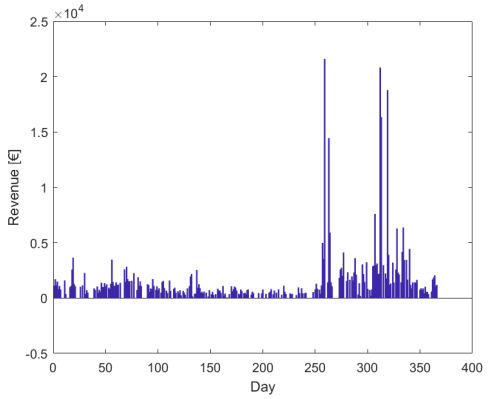

Figure 85: Revenue per day (RES-BESS)

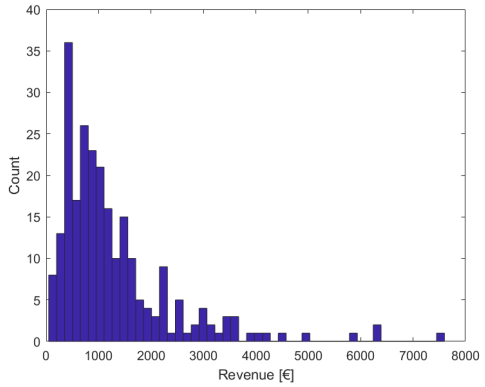

Figure 86: Revenue distribution (RES-BESS)

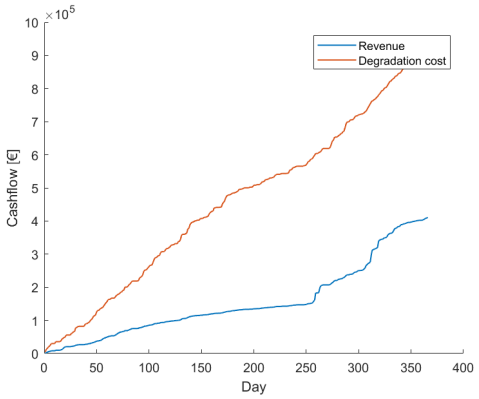

Figure 87: Cumulated revenue and degradation costs (RES-BESS)

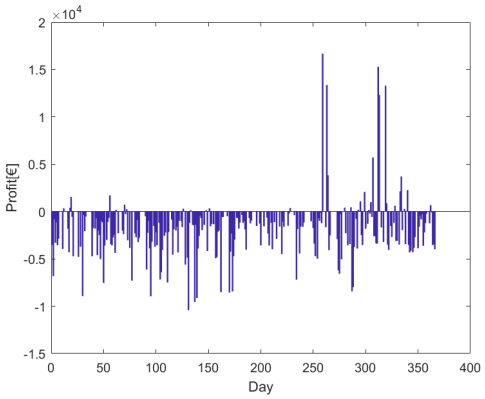

Figure 88: Profit per day considering degradation costs (RES-BESS)

The revenues presented in the following analysis are referred to the additional value produced by the ESS system in the day ahead electricity market. In particular, revenues are computed comparing the designed system (with RES and BESS) with the traditional system (with only RES). Therefore, the revenues obtained are the revenues produced by the RES+BESS system minus the revenues which would be produced without storing energy (RES revenues).

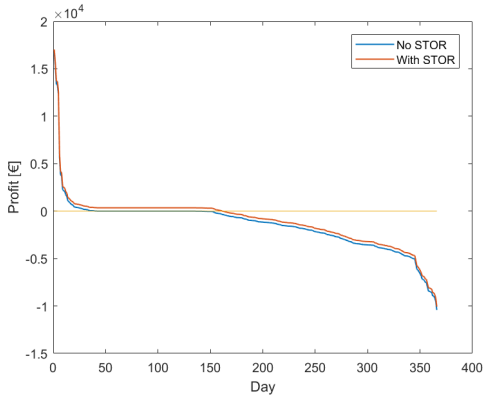

Figure 89: Number of profitable days (RES-BESS)

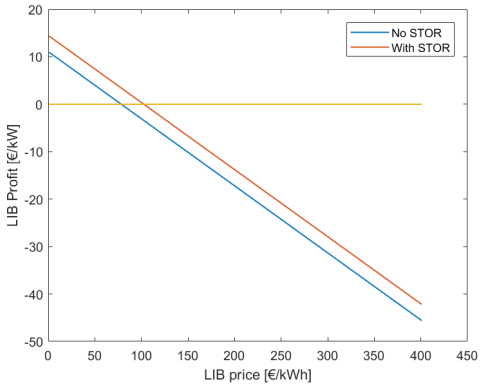

Figure 90: LIB price break even point (RES-BESS)

Figure 85 illustrates the revenues for each day during 2016. These values are very variable depending on the energy price volatility and on the stochastic RES. The same behavior is visible in Figure 86 which shows the revenue distribution (null revenues are filtered). From these figures it seems that the ESS can be highly profitable. However, as shown in Figure 87 and Figure 88 degradation costs overcomes revenues. More precisely, as illustrated in Figure 89 for only about 30 days throughout all 2016 the BESS results to be profitable. Nevertheless, the current decreasing trend of the LIB prices may make these applications more interesting from an economic poin of view. In particular, as shown in Figure 90 a LIB price lower than roughly 85 €/kWh could make this application profitable.

Moreover, operating also in the reserve market could improve the economic performance of the system. In particular, the Short Term Operating Reserve in UK as discussed in paragraph 2.2.3 can be an interesting additional source of revenue. A provider operating in this auction

market should gain on average 120 €/MW per day. This value has been extracted from the market data provided by the UK national grid [77]. Figure 90 shows how this additional source of revenue could make RES-BESS systems profitable with a LIB price lower than about 125 €/kWh.

Finally, it has to be mentioned than employing an ESS alongside renewable energy sources could help the RES feeders to control the power output (ramping) avoiding sanctions from the system operator. This third source of revenue cannot be easily evaluated.

5.3 Island Grid

The Island Grid (IG) is a part of the electrical grid fully or partially independent from an energetic point of view. This is possible thanks to the integration of distributed generators and energy storage systems. Generators usually consists in renewable energy sources (mainly wind turbines and PV panels). The energy storage system is necessary to cover the mismatch between production and demand which is crucial in an island grid. Moreover, in case of long insufficient production, the ESS can supply electrical energy while backup traditional generators are activated. Figure 91 gives an overview on the designed island grid. As it can be seen, this system is not fully isolated from the external grid. The energy production is provided by PV (2.49 MW average output) and Wind turbines (7.50 MW). The electrical load is represented by the residential district discussed in paragraph 5.1.2 and composed of 10.000 households. The ESS is a 60 MWH lithium ion battery. Both RES and ESS are sized after the design analysis described in the following paragraph.

The main target of the whole system is to minimize the amount of energy bought from the external grid. Therefore, the optimizer control the battery to cover the mismatch between production and demand making the residential district a partial island grid. Moreover, as a secondary target, the amount of energy sold to the grid is limited. In this way the exchanges in both direction with the external grid are limited.

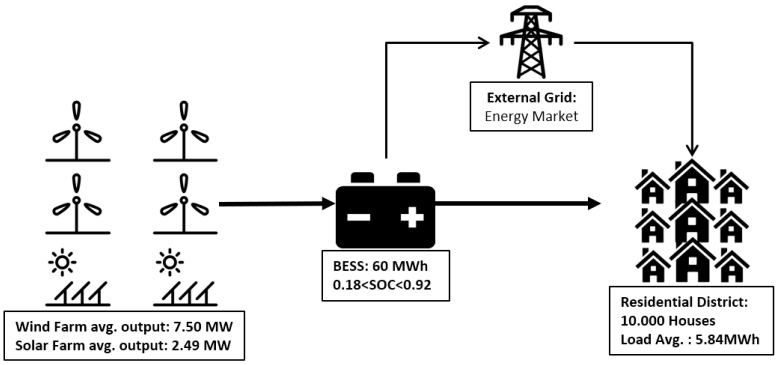

Figure 91: Island Grid (IG) overview

5.3.1 Design and Sizing Procedure

During the design procedure both RES and BESS penetrations should be investigated to find the optimal combination which minimizes the energy bought from the external grid. To achieve this task several simulations lasting one year are performed employing the optimizer. The LIB simulink model is not utilized in this preliminary design phase to avoid excessive computational effort. The RES penetration is expressed as the percentage of the average RES output compared

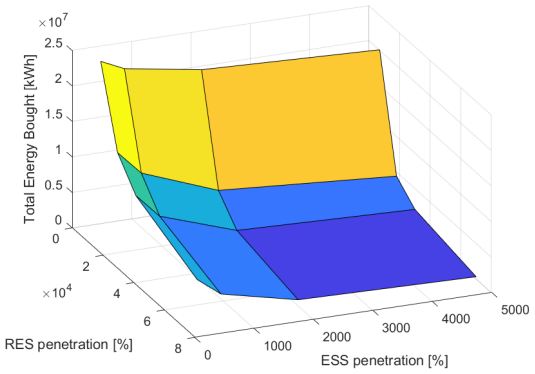

Figure 92: Power bought in 2016 for different RES and ESS penetrations 3D (IG)

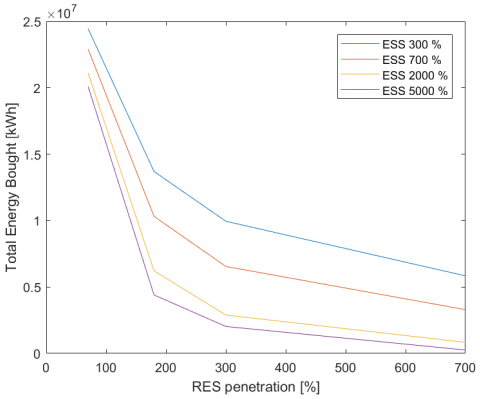

Figure 93: Power bought in 2016 for different RES and ESS penetrations (IG)

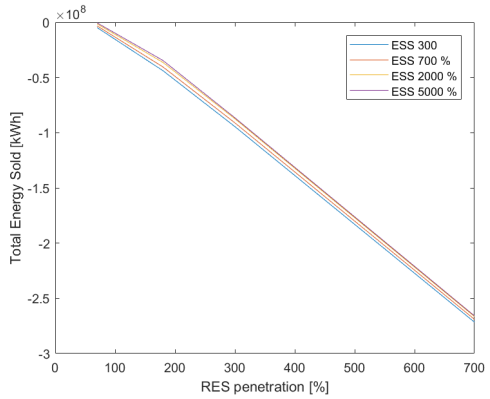

Figure 94: Power Sold in 2016 for different RES and ESS penetrations (IG)

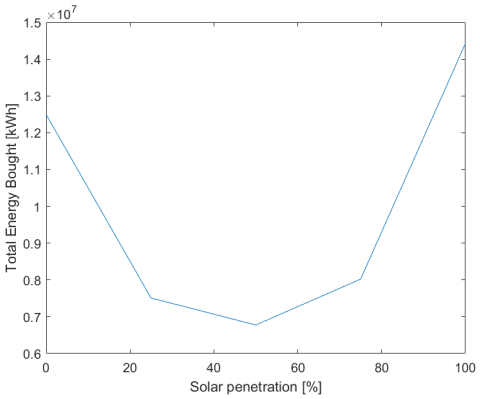

Figure 95: Power bought in 2016 for different solar penetrations (IG)

to the average electrical demand which is 5.8 MW. Similarly, The BESS penetration is expressed as the percentage of the nominal storage capacity compared to the average electrical demand. Figure 92 and Figure 93 shows the results of different simulations (performed with a solar:wind output ratio of 3:1). As expected higher BESS and RES penetrations minimize the energy bought form the external grid. As far as RES penetration is concerned, a value about 170 %

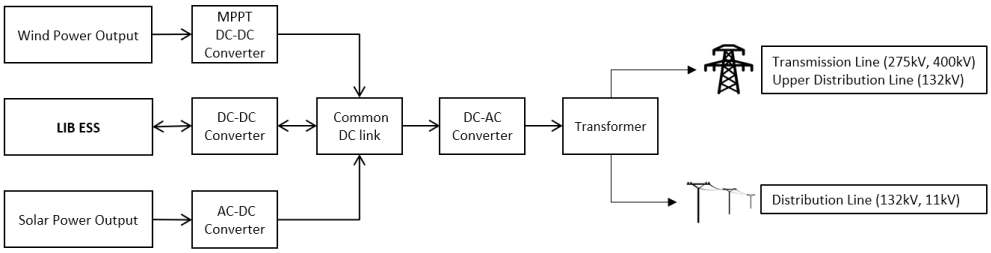

Figure 96: Island Grid BESS topology

(9.99 MW) is optimal considering that higher values strongly increase the energy sold to the external grid (Figure 93). Next, an ESS penetration of about 1000 % (60 MWh) is chosen as a trade off between investment costs and effectiveness (Figure 93).

At this point, knowing the RES and ESS penetations, the wind:solar ratio is studied. Figure 95 illustrates the results of the simulation for different solar outputs which are expressed as a percentage of the total RES output which is kept fixed. The simulations visible in Figure 95 demonstrate how a mix between different RES makes the production slightly less intermittent allowing the ESS to fulfill its duty effectively: a solar penetration of 50 % seems to be optimal. However, a percentage of 33 % (wind:solar ratio equal to 3:1) is chosen considering that it would be unrealistic to build such a large PV area in the East Midlands (UK).

Figure 96 gives an overview on the system topology in this application. The battery storage system and the renewable energy sources are connected through a common DC bus whose associated converters control the power fluxes. As an alternative, a common AC bus can be

designed as well. Energy is supplied to the residential district through the distribution line (132 kV or 11kV) or it is sold to the external grid through transmission lines.

5.3.2 Simulation Results

After the design procedure, a simulation of one year (2016) is performed initializing the BESS model with the design variables determined.

5.3.2.1 System analysis

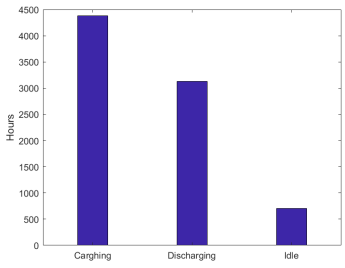

Figure 97: Charging, Discharging and Idle (IG)

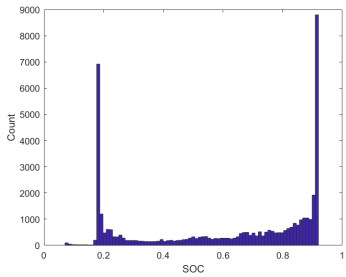

Figure 98: SOC distribution (IG)

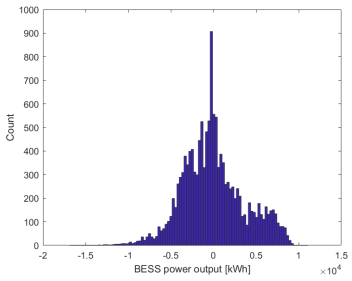

Figure 99: BESS power distribution (IG)

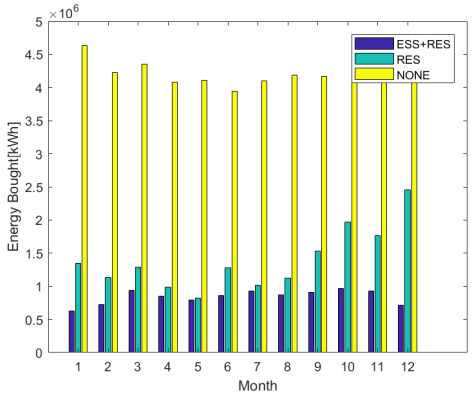

Figure 100: Energy bought monthly (IG)

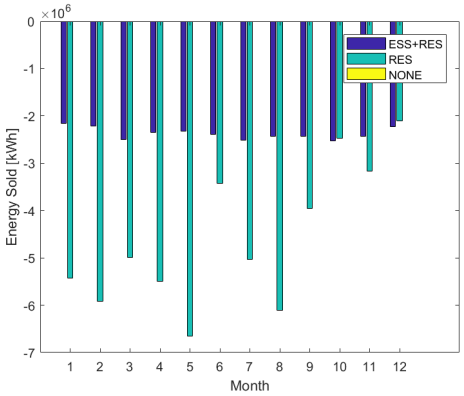

Figure 101: Energy sold monthly (IG)

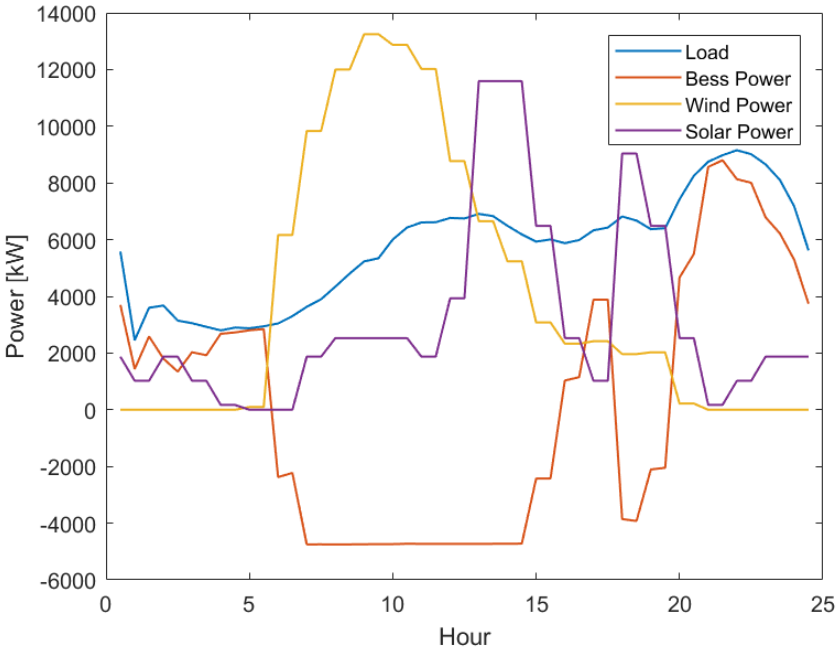

Figure 102: System power I/O on 01/08/2016 (IG)

In this application the energy produced by the RES is stored and supplied, when needed, to the load represented by the residential district. Figure 97 shows that the energy storage system stays idle for a limited amount of hours. In this specific application idle interval happens when the electrical demand is fully satisfied by the RES or when the energy storage is fully discharged. In particular, the BESS stays idle for about 7 % of the yearly operating hours meaning that it has been properly designed. As expected, RES low or over productions causes the ESS to stay at extreme state of charges as illustrated in Figure 98 which is not the best condition for aging. Figure 102 shows the BESS operating on a standard day (01/08/2016). It is visible, in

this case, how the system covers the midday demand peak with RES production whereas the evening peak is supplied by the energy storage. Figure 100 and Figure 101 demonstrates how integrating an ESS in system composed of RES and loads strongly reduces both energy sold and energy bought from the external grid making the system more independent.

5.3.2.2 Aging analysis

The BESS nominal capacity has been designed to be about six times the RES average output and ten times the average load. For this reason as shown in Figure 99 the BESS powers (charging and discharging), and thus, the current rates are very low (on average 0.1 C). As a consequence, as shown in Figure 103, the maximum temperatures reached by the cells throughout the simulation are limited. It has to be reminded that lower temperatures increase cycle aging effects due to the occurrence lithium plating. Therefore, damage is not as limited as expected with these low current rates. According to damage, at these operating conditions, the BESS has an expected life of roughly 8 years.

As far as calendar aging is concerned, the cells suffer the recurrent extreme SOC during operation (Figure 98). In fact, it has to be reminded that the best condition to hinder calendar aging is an intermediate SOC. On the other hand, the lower temperatures during operation decrease calendar aging impact. Overall, both calendar and cycle aging effects on the capacity are showed respectively in Figure 105 and Figure 106. The result of the capacity analysis is that an energy storage system operating in this manner can have an expected life about 7 years. There are not great differences between internal, border and corner cells due to the limited temperature gradient inside the cell module.

During the simulation, the impedances of the resistors are updated continuously to improve the accuracy of the simulation.

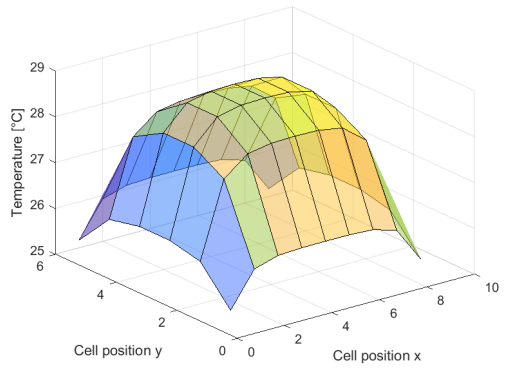

Figure 103: Max temperature reached by each cell during the simulation (IG)

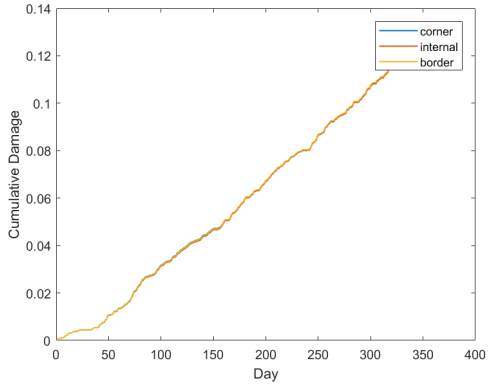

Figure 104: Cumulative damage (IG)

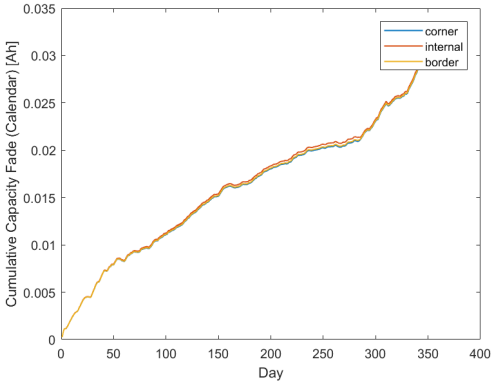

Figure 105: Cumulative capacity fade (calendar) (IG)

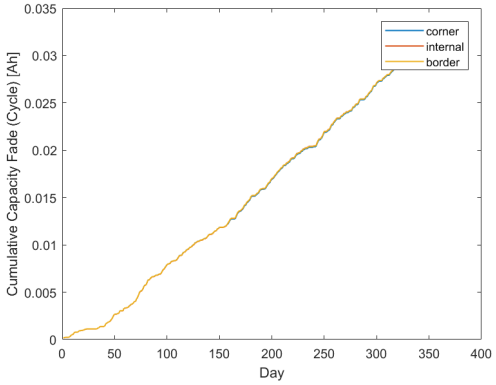

Figure 106: Cumulative capacity fade (cycle) (IG)

5.3.2.3 Economic results

The economic performance of energy storage systems operating in island grids cannot be easily assessed. In fact, employing a BESS in this application allows the distribution system operator to do without other devices needed in traditional grids where energy cannot be stored. In particular, island grids allow savings in terms of transmission lines, power conversion devices, regulating services (Voltage support, Frequency regulation, Operating Reserve) etc. Moreover, island grids strongly rely on distributed generators (mainly RES) and they allow to decrease the energy dissipation during transmission making the system more environmental sustainable.

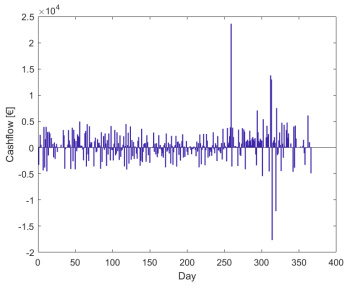

Figure 107: Revenue per day (IG)

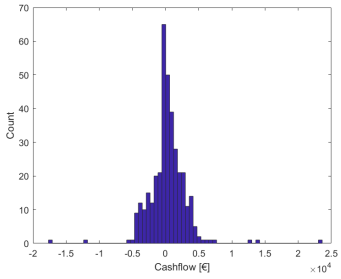

Figure 108: Revenue distribution (IG)

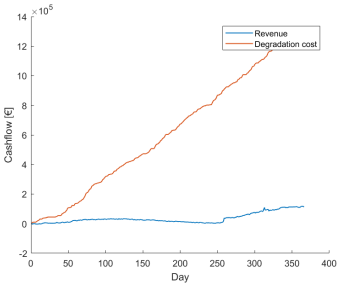

Figure 109: Cumulated revenue and degradation costs (IG)

Figure 107 and Figure 108 shows the revenue considering only the electricity market. This source of revenue is not really relevant in this application which has other economic targets as mentioned before. The revenues presented in these graphs are referred to the additional value

produced by the energy storage system. Therefore, these quantities are computed comparing the designed system (RES, BESS and LOAD) with the system with only RES and LOAD. in particular, the revenues obtained are the cashflows produced by the RES+BESS+LOAD system minus the cashflows which would be produced without storing energy. As expected, the yearly revenue is limited but positive. In fact, in normal weather conditions, the energy produced at night when electrical load and prices are low is stocked and sold during the day when prices and demand are higher.

As shown in Figure 109, the degradation costs heavily exceeds the revenue produced in the electricity market. However, as mentioned before, an island grid guarantees many further benefits to the distribution system operator which can be comparable with these aging costs. The degradation costs are computed starting from a lithium ion battery price of 190 €/kWh. Nowadays, NMC LIB prices hover between 170 and 320 €/kWh but they are expected to decrease [74] [75].

5.4 Energy Arbitrage

Energy Arbitrage consists in exploiting the energy price volatility by trading electrical energy in the electricity market. In this scenario, the battery energy storage system is a necessary device to store the energy exchanged. This decision making procedure is based on forecasting and optimization algorithms which control the battery energy storage system. The main target of the optimizer is to maximize profits considering cell aging as well: the cost function is shown in Equation 4.27. Figure 5 illustrates the distribution of the electricity prices on hourly basis in UK in 2016 [7]. As it can be noticed, great opportunities can be exploited by trading

electricity. Energy arbitrage applications usually involve enterprises or heavy industries with sufficient funds and know-how to operate in the energy market. Considering the volumes of the energy exchanged, the connection to the grid is generally at the upper distribution or transmission level. Further details about the energy arbitrage application are given in paragraph 2.1.1. Figure 110 gives an overview on the system whose sizing is described in the following paragraph. In addition to the energy market, to increase possible revenues this system has been designed to operate in the frequency regulation market as a secondary target. In particular, electricity is traded in the day ahead energy market while frequency regulation is provided in the Firm Frequency Response (FFR) market which has been described in paragraph 2.2.4.

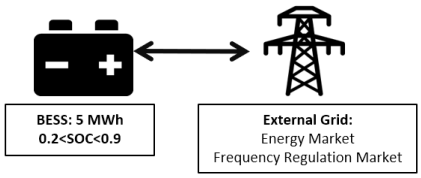

Figure 110: Energy arbitrage BESS overview

5.4.1 Design and Sizing Procedure

The sizing procedure is easier in comparison with the other two applications. In fact, in this case, the load and the RES are not involved in the system reducing the number of design variables. No relevant requirements are needed to operate in the day ahead energy market.

Instead, to provide the firm frequency response service, according to the UK national grid, a system must be able to supply or absorb at least 1 MW of electrical power. Moreover, this amount of power must be sustained for 20 seconds in case of primary response, for 30 minute in case of secondary response or indefinitely for high frequency response. The intervention times required (in the region between 10 and 30 seconds) can be easily satisfied by a LIB energy storage system. For practical reason, the system is designed to offer the primary and secondary response. Therefore, to meet these requirements (in terms of power and energy), a BESS with a nominal capacity of 5 MWh is chosen.

Figure 111 shows the system topology: the BESS is connected to the grid through DC-AC converters and transformers. These devices can be connected in parallel to achieve a higher system reliability.

Figure 111: Energy arbitrage BESS topology

5.4.2 Simulation Results

After the design process, a simulation of one year (2016) is performed initializing the BESS model with the design variables determined.

5.4.2.1 System analysis

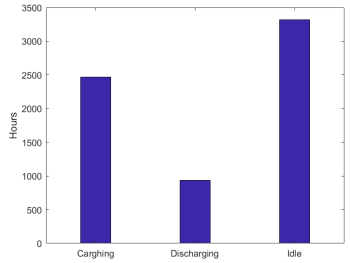

Figure 112: Charging, Discharging and Idle count (EA)

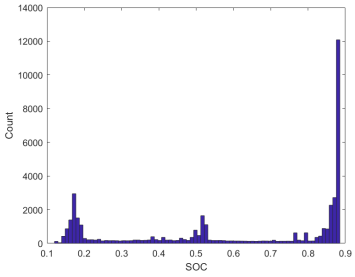

Figure 113: SOC distribution (EA)

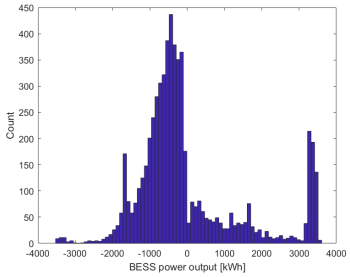

Figure 114: BESS power distribution (EA)

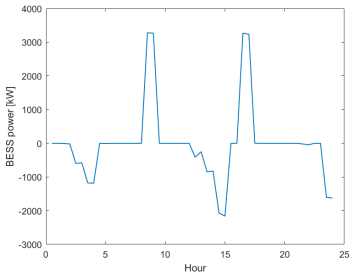

Figure 115: BESS power on a standard day of operation (EA)

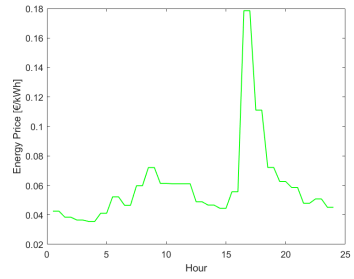

Figure 116: Energy prices on a standard day of operation (EA)

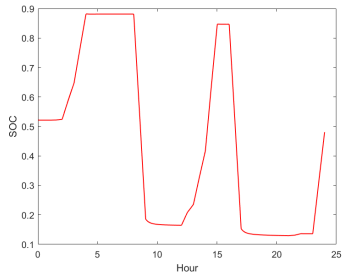

Figure 117: State Of Charge on a standard day of operation (EA)

To avoid excessive degradation because of aging and to maintain enough capacity to operate in the FFR market, the state of charge of the battery is always kept between 0.15 and 0.9. Figure 112 shows how the battery energy storage system stays idle for a large amount of hours waiting to exploit the volatility of electricity price. The difference between the total hours of

charging and discharging is due to the fact that the peaks of the energy price usually lasts a short time whereas the valleys (the drops) lasts longer as visible in Figure 116. For this reason, when electrical energy has to be sold, it is sold at a fast discharging rate to fully exploit the maximum price as shown in Figure 114. Figure 115, Figure 116 and Figure 117 illustrate how the system operates on a standard day (01/11/2016). As it can be seen electrical energy is stored when prices are lower and it is sold when prices are higher.

5.4.2.2 Aging analysis

The aging analysis is usually crucial in case of energy arbitrage. In fact, in this scenario the energy storage system is used heavily to respond to the volatility of the market. Therefore, as shown in Figure 118, the maximum temperatures reached by the cells are higher in comparison with the other applications. As expected, the internal cells suffer higher temperatures due to the less effective heat transfer: all these temperatures are within the operating range declared by the manufacturer.

To assess the remaining BESS lifetime both damage and capacity fade are analyzed. As far as damage is concerned, the BESS operating in this application accumulates about 35 % of damage per year meaning that it should operate for three years before reaching the end of life. In particular, as shown in Figure 119 and Figure 120, border and corner cells suffer higher damages due to the lower temperatures which accelerate lithium plating.

As illustrated in Figure 121, the final capacity fade is about 0.13 Ah per cell that is roughly 6 % of the nominal capacity. Therefore, the BESS would reach 80 % of the initial capacity after about 3 years. Both capacity and damage suggest an expected life of 3 years for a BESS

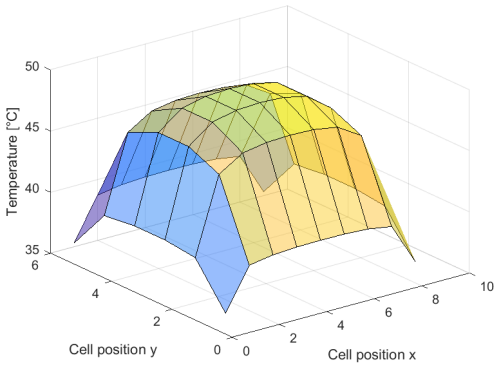

Figure 118: Max temperature reached by each cell during the simulation (EA)

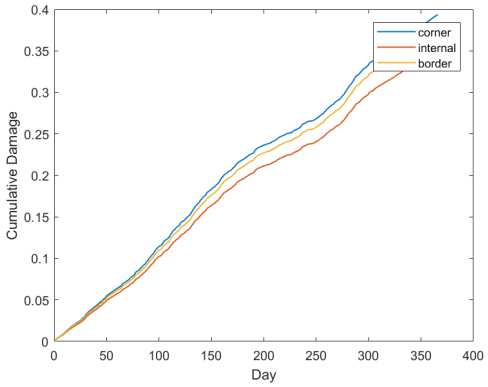

Figure 119: Cumulative damage (EA)

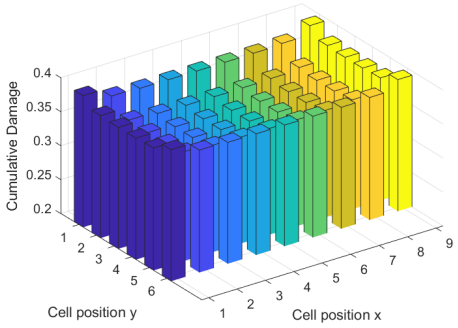

Figure 120: Final damage reached by each cell (EA)

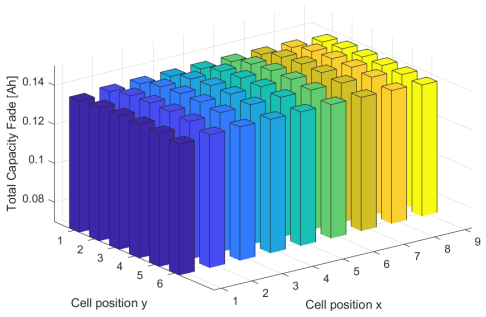

Figure 121: Final capacity fade reached by each cell (EA)

operating in energy arbitrage. In particular Figure 123 demonstrates how cycle aging has a stronger impact in comparison with calendar aging which is shown in Figure 122. Moreover, it has to be highlighted that calendar aging affects more internal cells which are subjected to higher average temperatures during operation.

Finally Figure 124 and Figure 125 give an overview the resistance increase. These values are continuously updated in the model during the entire simulation.

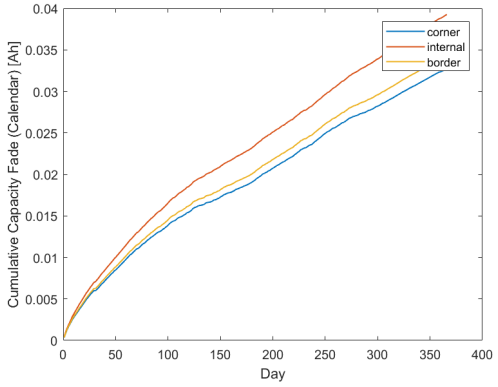

Figure 122: Cumulative capacity fade (calendar) (EA)

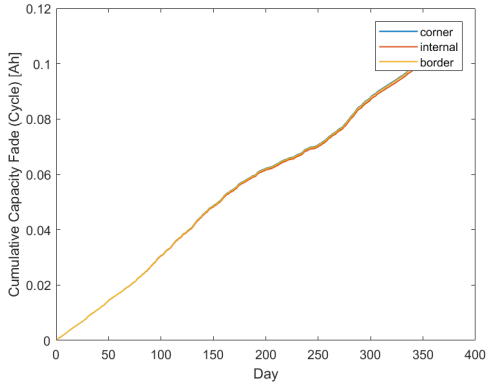

Figure 123: Cumulative capacity fade (cycle) (EA)

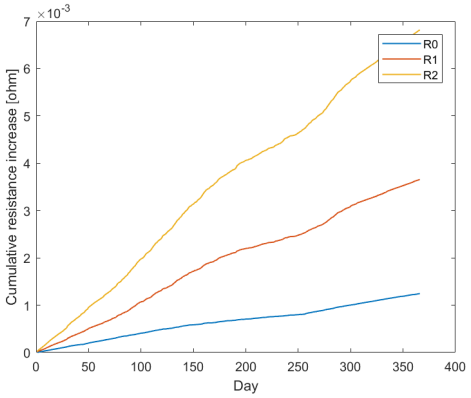

Figure 124: Resistances increase at SOC = 80 % for an internal cell (EA)

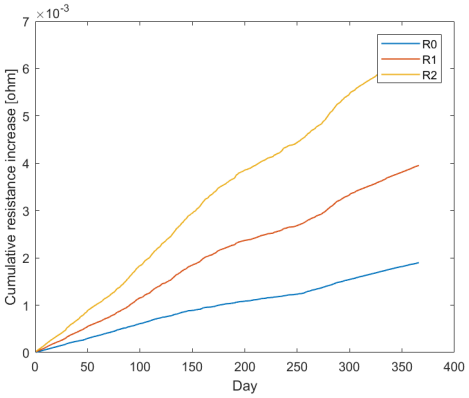

Figure 125: Resistances increase at SOC = 30 % for an internal cell (EA)

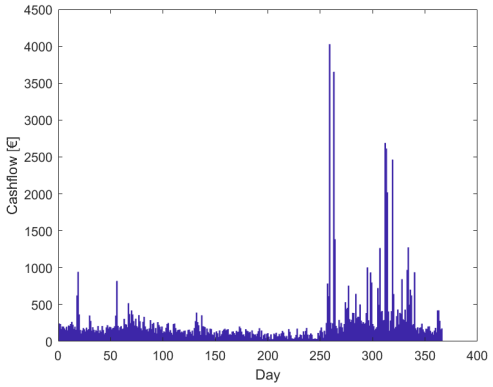

Figure 126: Revenue per day (EA)

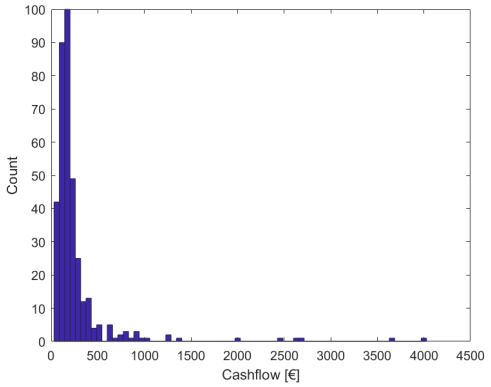

Figure 127: Revenues distribution (EA)

5.4.2.3 Economic results

It has to be highlighted that a high ESS penetration, which is not the case at present, would damp the volatility of the energy prices improving the performance of the grid but decreasing the profitability of an ESS operating in energy arbitrage. For this reason ESS can be considered price taker or price maker according to their total influence on the market. In this analysis it is assumed the price taker approach.

Figure 126 shows the revenues per day of the system. These values strongly depends on the volatility of the electricity prices. Also in this case the degradation costs, assuming a LIB price about 190 €/kW, overcomes possible revenues as illustrated in Figure 128. The degradation costs are computed considering the accumulated damages.

As demonstrated in Figure 129 and Figure 130 only in some days (about 15) the system operates in positive. However, as shown in Figure 130 and Figure 130, providing firm frequency

response can add a further source of revenue improving the profitability. Unfortunately, also in this case the system is not economically sustainable. In fact, as illustrated in Figure 131, the Lithium Ion battery should be cheaper than 90 €/Kw (with FFR) and 60 €/Kw (without FFR) to make this application interesting. Nowadays, NMC LIB prices hover between 170 and 320 €/kWh but they are expected to decrease [74] [75]. For example, according to Bloomberg they should be lower than 100 €/kWh by 2030 [76] which would make energy arbitrage sustainable.

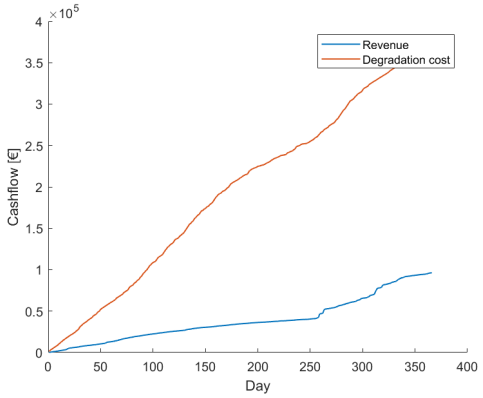

Figure 128: Cumulated revenue and degradation costs (EA)

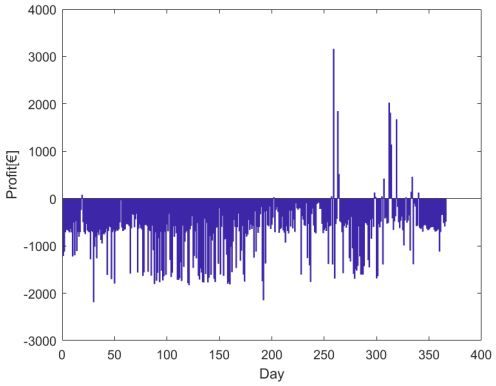

Figure 129: Profit per day considering degradation costs(EA)

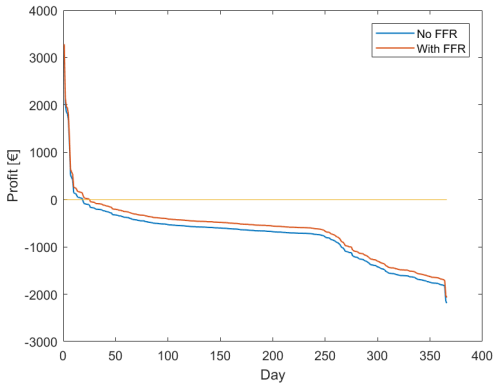

Figure 130: Number of profitable days (EA)

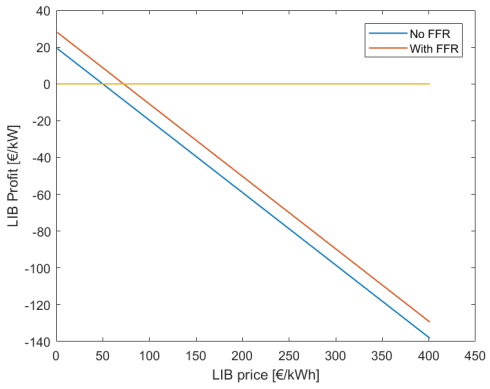

Figure 131: LIB price break even point (EA)

CHAPTER 6

CONCLUSION

The present thesis research describes an energy storage system model and its implementation in the electrical grid. In particular, some applications were analyzed and discussed: RES-BESS, island grid and energy arbitrage. This work is justified by the fact that modern smart grids require ESS in order to achieve higher standards of sustainability and effectiveness. Moreover, the increasing penetration of renewable energy sources makes the integration of energy storage systems necessary.

The *BESS model* was built in order to simulate a NMC lithium-ion energy storage system integrated in an electrical grid considering several aspects: electrical connections, thermal behavior, aging prediction, controlling and economic performance. To achieve this task a rich bibliographic research was performed and numerous personal contributions were added. The value of this model derives from the fact that it takes into account the whole scenario with a high level of detail. Therefore, the model can produce accurate simulations whose results are reliable and meaningful. In particular, a great attention was devoted to the aging model which was built starting from large sets of experimental data.

A simulation of one year was performed employing the energy storage system in three relevant applications. In all cases the ESS was designed after an accurate design procedure according to the different requirements. In RES-BESS it was demonstrated how the storage system can manage to control the sale of the electrical energy produced by renewable energy

sources increasing revenues. Next, it was illustrated how an ESS implemented in a smart grid can minimize the exchanges of electricity with the external grid. Finally, in energy arbitrage it was proved how the ESS can produce revenues by trading electrical energy. In all cases, but especially in energy arbitrage, the results of the simulations suggest that, nowadays, the degradation costs can be relevant overcoming possible revenues or values added. However, the decreasing price of lithium ion batteries as well as their technical features, which are improving, can make these applications really interesting in the near future.

Further developments should aim at building ESS models based on other technologies in order to compare different solutions.

APPENDIX

CELL DATA

TABLE XI: RC PARAMETERS AT T=20 ℃

SOC	**R0 [ohm]**	**R1 [ohm]**	**R2 [ohm]**	**C1 [F]**	**C2 [F]**
0	0.03996	0.0900	0.3985	700	90
0.025	0.04298	0.0150	0.0500	773	662
0.1	0.04911	0.0136	0.0498	643	1592
0.2	0.04391	0.0090	0.0482	747	1598
0.3	0.04596	0.0110	0.0489	788	1599
0.4	0.04454	0.0069	0.0447	703	1593
0.5	0.04583	0.0078	0.0326	740	1497
0.6	0.04765	0.0132	0.0452	783	1598
0.7	0.04826	0.0132	0.0446	779	1593
0.8	0.04793	0.0124	0.0448	752	1440
0.9	0.04808	0.0114	0.0388	729	1590
1	0.04403	0.0064	0.0353	700	1553

APPENDIX (continued)

TABLE XII: RC PARAMETERS AT T=45 °C

SOC	R0 [ohm]	R1 [ohm]	R2 [ohm]	C1 [F]	C2 [F]
0	0.0370	0.0542	0.2200	111	80
0.025	0.0440	0.0130	0.0351	120	600
0.1	0.0454	0.0094	0.0371	126	644
0.2	0.0440	0.0056	0.0277	209	854
0.3	0.0426	0.0050	0.0254	256	908
0.4	0.0419	0.0047	0.0234	255	902
0.5	0.0419	0.0041	0.0214	288	823
0.6	0.0409	0.0069	0.0199	185	864
0.7	0.0408	0.0079	0.0205	175	745
0.8	0.0407	0.0077	0.0207	175	737
0.9	0.0404	0.0076	0.0213	168	770
1	0.0406	0.0058	0.0266	214	923

T [°C]	I [C]	DOD[%]	SOC=100%	SOC=90%	SOC=80%	SOC=70%	SOC=60%	SOC=50%	SOC=40%	SOC=30%	SOC=20%	SOC=10%	SOC=0%
20	1	25	2.84E-06	1.91E-06	2.18E-06	2.70E-06	1.37E-06	2.98E-06	2.96E-06	3.07E-06	2.46E-06	3.31E-06	3.02E-05
20	1	50	-3.77E-07	-1.12E-06	-1.38E-06	3.27E-08	-3.10E-06	-2.50E-06	-1.57E-06	-1.98E-06	-1.74E-06	-5.73E-06	4.25E-05
20	1	60	-1.59E-05	-1.31E-05	-5.07E-06	-1.59E-05	-1.87E-05	-1.97E-05	-1.85E-05	-1.64E-05	-1.55E-05	-1.59E-05	5.15E-05
20	1	75	-2.68E-06	-4.84E-06	-6.83E-06	-6.84E-06	-8.81E-06	-8.03E-06	-8.86E-06	-9.35E-06	-1.46E-05	-1.77E-05	6.10E-05
20	1	80	-9.46E-07	8.81E-06	5.81E-06	6.30E-06	1.83E-06	5.22E-06	8.02E-07	5.07E-06	6.55E-06	1.28E-06	7.15E-05
20	1	90	1.35E-06	3.88E-06	-1.35E-06	1.88E-06	1.14E-06	5.55E-06	5.18E-06	5.57E-06	2.62E-06	5.12E-07	9.95E-05
20	1	100	2.88E-05	1.26E-05	1.45E-05	1.95E-05	3.73E-05	5.29E-05	5.49E-05	6.40E-05	7.69E-05	1.04E-04	1.14E-04
20	2	25	7.26E-07	1.03E-06	-7.63E-07	1.64E-06	-2.19E-06	-7.19E-07	-4.56E-07	-9.93E-07	-1.11E-06	-1.60E-06	3.68E-05
20	2	50	-1.37E-05	-6.88E-06	-8.40E-06	-9.26E-06	-1.16E-05	-1.08E-05	-1.10E-05	-1.44E-05	-1.54E-05	-2.31E-05	4.37E-05
20	2	75	1.76E-05	1.25E-05	1.32E-05	1.33E-05	1.55E-05	1.45E-05	9.73E-06	1.72E-05	7.67E-06	-2.80E-06	6.11E-05
20	2	100	2.30E-05	1.06E-05	9.87E-06	1.33E-05	1.40E-05	2.24E-05	2.44E-05	2.91E-05	3.58E-05	5.81E-05	1.24E-04
45	1	50	1.90E-05	1.60E-05	1.62E-05	1.70E-05	1.66E-05	1.90E-05	1.90E-05	1.92E-05	1.80E-05	1.54E-05	2.67E-05
45	1	100	3.30E-05	2.07E-05	2.28E-05	2.66E-05	3.38E-05	4.48E-05	4.59E-05	5.01E-05	5.47E-05	6.31E-05	6.92E-05
45	2	50	1.87E-05	1.71E-05	1.72E-05	1.84E-05	1.72E-05	2.02E-05	2.11E-05	2.11E-05	1.95E-05	1.78E-05	2.99E-05
45	2	100	3.13E-05	2.13E-05	2.38E-05	2.58E-05	3.38E-05	4.70E-05	4.88E-05	5.29E-05	5.81E-05	6.56E-05	7.10E-05

Figure 132: β_0 [ohm/EFC] cycle aging coefficients for each operating condition at specific SOC

APPENDIX (continued)

T [°C]	I [C]	DOD[%]	SOC=100%	SOC=90%	SOC=80%	SOC=70%	SOC=60%	SOC=50%	SOC=40%	SOC=30%	SOC=20%	SOC=10%	SOC=0%
20	1	25	5.85E-06	5.16E-06	4.65E-06	3.53E-06	5.21E-06	5.99E-06	6.43E-06	6.85E-06	9.26E-06	1.51E-05	-5.24E-05
20	1	50	1.28E-05	1.18E-05	1.21E-05	8.87E-06	1.06E-05	1.30E-05	1.25E-05	1.34E-05	1.48E-05	2.73E-05	-1.37E-04
20	1	60	5.27E-06	5.90E-06	-2.11E-06	8.01E-06	5.43E-06	1.06E-05	1.01E-05	6.92E-06	6.03E-06	5.79E-06	-2.69E-04
20	1	75	2.03E-05	1.80E-05	2.08E-05	1.95E-05	2.26E-05	2.04E-05	2.21E-05	2.20E-05	2.72E-05	4.26E-05	2.79E-05
20	1	80	8.53E-06	-1.89E-06	1.91E-06	5.99E-08	2.41E-06	2.62E-06	8.44E-06	3.94E-06	4.02E-06	1.83E-05	-1.84E-04
20	1	90	8.66E-06	4.80E-06	1.15E-05	6.63E-06	5.35E-06	4.61E-06	6.00E-06	6.88E-06	1.48E-05	4.37E-05	-1.38E-04
20	1	100	2.96E-05	1.68E-05	1.87E-05	1.99E-05	6.00E-05	5.15E-05	5.37E-05	6.18E-05	9.50E-05	2.18E-04	7.77E-01
20	2	25	3.55E-06	3.54E-06	4.94E-06	1.30E-06	3.92E-06	5.38E-06	5.60E-06	6.74E-06	8.94E-06	1.96E-05	2.39E-05
20	2	50	9.66E-07	-2.22E-06	-3.95E-08	-2.12E-06	-6.28E-06	-1.77E-06	-4.83E-07	2.02E-06	1.45E-06	1.00E-05	-2.82E-04
20	2	75	1.28E-06	6.36E-06	6.52E-06	3.56E-06	-6.25E-07	6.85E-06	1.32E-05	5.90E-06	1.84E-05	2.79E-05	-2.64E-04
20	2	100	2.90E-05	1.84E-05	2.22E-05	1.84E-05	3.08E-05	3.35E-05	3.29E-05	3.69E-05	5.67E-05	1.31E-04	1.08E-03
45	1	50	1.31E-05	6.94E-06	7.30E-06	5.14E-06	5.80E-06	8.62E-06	8.42E-06	7.81E-06	9.07E-06	9.81E-06	-8.09E-05
45	1	100	2.71E-05	1.51E-05	1.49E-05	1.40E-05	3.46E-05	3.20E-05	3.19E-05	3.45E-05	4.65E-05	8.03E-05	4.01E-05
45	2	50	1.46E-05	6.32E-06	6.99E-06	3.99E-06	6.36E-06	8.99E-06	7.95E-06	8.17E-06	1.03E-05	1.17E-05	-8.26E-05
45	2	100	2.85E-05	1.45E-05	1.35E-05	1.40E-05	4.02E-05	3.48E-05	3.39E-05	3.76E-05	4.97E-05	8.36E-05	4.38E-05

Figure 133: β_1 [ohm/EFC] cycle aging coefficients for each operating condition at specific SOC

T [°C]	I [C]	DOD[%]	SOC=100%	SOC=90%	SOC=80%	SOC=70%	SOC=60%	SOC=50%	SOC=40%	SOC=30%	SOC=20%	SOC=10%	SOC=0%
20	1	25	-1.50E-06	2.78E-07	-1.49E-06	-8.93E-07	1.22E-05	1.53E-05	1.98E-05	1.78E-05	1.33E-05	5.74E+05	-4.85E-05
20	1	50	-1.18E-05	-5.08E-06	-7.77E-06	-7.00E-06	8.99E-06	1.73E-05	2.23E-05	1.61E-05	2.20E-05	3.27E-02	-1.47E-04
20	1	60	-9.09E-07	2.91E-06	1.57E-06	-4.35E-06	1.74E-05	3.60E-05	4.42E-05	4.24E-05	4.95E-05	8.70E-03	8.41E-05
20	1	75	-1.86E-05	-4.72E-06	-4.00E-06	-4.45E-08	1.45E-05	1.98E-05	2.47E-05	2.05E-05	2.41E-05	1.37E-02	-4.79E-04
20	1	80	7.41E-06	8.07E-06	4.61E-06	5.38E-06	3.42E-05	5.11E-05	5.64E-05	6.14E-05	6.37E-05	7.57E-02	3.04E-04
20	1	90	9.35E-06	3.32E-06	-2.39E-06	5.29E-07	2.67E-05	4.72E-05	6.27E-05	5.74E-05	6.12E-05	5.75E-02	2.79E-04
20	1	100	-1.03E-05	1.56E-04	2.98E-05	6.97E-03	-1.24E-05	-1.82E-05	-2.03E-05	-2.14E-05	-2.18E-05	5.77E-06	9.93E-01
20	2	25	-2.24E-06	-2.92E-06	-5.90E-06	-4.62E-06	1.30E-05	2.68E-05	3.46E-05	2.93E-05	2.24E-05	3.25E+00	-1.15E-04
20	2	50	2.47E-06	7.16E-06	2.22E-07	-4.03E-06	3.69E-05	6.09E-05	7.27E-05	6.22E-05	6.38E-05	1.10E-02	-2.14E-05
20	2	75	4.14E-05	9.50E-06	6.54E-06	7.76E-06	6.50E-05	1.17E-04	1.82E-04	1.86E-04	1.56E-04	1.03E-03	-2.27E-04
20	2	100	-1.49E-05	1.64E-05	-9.84E-07	8.79E-06	2.40E-05	8.12E-06	1.94E-05	1.07E-05	7.56E-06	3.67E-03	9.48E-04
45	1	50	4.23E-06	1.78E-05	1.38E-05	1.50E-05	5.40E-05	2.99E-05	3.95E-05	4.01E-05	3.78E-05	1.19E-02	-1.74E-04
45	1	100	1.28E-05	2.12E-04	4.46E-05	1.13E-03	4.50E-06	-9.23E-06	-8.92E-06	-1.46E-05	-1.83E-05	3.73E-04	-1.75E-04
45	2	50	7.34E-07	2.04E-05	1.52E-05	1.63E-05	6.80E-05	3.12E-05	4.23E-05	3.53E-05	3.11E-05	1.20E-01	-1.71E-04
45	2	100	-1.38E-06	2.39E-04	4.82E-05	5.29E-03	2.85E-06	-8.46E-06	-9.53E-06	-1.54E-05	-1.94E-05	1.93E-03	-1.60E-04

Figure 134: β_2 [ohm/EFC] cycle aging coefficients for each operating condition at specific SOC

CITED LITERATURE

1. A world turned upside down, feb 2017. https://www.economist.com/briefing/2017/02/25/a-world-turned-upside-down. [Online; accessed 05/04/2018].

2. Husev, O.: Smart grid as a future grid of a power distributed systems. Technical report, Chernihiv National University of Technology, apr 2016.

3. Brouwer, A. S., Van Den Broek, M., Seebregts, A., and Faaij, A.: Impacts of large-scale intermittent renewable energy sources on electricity systems, and how these can be modeled. Renewable and Sustainable Energy Reviews, 33:443–466, 2014.

4. The worlds renewable electricity capacity is set to rise sharply over the next five years, the international energy agency (iea) says, expanding 43% on todays levels., oct 2017. https://www.carbonbrief.org/iea-renewable-electricity-set-to-grow-40-globally-by-2022. [Online; accessed 04/04/2018].

5. Amin, M.: Smart grid. PUBLIC UTILITIES FORTNIGHTLY, 2015.

6. Scrosati, B. and Garche, J.: Lithium batteries: Status, prospects and future. Journal of Power Sources, 195(9):2419–2430, 2010.

7. Nordpool historical market data, may 2017. https://www.nordpoolgroup.com/historical-market-data/. [Online; accessed 24/05/2018].

8. Fares, R. L. and Webber, M. E.: A flexible model for economic operational management of grid battery energy storage. Energy, 78:768–776, 2014.

9. Chamana, M., Mazhari, I., Parkhideh, B., and Chowdhury, B. H.: Multi-mode operation of different pv/bess architectures in a microgrid: Grid-tied and island mode. In T&D Conference and Exposition, 2014 IEEE PES, pages 1–5. IEEE, 2014.

10. Heymans, C., Walker, S. B., Young, S. B., and Fowler, M.: Economic analysis of second use electric vehicle batteries for residential energy storage and load-levelling. Energy Policy, 71:22–30, 2014.

CITED LITERATURE (continued)

11. Grid, N.: Demand turn up, July 2018. https://www.nationalgrid.com/uk/electricity/balancing-services/reserve-services/demand-turn?overview. [Online; accessed 05/07/2018].

12. Toshiba to supply japan's largest lithium-ion battery energy storage system for tohoku electric power company, may 2015. https://www.toshiba.co.jp/about/press/2015_05/pr2901.htm. [Online; accessed 15/05/2018].

13. Burke, S. L. H. Z. A.: A first-order transient response model for lithium-ion batteries of various chemistries: Test data and model validation. Technical report, Institute of Transportation Studies - University of California, Davis, 2012.

14. Oudalov, A., Cherkaoui, R., and Beguin, A.: Sizing and optimal operation of battery energy storage system for peak shaving application. In Power Tech, 2007 IEEE Lausanne, pages 621–625. IEEE, 2007.

15. Abdelrazek, S. A. and Kamalasadan, S.: Integrated pv capacity firming and energy time shift battery energy storage management using energy-oriented optimization. IEEE Transactions on Industry Applications, 52(3):2607–2617, 2016.

16. Lawder, M. T., Suthar, B., Northrop, P. W., De, S., Hoff, C. M., Leitermann, O., Crow, M. L., Santhanagopalan, S., and Subramanian, V. R.: Battery energy storage system (bess) and battery management system (bms) for grid-scale applications. Proceedings of the IEEE, 102(6):1014–1030, 2014.

17. Grid, N.: Fast reserve, may 2018. https://www.nationalgrid.com/uk/electricity/balancing-services/reserve-services/fast-reserve?overview. [Online; accessed 14/05/2018].

18. Grid, N.: Short term operating reserve, July 2018. https://www.nationalgrid.com/uk/electricity/balancing-services/reserve-services/short-term-operating-reserve-stor?overview . [Online; accessed 04/07/2018].

19. Grid, N.: Firm frequency response, July 2018. https://www.nationalgrid.com/uk/electricity/balancing-services/frequency-response-services/firm-frequency-response?getting-paid. [Online; accessed 06/07/2018].

20. Divya, K. and Østergaard, J.: Battery energy storage technology for power systemsan overview. Electric Power Systems Research, 79(4):511–520, 2009.

CITED LITERATURE (continued)

21. Curtis, M.: Overview of the uk demand response market epfl workshop. Technical report, University of Reading, sep 2015.

22. Colthorpe, A.: California batterys black start capability hailed as major accomplishment in the energy industry. Energy Storage News, may 2017.

23. Stan, A.-I., Świerczyński, M., Stroe, D.-I., Teodorescu, R., and Andreasen, S. J.: Lithium ion battery chemistries from renewable energy storage to automotive and back-up power applicationsan overview. In Optimization of Electrical and Electronic Equipment (OPTIM), 2014 International Conference on, pages 713–720. IEEE, 2014.

24. Raineri, R., Rios, S., and Schiele, D.: Technical and economic aspects of ancillary services markets in the electric power industry: an international comparison. Energy policy, 34(13):1540–1555, 2006.

25. Aamir, M., Kalwar, K. A., and Mekhilef, S.: uninterruptible power supply (ups) system. Renewable and sustainable energy reviews, 58:1395–1410, 2016.

26. Vazquez, S., Lukic, S. M., Galvan, E., Franquelo, L. G., and Carrasco, J. M.: Energy storage systems for transport and grid applications. IEEE Transactions on Industrial Electronics, 57(12):3881–3895, 2010.

27. Battke, B., Schmidt, T. S., Grosspietsch, D., and Hoffmann, V. H.: A review and probabilistic model of lifecycle costs of stationary batteries in multiple applications. Renewable and Sustainable Energy Reviews, 25:240–250, 2013.

28. Sortomme, E. and El-Sharkawi, M.: Optimal power flow for a system of microgrids with controllable loads and battery storage. In Power Systems Conference and Exposition, 2009. PSCE'09. IEEE/PES, pages 1–5. IEEE, 2009.

29. Tan, K. M., Ramachandaramurthy, V. K., and Yong, J. Y.: Integration of electric vehicles in smart grid: A review on vehicle to grid technologies and optimization techniques. Renewable and Sustainable Energy Reviews, 53:720–732, 2016.

30. Association, E. S.: Energy storage technologies, jun 2018. http://energystorage.org/energy-storage/energy-storage-technologies. [Online; accessed 12/06/2018].

31. Zhao, H., Wu, Q., Hu, S., Xu, H., and Rasmussen, C. N.: Review of energy storage system for wind power integration support. Applied Energy, 137:545–553, 2015.

CITED LITERATURE (continued)

32. Luo, X., Wang, J., Dooner, M., and Clarke, J.: Overview of current development in electrical energy storage technologies and the application potential in power system operation. Applied energy, 137:511–536, 2015.

33. Doe energy storage database, jul 2018. https://www.energystorageexchange.org/. [Online; accessed 01/07/2018].

34. Nitta, N., Wu, F., Lee, J. T., and Yushin, G.: Li-ion battery materials: present and future. Materials today, 18(5):252–264, 2015.

35. Bu-301a: Types of battery cells, jul 2017. https://batteryuniversity.com/learn/article/types_of_battery_ [Online; accessed 08/07/2018].

36. Julien, C. M., Mauger, A., Zaghib, K., and Groult, H.: Comparative issues of cathode materials for li-ion batteries. Inorganics, 2(1):132–154, 2014.

37. Yazami, R.: Surface chemistry and lithium storage capability of the graphite–lithium electrode. Electrochimica acta, 45(1-2):87–97, 1999.

38. Broussely, M., Biensan, P., Bonhomme, F., Blanchard, P., Herreyre, S., Nechev, K., and Staniewicz, R.: Main aging mechanisms in li ion batteries. Journal of power sources, 146(1-2):90–96, 2005.

39. Vetter, J., Novak, P., Wagner, M. R., Veit, C., Möller, K.-C., Besenhard, J., Winter, M., Wohlfahrt-Mehrens, M., Vogler, C., and Hammouche, A.: Ageing mechanisms in lithium-ion batteries. Journal of power sources, 147(1-2):269–281, 2005.

40. Dees, D. W., Battaglia, V. S., and Bélanger, A.: Electrochemical modeling of lithium polymer batteries. Journal of power sources, 110(2):310–320, 2002.

41. Li, S. and Ke, B.: Study of battery modeling using mathematical and circuit oriented approaches. In Power and Energy Society General Meeting, 2011 IEEE, pages 1–8. IEEE, 2011.

42. Swierczynski, M., Stroe, D. I., Stan, A.-I., Teodorescu, R., and Sauer, D. U.: Selection and performance-degradation modeling of limo _{2}/li _{4} ti _{5} o _{12} and lifepo _{4}/c battery cells as suitable energy storage systems for grid integration with wind power plants: An example for the primary frequency regulation service. IEEE transactions on Sustainable Energy, 5(1):90–101, 2014.

CITED LITERATURE (continued)

43. Sony Energy Devices Corporation Device Solutions Business Group, S. C.: Lithium ion rechargeable battery technical information. model number us18650v3. http://www.batteryspace.com/prod-specs/9091_specification.pdf. [Online; accessed 02/04/2018].

44. Zhang, L., Peng, H., Ning, Z., Mu, Z., and Sun, C.: Comparative research on rc equivalent circuit models for lithium-ion batteries of electric vehicles. Applied Sciences, 7(10):1002, 2017.

45. Stiaszny, B., Ziegler, J. C., Krauß, E. E., Zhang, M., Schmidt, J. P., and Ivers-Tiffée, E.: Electrochemical characterization and post-mortem analysis of aged limn2o4–nmc/graphite lithium ion batteries part ii: Calendar aging. Journal of Power Sources, 258:61–75, 2014.

46. Linden, D. and Reddy, T. B.: Handbook of batteries. 3rd. McGraw-Hill, 2002.

47. Ecker, M., Gerschler, J. B., Vogel, J., Käbitz, S., Hust, F., Dechent, P., and Sauer, D. U.: Development of a lifetime prediction model for lithium-ion batteries based on extended accelerated aging test data. Journal of Power Sources, 215:248–257, 2012.

48. Maleki, H., Al Hallaj, S., Selman, J. R., Dinwiddie, R. B., and Wang, H.: Thermal properties of lithium-ion battery and components. Journal of the Electrochemical Society, 146(3):947–954.

49. Bmz energy storage systems take you on the bright side, may 2018. https://www.bmz-group.com/dokumente/Produktbroschueren/Broschuere-ESS_EN.pdf. [Online; accessed 07/05/2018].

50. Chatzinikolaou, E. and Rogers, D. J.: A comparison of grid-connected battery energy storage system designs. IEEE Transactions on Power Electronics, 32(9):6913–6923, 2017.

51. Kenney, B., Darcovich, K., MacNeil, D. D., and Davidson, I. J.: Modelling the impact of variations in electrode manufacturing on lithium-ion battery modules. Journal of Power Sources, 213:391–401, 2012.

52. Ling, Z., Wang, F., Fang, X., Gao, X., and Zhang, Z.: A hybrid thermal management system for lithium ion batteries combining phase change materials with forced-air cooling. Applied energy, 148:403–409, 2015.

CITED LITERATURE (continued)

53. Maleki, H., Al Hallaj, S., Selman, J. R., Dinwiddie, R. B., and Wang: Thermal properties of lithium ion battery and components. Journal of the Electrochemical Society, pages 947–954, 1999.

54. Prasad, G. K. and Rahn, C. D.: Model based identification of aging parameters in lithium ion batteries. Journal of power sources, 232:79–85, 2013.

55. Schmitt, J.: Modeling of Aging Effects and Extended Kalman Filter Based State of Charge Estimation of Lithium-Ion Batteries. Master's thesis, Fraunhofer Institute for Solar Energy Systems, 2016.

56. Maheshwari, A., Heck, M., and Santarelli, M.: Cycle aging studies of lithium nickel manganese cobalt oxide-based batteries using electrochemical impedance spectroscopy. Electrochimica Acta, 273:335–348, 2018.

57. Schmitt, J., Maheshwari, A., Heck, M., Lux, S., and Vetter, M.: Impedance change and capacity fade of lithium nickel manganese cobalt oxide-based batteries during calendar aging. Journal of Power Sources, 353:183–194, 2017.

58. Ecker, M., Gerschler, J. B., Vogel, J., Käbitz, S., Hust, F., Dechent, P., and Sauer, D. U.: Development of a lifetime prediction model for lithium-ion batteries based on extended accelerated aging test data. Journal of Power Sources, 215:248–257, 2012.

59. Stroe, D.-I., Swierczynski, M., Stroe, A.-I., Teodorescu, R., Laerke, R., and Kjaer, P. C.: Degradation behaviour of lithium-ion batteries based on field measured frequency regulation mission profile. In Energy Conversion Congress and Exposition (ECCE), 2015 IEEE, pages 14–21. IEEE, 2015.

60. You, S. and Rasmussen, C. N.: Generic modelling framework for economic analysis of battery systems. 2011.

61. Badey, Q., Cherouvrier, G., Reynier, Y., Duffault, J., and Franger, S.: Ageing forecast of lithium-ion batteries for electric and hybrid vehicles. Curr. Top. Electrochem, 16:65–79, 2011.

62. Baghdadi, I., Mathieu, R., Briat, O., Gyan, P., and Vinassa, J.-M.: Lithium-ion battery ageing assessment based on a reduced design of experiments. In IEEE Vehicle Power and Propulsion Conference, VPPC, 2017.

CITED LITERATURE (continued)

63. Safari, M., Morcrette, M., Teyssot, A., and Delacourt, C.: Life-prediction methods for lithium-ion batteries derived from a fatigue approach i. introduction: capacity-loss prediction based on damage accumulation. Journal of The Electrochemical Society, 157(6):A713–A720, 2010.

64. for Environmental Data Analysis CEDA, C.: , , jun 2018. http://data.ceda.ac.uk/badc/ukmo-midas/data/WM/yearly_files/. [Online; accessed 16/06/2018].

65. EWT: Dw54, jun 2018. https://ewtdirectwind.com/products/dw54/. [Online; accessed 02/06/2018].

66. (CAMS), C. A. M. S.: , , jun 2018. http://www.soda-pro.com/web-services/radiation/cams-radiation-service. [Online; accessed 18/06/2018].

67. Masters, G. M.: Renewable and efficient electric power systems. John Wiley & Sons, 2013.

68. et al, R.: Domestic electricity use: a high-resolution energy demand model. Master's thesis, Loughborough University, 2010.

69. Buffo, G.: Modeling, techno-economic analysis and optimal operation of a Reversible Solid Oxide Cell (ReSOC) polygeneration system. Master's thesis, Politecnico di Torino, 2017.

70. Mrs. Ramalakshmi, M. J. G.: Grid connected pv/wind (gcpw) hybrid system with improved power quality. Research and Reviews, 2012.

71. Hesse, H. C., Schimpe, M., Kucevic, D., and Jossen, A.: Lithium-ion battery storage for the grida review of stationary battery storage system design tailored for applications in modern power grids. Energies, 10(12):2107, 2017.

72. Cordova, F. M. and Yanine, F. F.: Homeostatic control of sustainable energy grid applied to natural disasters. International Journal of Computers Communications & Control, 8(1):50–60, 2013.

73. Conrad: Sony us18650v3 non-standard battery (rechargeable) 18650 flat top li-ion 3.7 v 2250 mah, 2018. https://www.conrad.com/ce/en/product/1558868/Sony-US18650V3-Non-standard-battery-rechargeable-18650-Flat-top-Li-ion-37-V-2250-mAh. [Online; accessed 04/04/2018].

CITED LITERATURE (continued)

74. Patry, G., Romagny, A., Martinet, S., and Froelich, D.: Cost modeling of lithium-ion battery cells for automotive applications. Energy Science Engineering, 3(1):71–82, 2015.

75. KANE, M.: Lux research forecasts $ 172/kwh for li-ion batteries in 2025, jun 2011. https://insideevs.com/lux-research-forecast-172kwh-of-li-ion-batteries-in-2025/. [Online; accessed 25/06/2018].

76. Watanabe, C.: Why battery cost could put the brakes on electric car sales. Bloomberg, nov 2017.

77. Short term operating reserve (stor), market information and tender round results, aug 2018. https://www.nationalgrideso.com/balancing-services/reserve-services/short-term-operating-reserve-stor?market-information. [Online; accessed 02/08/2018].

VITA

NAME	Francesco Rebaudi
EDUCATION	
	Master of Science in Mechanical Engineering, University of Illinois at Chicago, USA, 2017-present
	Master of Science in Mechanical Engineering , Polytechnic of Turin, Italy, 2016-present
	Alta Scuola Politecnica, Polytechnic of Turin and Polytechnic of Milan, Italy, 2017-2018
	Bachelor's Degree in Mechanical Engineering , Università di Genova, Italy, 2013-2016
LANGUAGE SKILLS	
Italian	Native speaker
English	Full working proficiency
	2015 : IELTS examination (7/9)
	Fall 2017 : One Semester of study abroad in Chicago, Illinois
	A.Y. 2016-2018 : Lessons and exams attended exclusively in English
French	Advanced speaker
SCHOLARSHIPS	
2014-2016	Italian scolarship for ISSUGE students
2016-2018	Full tuition waiver at Polito for Alta Scuola Politecnica students
2017	Italian scholarship for extra-EU destinations
2017	Italian scholarship for TOP-UIC students
TECHNICAL SKILLS	
Intermediate level	Python, SolidWorks
Advanced level	C, C++, Fortran, Simulink, Latex
Proficient level	MATLAB, MS OFFICE (Word, Excel, Power Point, Outlook)

VITA (continued)

WORK EXPERIENCE AND PROJECTS

Fall 2017	Stochastic Analysis on a Truss to Determine its Reliability: The truss was modeled in MATLAB employing the finite elements method. Next, the statistical analysis was performed with Monte Carlo iterations producing probability distribution functions.
June 2017 - September 2018	Design and Innovate Salesforce Processes (DISP) at Procter and Gamble: DISP project was developed in collaboration between Procter and Gamble and Alta Scuola Politecnica in order to examine why the sales volume of Gillette, one of its leading brands, has dropped over the past years and to recommend ways of addressing this issue. DISP team exploited new technologies and business models to protect Gillette leadership. The project scope touched different fields, from digital transformation, to data analysis, to marketing and communication strategy; the goal was to design a seamless and effective omnichannel purchase experience
Spring 2017	Kaplan turbine speed increaser: static and fatigue resistance was studied in order to design a speed increaser integrated in a Kaplan turbine. The components considered included: the bearings, the shafts and the different gears. The sizing procedure was accomplished according to the FKM standards
Spring 2017	Solar Energy Equipment: a solar energy collector was designed for a residential building in Turin. The target was supplying hot sanitary water as well as heat to the users. The whole design procedure was accomplished exploiting FEM, exergy, entropy and energy analysis.
Spring 2016	BS thesis research, Calculation code for axial-flow compressors design: It was developed a calculation code *compressore RR*which, from some input parameters chosen by the designer, determines the geometries of an axial compressor and verifies its performances. This calculation code, written in FORTRAN, was verified with the bidimensional calculation code *SLMCC* developed by DIME of the University of Genoa.